Fall 12-2008

The Relationship Betweeen Dynamic and Chemical Factors on the Morphology in AOT-Water-Polymer Systems

Jolanta Elzbieta Marszalek
University of Southern Mississippi

The University of Southern Mississippi

THE RELATIONSHIP BETWEEN DYNAMIC AND CHEMICAL FACTORS ON THE MORPHOLOGY IN AOT-WATER-POLYMER SYSTEMS

by

Jolanta Elżbieta Marszałek

Abstract of a Dissertation
Submitted to the Graduate Studies Office
of The University of Southern Mississippi
in Partial Fulfillment of the Requirements
for the Degree of the Doctor of Philosophy

December 2008

The University of Southern Mississippi

THE RELATIONSHIP BETWEEN DYNAMIC AND CHEMICAL FACTORS ON THE MORPHOLOGY IN AOT-WATER-POLYMER SYSTEMS

by

Jolanta Elżbieta Marszałek

A Dissertation
Submitted to the Graduate Studies Office
of The University of Southern Mississippi
in Partial Fulfillment of the Requirements
for the Degree of Doctor of Philosophy

Approved:

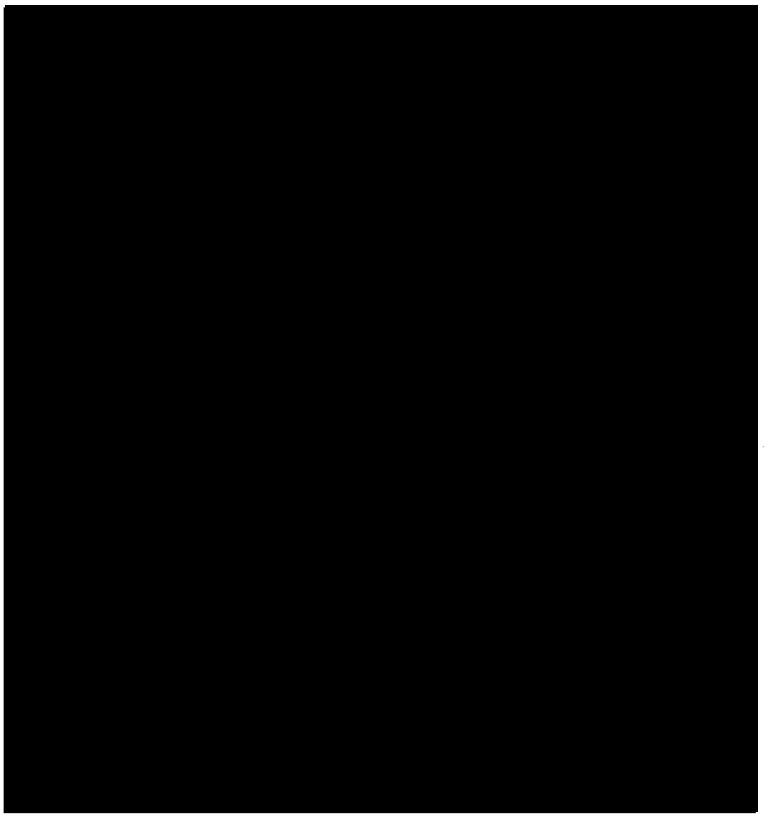

December 2008

ABSTRACT

THE RELATIONSHIP BETWEEN DYNAMIC AND CHEMICAL FACTORS

ON THE MORPHOLOGY IN AOT-WATER-POLYMER SYSTEMS

by Jolanta Elżbieta Marszałek

December 2008

Photopolymerization of reverse microemulsion demonstrates strong influences from dynamical and chemical factors on morphology of formed polymer systems. Upon polymerization the clear microemulsion with nanoscale structures transforms into opaque films with larger aggregates that scatter light. Studied here were microemulsions based on acrylate and on thiol-ene chemistries.

The difference in the two reaction mechanisms results in the phase separation occurring at different stages of the material formation. Consequently, the morphology of the material demonstrates distinct dissimilarities in the two systems. In addition, the chemical structure of the monomers promotes these morphological differences.

When the microemulsion is composed of acrylate and diacrylate monomers, the formed polymer has two different structures. Large sphere-shaped structures are formed from the aggregation of the nanometer-sized droplets in the microemulsion. The droplets, which are mainly filled with water, are large enough to scattering visible light and give the films their opacity. However, they are too small to be observable under an optical microscope. Secondly, some portion of the surfactant self-assembles into a

bilayer structure connecting the larger pools of water. The structure of the film was evaluated by Small Angle Neutron Scattering and Ultra-Small Angle Neutron Scattering.

In the case of microemulsions based on thiol-ene chemistry, the film's morphology is considerably different. Large droplets with size varying from 2 to 100 μm are visible in the films under the magnification of the optical microscope. In addition, the surfactant is more readily excluded from the polymer network than with acrylates; thus, the aggregates are filled not only with water but also with so-called aqueous phase composed of water and surfactant.

The morphology of both systems is sensitive to the rate of the polymerization. The thiol-ene microemulsions were able to self-polymerize, which resulted in phase separation of the material. Resulting two layers were analyzed. The top layer contained mainly polymer. The lower stratum was water-rich with a small amount of polymer confined in droplets. This result proved that films formed through light induced reaction are frozen in a far-form-equilibrium state.

To My Daughter, Anna Sophia Kempke

ACKNOWLEDGMENTS

Foremost I want to thank God for love, friendship, and the gift of an analytical mind.

I thank my adviser; Dr. John A. Pojman, for aiding in the development of research skills, inspiring creativity, and encouraging independent thinking. His excellent support and words of encouragement are an integral part of his teaching and are deeply appreciated. In addition, I extend my gratitude to him for providing me with the opportunity to present results at national conferences. It has been an honor to work with Dr. Pojman, and I will always be grateful for his help.

Support from the other committee members, Dr. Paige Phillips, Dr. Charles Hoyle, Dr. Joe Whitehead, and Dr. Douglas Masterson has been very important and has aided in the successful completion of this graduate research.

Past and present members of the Pojman, Phillips, and Hoyle Research Groups, especially Chris Bounds, Zulma Jimenez, David Heaps, Michelle McCluskey, Tolecia Clark, and Justin Chan, have been a great help in accessing the instruments. I have benefited greatly from many discussions and brainstorming sessions we conducted.

Also, I extend my special thanks to my friends and family outside of the University of Southern Mississippi. I would like to thank my parents Zofia and Ryszard, and my brother Piotr, for their unconditional support and encouragement as I pursued this goal. My special "Thank You" goes to Roberto Kempke and Deles and Truett Roberts whose help and love during my last years at USM was priceless and without which I would not be where I am now.

TABLE OF CONTENTS

LIST OF TABLES

TABLE

LIST OF ILLUSTRATIONS

FIGURE

CHAPTER I

INTRODUCTION

The inspiration for this work comes from polymer-dispersed liquid crystals (PDLCs), which are biphasic networks created by polymerizing a homogeneous mixture of liquid crystal and monomer mixture that upon polymerization forms a phase-separated material composed of liquid crystal droplets within a polymer matrix.(1-3)

Before the work on this dissertation was begun, thin films with water droplets distributed throughout had been produced in our group. The films were prepared through photopolymerization of microemulsions based on an acrylate monomer. The continuous phase of the microemulsions was based on dodecyl acrylate, and the surfactant used to produce water-in-oil arrangement was bis(2-ethylhexyl) sodium sulfosuccinate (AOT). The photopolymerization of the microemulsions produced opaque films. The opaqueness of the films was understood to be the result of the aggregation of the initially nanometer-sized water droplets into droplets large enough to scatter visible light.

We assumed that the occurrence of the aggregates in the films was a result of fast polymerization rates of the systems. We further supposed that if the reaction would be conducted infinitely slowly, it would result in two separate phases of the material. In addition, we believed that the history of the polymerization would be imprinted on the formed material. Thus, we chose two systems with different polymerization mechanisms to examine their influence on the morphology of the films. We assumed that the different paths of polymer formation would result in the occurrence of phase separation at different

conversions of the reaction. Also, we expected that the chemical structures of the monomers would influence the morphology of the formed polymeric materials.

In order to assess the validity of our assumptions, we aimed to answer the following questions:

- How is the stability of the microemulsion distorted by the presence of the polymer? At what polymer load does the microemulsion separate into distinct phases? How is the morphology of the final material affected by the phase separation process? Is the morphology of the final product the equilibrium structure or is the morphology the result of the system being trapped in a nonequilibrium state? Can the equilibrium in the material based on polymerized microemulsion be reached? We hypothesized that if the polymerization were conducted reversibly, i.e., infinitely slowly, then the system would separate into two phases. In addition to influence from the rate and mechanism of polymerization, the observed structures would be a function of the thermodynamic interactions of the water, surfactant, monomer and polymer. We predicted that the polymerization forms material, which captures the aqueous phase within the polymer. We reasoned that the high viscosity caused by crosslinking of the polymer matrix facilitated the trapping of the aqueous phase. This material was believed to be in a nonequilibrium state. The analysis of these questions and hypotheses, presented in Chapter 5, was aimed to give a glimpse of the polymerization reaction.

- What is the size distribution of the water micelles in the microemulsions? Is this distribution a function of the amount of water or only the water-to-surfactant ratio?

How does the type of the monomer affect the size distribution? How large is the stable reverse microemulsion, L_2, region for the monomers? This set of questions was designed to characterize the starting material, namely the microemulsions. We were able to characterize the microemulsions based on the acrylates by Small Angle Neutron Scattering, and the analysis of our data is presented in Chapter 4. Many researchers characterized the size and shape of the microemulsions' structures. These are discussed in more detail in Chapter 2.

- How does chain-growth versus step-growth polymerization influence the aggregation of the aqueous phase? How does the amount of water in the microemulsion affect the size of the aggregates? What is the influence of the water-to-surfactant ratio on the domains? Are the water droplets smaller in the polymerized film, when the system is composed of multifunctional monomers? In Chapter 3 and 6 we addressed these questions by examining how the structural features of the monomers affected the morphology and phase separation in the films.

References

(1) P Drzaic: Putting liquid crystal droplets to work: a short history of polymer dispersed liquid crystals. Liquid Crystals 33 (2006) 1281.

(2) AF Senyurt, G Warren, JB Whitehead, CE Hoyle: Matrix physical structure effect on the electro-optic characteristics of thiol-ene based H-PDLS films. Polymer 47 (2006) 2741.

(3) LV Natarajan, CK Shepherd, DM Brandelik, RL Sutherland, S Chandra, VP Tondiglia, D Tomlin, TJ Bunning: Switchable Holographic polymer-dispersed liquid crystal reflection gratings based on thiol-ene photopolymerization. Chemistry of Matrials 15 (2003) 2477.

(4) M Kotlarchyk, S-H Chen: Analysis of small angle neutron scattering spectra from polydispersed interacting colloids. Journal of Chem Phys 79 (1983) 2461.

CHAPTER II

REVIEW OF THE LITERATURE

Microemulsions

The solubility of water in oil can be easily improved by addition of a surfactant. Microemulsions are systems in which droplets of water or oil are dispersed into small size domains that form thermodynamically stable, clear mixtures. Depending on the composition, they are dispersions of either oil-in-water or water-in-oil. The surfactant absorbs on the oil-water interface and lowers the interfacial tension between oil and water. The average size of the dispersed aggregates ranges between 5 and 100 nm.

The first report of preparing a microemulsion with the use of a surfactant to form a clear homogeneous solution, can be found in an article by Hoar and Schulman in 1943.(1) Shortly after sodium bis(2-ethylhexyl) sulfosucciate (AOT) was introduced as an excellent surfactant to form water-in-oil microemulsions in ternary arrangements.(2)

The microemulsions are called ternary mixtures, when only one surfactant is present in the system; and quaternary mixtures when the microemulsions are formed with the help of a surfactant and co-surfactant. Depending on the composition, the microemulsions display a variety of phases. A classification introduced by P. A. Winsor,(3) which is widely used in describing the phase-forming scenarios, is presented in Figure 2.1, and can be described as following:

- dispersion of oil-in-water (direct microemulsion) in contact with excess oil – Winsor I

- dispersion of water-in-oil (reverse microemulsion) in presence of excess water – Winsor II

- both oil-in-water and water-in-oil dispersions are present in the same domain in a mixed state in contact with water and oil – Winsor III

- a homogeneous phase of either oil-in-water or water-in-oil are observed with no excess of oil or water – Winsor IV

The phase-forming behavior depends on a number of factors, e. g., type of oil, polarity of medium, type of surfactant, presence of additives, temperature, and pressure.(4) The phase can attain different morphology like chains, spheres, lamellae, mesophase, liquid crystalline, and gel-like structures.

Determination of the actual structure of the microemulsion is a challenging problem due to very complex internal interactions and special assembly of the components. Advanced physical techniques are necessary to unravel these complicated structures. Small angle neutron scattering (SANS), small angle X-ray scattering (SAXS), dynamic light scattering (DLS), transmission electron microscopy (TEM), nuclear magnetic resonance (NMR), and time resolved fluorescence quenching (TRFQ) are among the most useful ones. Other methods include conductance, viscosity, ultrasonic interferometry, infrared spectroscopy, ultrasonic absorption, dielectric permittivity, thermal conductivity, and calorimetry.(5)

AOT

Aerosol® OT is a registered trademark, firstly registered with American Cyanamid Company, now CYTEC Industries, and it is the commercial name of sodium bis(2-ethylhexyl) sulfosucciate, commonly known as AOT. The surfactant molecule is shown in Figure 2.2. The linear length of the molecule is 11 Å and the maximum cross-section area of the polar head is about 55 Å.(6)

When exposed to acid or base the AOT hydrolyzes into 2-ethyl-1-hexanol shown in Figure 2.3. This highly surface-active alcohol can function as a co-surfactant and affect the micellar size and the rate of exchange between micelles. At neutral pH reverse micelles containing solubilized water show only 0.1 % decomposition of the AOT during a three-day period.(7)

A typical phase diagram for water-AOT-isooctane at 25 °C displays a large, Winsor IV, water-in-oil phase called L_2. In the Figure 2.5 we show a characteristic ternary phase diagram of AOT/isooctane/water as determined by Tanamushi(8) and recently confirmed with computer simulation by Yuan.(9) The existence of the extended isotropic transparent phase is a distinctive feature of AOT-based microemulsions.

Formation of the Microemulsion

Upon addition of AOT into a non-polar solvent, the aggregation of the surfactant occurs. The two alkyl chains of AOT increase the effective volume of the molecule giving large effective packing parameter. This leads to easier formation of the reverse micellar aggregates. The process of surfactant aggregation is believed to be dominated by solvophilic interactions involving the head groups. The sulfonated head groups are

ordered forward to the interior of the aggregates, thus avoiding interaction with the solvent. The micellar stability in apolar solvents comes mainly from hydrogen-bonding, dipole-dipole, dipole-induced dipole, and dispersion interactions.(6) AOT displays strong monomer – n-mer association in non-polar environments. Aggregation numbers of AOT range from 12 to 40 in these systems. The minimum radius of the inverted micelles in absence of water is calculated to be 12 Å. However, the smallest detected hydrodynamic radius is 15 Å,(6) which was attributed to ever-present water in AOT, actually giving the length of the AOT-H_2O pair. Others(10) hypothesized that the length of 15 Å is a result of AOT molecules stacking on top of each other.

The critical micelle concentration (CMC) for AOT, at which the micelles are spontaneously formed, has been shown to be on the order of mM for series of polar and non-polar solvents, and the CMC did not show polarity dependence.(11)

The solubilization of water in AOT-oil solutions has been described as a three-step process.(12) First, the hydration of the head group occurs; next, the micelles swell with the addition of water; and, finally, the phases separate. The process of solubilization is endothermic, and so it is driven by an increase in entropy.(13)

The solubilization of water in AOT depends on many factors that affect the packing parameter of the surfactant. The oil penetrates the surfactant's tail, increasing the apparent volume. Hydrocarbons similar to the surfactant will be most effective in penetrating the surfactant layer, thus the solubility of water decreases as the carbon number of alkanes increases.(14)

Temperature has a strong effect on the phase structure of the microemulsions. At lower temperatures, the water-in-oil system separates into a two-phase system (Winsor II) and a Winsor I – instability phase. A representative phase diagram for AOT-water-heptane at [AOT] = 0.1 M is shown in Figure 2.5.(15) A temperature increase results in a decrease in the rigidity of the immediate vicinity of the surfactant layer in the interfacial region, especially above 60°C.(13)

The addition of electrolytes decreases the solubilization of water in an AOT solution. The increase in sodium chloride concentration decreases the head-group repulsions and consequently decreases the effective head group area, thus decreasing the packing parameter.(16)

Even though the microemulsions are thermodynamically stable there is a kinetic delay in attaining their equilibrium size distribution. Carballido-Landeira et al.(17) determined, through dynamic light scattering, that the constant hydrodynamic radii were only reached after 24-hours of mixing.

States of Water in Microemulsion

It has been shown that, depending on the water-to-surfactant ratio, the water exhibits different states of association with the surfactant. As early as 1979 Zinsli(18) proposed a model in which two types of water exist within the microemulsion droplets. Subsequently, the nature of the trapped water has been studied by means of a large variety of experimental techniques; namely, fluorescence(18), IR and Raman(19-21), NMR(22-24), DCS measurements(12,25), light scattering and photon correlation.(6) From these studies a picture of water within micelles can be visualized.

In the microemulsion there are three types of water referred to as *trapped*, *bound*, and *free*. The *trapped* water is bound to the ionic head groups of the surfactant at the interface of the micelles. *Free* water has more bulk-like characteristics away from the interface. Between these two, *bound* water appears as a layer of water attached to the interface through hydrogen bonding. *Trapped* water in these models, in comparison to the *free* water, has restricted mobility – both translational and rotational(26), increased viscosity, a diminished hydrogen bonding network(21), less polarity, and smaller dielectric constant(27). The properties of the surfactant-affected water are strongly dependent on $W = [H_2O]/[AOT]$. In a water-AOT-toluene system, only *trapped* water is present below $W < 4$. Swollen micelles with *bound* water are formed when W is between 4 and 12, and, when $W > 12$, *free* bulk-like water builds up in the interior of the micelles(28). Ladanyi et al.(29) successfully conducted Molecular Dynamic simulations confirming the above model, though with a slight shift of the W values.

Often in the literature(5), the structures with $W > 12$ are referred to as water-in-oil microemulsions, while, below that value, the AOT aggregates are called reverse micelles.

Applications of Microemulsions

Reverse micellar solutions of AOT have been exploited in different applications, including: enzyme activity studies, cryoenzymology, liquid-liquid extractions of proteins, sol-gel preparations, polymerizations, and nanoparticle preparations. The systems are very attractive because they are optically transparent and therefore the changes in the system can be followed by different spectrophotometric methods. Moreover, both hydrophilic and hydrophobic components can be solubilized in these systems.

Additionally, there are parameters like water pool size, surfactant concentration, pH of the water pool, which can be easily tuned to effect changes in the system under study.(5)

Several enzymes and proteins have by now been solubilized in reverse micellar solutions of AOT-hydrocarbon systems (usually isooctane or n-octane). It has been shown that the enzymes solubilized in AOT microemulsion maintain activity on levels comparable to that found in aqueous solutions. There are cases where the enzyme activity in reverse micellar solutions was found to be much higher than the enzyme activity in aqueous mediums.(30)

Use of the microemulsion structure as a template for the synthesis of polymeric materials has received a considerable amount of attention.(31-34) Typically, microemulsion polymerizations are used in the synthesis of well-defined, nanometer-sized polymer particles with a narrow size distribution. The inherent properties of microemulsion systems allow a large degree of control over the polymerization process and, ultimately, the types of polymer particles which can be synthesized.(34) Specifically, inverse-microemulsion polymerization is an attractive approach to the synthesis of high-molecular-weight water-soluble polymers,(34,35) as well as difficult to dissolve polymers(36) such a polyaniline(37) or polythiophene(38). As mentioned above, in the restricted environment of inverse micelles, water exhibits unique physical and chemical properties that facilitate the synthesis of various types of inorganic solid colloidal particles (e.g. metals, metal carbonates, semiconductors).(39-41)

Although there have been several studies demonstrating the ability of carrying out polymerization reactions *within* the micelles of a microemulsion,(38,42) there has been little work on polymerizations that occur throughout the continuous phase of the reverse

microemulsion.(43-45) These studies were concerned with polymerization of a monomer in a bicontinuous microemulsion (Winsor III) to form porous polymers which could be utilized as membranes.(46) Because the resulting polymers often did not reflect the original microstructure, polymerizable surfactants were introduced.(47,48) In another attempt to preserve the lamellar nanostructure of the microemulsion, a small amount of crosslinking throughout the oil phase resulted in nanostructured polyacrylamide hydrogels.(49)

Scattering Theory

Both scattering and absorption remove energy from a beam of light traveling through a medium; the beam is attenuated. This attenuation, also called extinction, is seen when one looks directly at the light source. However, whether the absorption or scattering is mainly responsible for the extinction cannot be judged by observation alone. Thus

Extinction = scattering + absorption

If light traverses through a perfectly homogeneous media, there is no scattering present.

Figure 2.6 shows interfering light of intensity I_o entering a glass cylinder filled with an inhomogeneous scatterer. On the other end of the cylinder light intensity, $I < I_o$, emerges. For a smoke-filled cylinder of a given density the outgoing intensity depends exponentially on the length of the cylinder, d, and the absorption coefficient α

$$I = I_o e^{-\alpha d} \qquad \text{Equation 2.1}$$

The absorption coefficient measures the rate of light loss from the direct beam. The absorption coefficient often consists of two parts: true absorption, α_a, and absorption due to scattering, α_s. In Figure 2.6, true absorption represents the energy converted into heat motion, while scattering is represented by the I_s.

Scattering is most efficient when the wavelength of the light is of a comparable value to the scatterers' size. Coherent scattering appears when all waves leave the scatterer in phase with each other.

Lord Rayleigh gave the first quantitative description of scattered light intensity applicable for objects that had refraction indexes different from the surroundings.

$$I_s = k\frac{1}{\lambda^4} \qquad \text{Equation 2.2}$$

When looking at scattering with respect to a microemulsion system, there are two possible scenarios. In the first the scatterers, micelles, are well separated, and there is no interference of the scattered light. This is a dilute system. In the second, the particles "see" each other, and the inter-particle interference is considerable.

For the dilute systems, where the scattering particles are separated by large enough distances so that no interference occurs between scattering from different particles, the intensity of elastic scattered radiation is given simply by the product of the number of scatterers, N, and the scattered intensity of a single particle.(50) This can be expressed in a general way as

$$I(Q) = K\,N\,P(Q) \qquad \text{Equation 2.3}$$

where Q is the magnitude of the scattering vector, given by

$$Q = \frac{4n\pi}{\lambda}\sin\theta \qquad \text{Equation 2.4}$$

where n is the solution refractive index, λ is the incident wavelength in a vacuum, and θ is half of the scattering angle.

P(Q) is the form factor of the particle, and K is a constant that is a function of the type of radiation used and the sample properties. For a homogeneous sphere of radius R the form factor can be written as:

$$P(Q) = v_o^{\,2}\Phi^2(QR) \qquad \text{Equation 2.5}$$

where v_o is the sphere volume and

$$\Phi(QR) = \frac{3}{(QR)^3}[\sin(QR) - QR\cos(QR)] \qquad \text{Equation 2.6}$$

Thus, for a system of N identical spherical particles, representing micelles the scattered intensity is

$$I(Q) = K\ N\ v_o^{\,2}\Phi^2(QR) \qquad \text{Equation 2.7}$$

The maxima in the form factor are calculated to occur at

$$QR = 5.76, 9.10, \ldots \qquad \text{Equation 2.8}$$

Therefore, the radius of the sphere can be calculated from the location of the intra-particle peaks in the scattering curve.

As the density of scattering particles increases, inter-particle interference becomes significant. In order to include the effect of particle interference on the scattering intensity, Zernike and Prins(51) introduced a structure factor S(Q) that describes the interference of the scattered light. For monodisperse particles:

$$I(Q) = K\,N\,P(Q)\,S(Q) \qquad \text{Equation 2.9}$$

and S(Q), the interference factor, is given by

$$S(Q) = 1 + 4\pi m \int_0^\infty (g(r) - 1)\frac{\sin(Qr)}{Qr} r^3 dr \qquad \text{Equation 2.10}$$

Here, m is the particle number density, and g(r) is the radial distribution function describing the arrangement of the particles.

Fournet(52), through modification of the liquid-state theories, recalculated g(r) to take into account three-body interactions obtaining the following result for the scattered intensity:

$$I(Q) = K\,N\,P(Q)\,[1 - n(2\pi)^{3/2}\,\varepsilon\beta(Q)]^{-1} \qquad \text{Equation 2.11}$$

where ε is a factor close to unity and

$$\beta(Q) = \frac{2}{\sqrt{2\pi}} \int_0^\infty (e^{-\phi(r)/kT} - 1)\frac{\sin(Qr)}{Qr} r^3 dr \qquad \text{Equation 2.12}$$

Fournet's formula can also be solved for a system of hard spheres with $\phi(r) = \infty$ for $0 < r < 2R$ and $\phi(r) = 0$ for $r > 2R$:

$$I(Q) = K\,N\,v_o^2\Phi^2(QR)[1 + 8\,n\,v_o\,\varepsilon\,\Phi(2QR)]^{-1} \qquad \text{Equation 2.13}$$

Small-Angle Neutron Scattering (SANS)

Over the past three decades, small-angle neutron scattering (SANS) has proven to be a useful tool in examining the structure of water-in-oil (and oil-in-water) microemulsion systems.(53-60) In scattering techniques, the waves scattered at a given angle by all points in the sample interfere with each other to produce one point in an interference pattern. The interference is then transformed to reconstruct an image of all correlations within the sample. The wavelength of the neutron and X-ray radiations are less than 1 nm, thus they can be used in measuring the specific distances in microemulsions that are of a similar scale. In particular, measurements at low angles provide adequate interference to derive information about the species. In the small angle methods the measured intensity is correlated with the number density of scatterers, and the particle size and structural correlations are derived by application of various models. SANS measurements of microemulsions, with use of different contrast techniques, allow direct evaluation of apparent water pools and hard sphere radii.

In summation and with respect to neutron scattering, the total scattering function, I(Q), of a microemulsion system can be described by the product of the contributions from the shape of the scattering particle (i.e., the form factor), F(Q), and the spatial distribution of the scattering particles (i.e., the structure factor), S(Q). It is given by the following relation

$$I(Q) = \kappa\left|\langle F(Q)\rangle\right|^2 \langle S(Q)\rangle \qquad \text{Equation 2.14}$$

where κ is the number density of the scattering particles, and the brackets, $\langle\rangle$, represent the ensemble average due to thermal fluctuations.

Our present work uses a core-shell model for spherical droplets for F(Q), which considers the core to be polydisperse, and the shell to consist of a monolayer of the surfactant molecules. The polydispersity is taken into account by weighting the form factor by a probability function described by the Schulz distribution.(61-63) This is a common technique used to describe the polydispersity of droplet sizes in microemulsions. The form factor, F(Q), for a spherical core-shell particle can be expressed by

$$F(Q) = V_c(\rho_c - \rho_s)\cdot F_0(QR_c) + V_s(\rho_s - \rho_{solv})\cdot F_0(QR_s) \qquad \text{Equation 2.15}$$

where V_c and V_s are the volumes of the particles with radii of the core R_c and of the shell, R_s.(64) Neutron-scattering length densities of the core, the shell, and the solvent are ρ_c, ρ_s, ρ_{solv}, respectively. The function $F_o(x)$ is a first-order spherical Bessel function of the first kind and is given by

$$F_0(x) = 3\frac{\sin x - x\cos x}{x^3} \qquad \text{Equation 2.16}$$

The contribution to I(Q) from the structure factor, S(Q), for the spherical core-shell particles has been modeled assuming hard-sphere interactions. This approach has been found to describe scattering from micoremulsions quite well.(62,65) The model structure factor employed here is based on the Percus-Yevick approximation.(66)

SANS study of microemulsions formed from low-density alkanes with AOT has established that droplet structure depends on the alkane's density. High alkane density produces randomly distributed, monodisperse, weakly-interacting droplets, whereas lower density produces an increase in droplet interaction leading to cluster formation.(67)

Studies by Kotlarchyk and coworkers(62,63,68-71) have used SANS to elucidate the structure in pure three-component AOT-D_2O-alkane systems. Their results have

shown that the droplets in such systems are polydisperse spheres and weakly-interacting at room temperature. Furthermore, they showed that the droplet radius increased linearly with an increase in the molar ratio of D_2O to AOT ($W=[D_2O]/[AOT]$). In particular, they found, empirically, that the mean droplet radius <r> could be expressed in terms of W using the following equation(62)

$$\langle r \rangle = \frac{3v_{D_2O}}{a_0} W + \frac{3V_H}{a_0} \qquad \text{Equation 2.17}$$

where v_{D2O} is the specific volume of a D_2O molecule, V_H is the volume of the water-penetrated portion of a single AOT head group, and a_o is the area per AOT head group on the water-core surface. In related work by Kotlarchyk and coworkers,(63) modeling of the SANS data was accomplished using a form factor for polydisperse hard spheres and a structure factor taking into account contributions from inter-particle interactions and density fluctuations.

Photopolymerization

Light-induced polymerization is a technique that permits a rapid conversion of liquid materials into rubbery or glassy polymers, even at room temperatures. It is a useful and environmentally friendly method for producing coatings with a range of properties depending on the composition of the pre-polymerization mixture.

The term photopolymerization actually represents a light-induced chain reaction, where light serves as a radical or cation generator, which in turns starts radical-chain propagation. In classical terms of chain-radical propagation, the following steps can be distinguished:

Dissociation: $In \xrightarrow[k_d]{} 2R^{\bullet}$

Initiation: $R^{\bullet} + M \xrightarrow[k_i]{} RM^{\bullet}$

Propagation: $RM_i^{\bullet} + M \xrightarrow[k_p]{} RM_{i+1}^{\bullet}$

Termination: $RM_i^{\bullet} + RM_j^{\bullet} \xrightarrow[k_{tc}]{} RM_{i+j}R$

$RM_i^{\bullet} + RM_j^{\bullet} \xrightarrow[k_{td}]{} RM_i + RM_i$

where In is an initiator, M a monomer, $R^{\bullet}$ a primary radical, $RM_i^{\bullet}$ a growing polymer chain with leaving radical, and RM_i and $RM_i R$ are "dead" polymer chains. The rate constants k_d, k_i, k_p, k_t refer to decomposition, initiation, propagation, and termination, respectively. The termination may either occur through combination (k_{tc}) or disproportionation (k_{td}).

When a few assumptions are made, the rate law of the polymerization can be written. First, the so-called steady-state assumption requires that the total free-radical concentration remains constant during the reaction, because the rate of radical production is equal to the rate of radical termination. In addition, one needs to assume that the reactivity of radicals is size independent, and also that there is no chain transfer during radical propagation.(73)

$$R_p = k_p[M]\sqrt{\frac{R_i}{2k_t}} \qquad \text{Equation 2.23}$$

The rate of initiation R_i for a light-induced system becomes:

$$R_i = 2\varphi I_a \qquad \text{Equation 2.24}$$

in which φ is the quantum efficiency of the initiator, and I_a is intensity of absorbed light, which at low absorbance is equal to:

$$I_a = 2.3\ \varepsilon\ I_o\ [In]\ d \qquad \text{Equation 2.25}$$

where ε is the molar extinction coefficient at the wavelength of radiation, I_o is the incident intensity, and d is the thickness of the sample. For very thin samples the rate of polymerization becomes:

$$R_p = k_p[M]\sqrt{\frac{2.3\ \varepsilon\ \varphi\ I_o[In]\ d}{k_t}} \qquad \text{Equation 2.26}$$

However, for thicker samples the Beer's law should be included in the rate expression giving:

$$R_p = k_p[M]\sqrt{\frac{\varphi\ I_o(1-10^{-\varepsilon[In]d})}{k_t}} \qquad \text{Equation 2.27}$$

Acrylates

Acrylates are the most commonly used precursors for photopolymerization because of their low cost, good final properties, and wide range of applications. Multifunctional acrylates, that form thermosets upon polymerization, are used as protective coatings, UVis curable inks etc.

It has been shown that in chain-growth polymerization of multifunctional acrylates, the networks have inhomogeneous structures with high-density regions formed at low double-bond conversion.(74) The heterogeneous network of multifunctional acrylates results in very broad glass transition temperatures of glassy polymers with a wide distribution of dense regions. Acrylate polymerization is also inhibited by oxygen.(75)

Thiol-ene Chemistry

Thiol-enes are photo-curable systems that polymerize by a free-radical step growth reaction. The mechanism, depicted in Figure 2.7,(76) involves two steps: an initial addition of the thiyl radical to the carbon of an ene (step A in Propagation) and a succeeding hydrogen abstraction of a thiol group by a carbon-centered radical to give a thiyl radical (step B). Termination occurs by radical–radical coupling.

Multifunctional thiols will copolymerize with almost any multifunctional ene, and the reaction mechanism affords delayed gelation, high conversion, and uniform crosslink densities; this results in the ability to produce products with unique physical and mechanical properties.(77)

The properties of the thiol– ene networks originate from the following facts: the thiol-enes photopolymerize very rapidly in air in comparison with traditional acrylates; they can be photocured without the addition of a photoinitiator, although the addition of the photoinitiator drastically increases potopolymerization rates; the rheology of the initial unpolymerized resin as well as the properties of the final film can be easily modified with a wide variety of enes.

The films have highly uniform crosslink density that ensures optimum mechanical performance. The thioether linkages formed during the polymerization process are flexible and serve as efficient antioxidants for the crosslinked network. The films exhibit excellent weatherability. The adhesion of thiol–ene-based clear coatings to a large variety of substrates, including plastics, metals, glass, and wood, is outstanding because of the late gelation process, and the nature of the thioether groups that promote adhesion.(78)

Roper et al.(79) used a thiol-ene system as a base of a pigmented photocurable resin. The thiol-ene resin not only photopolymerized in the air, but also resulted in high conversions of monomers. As it is well known, high conversions significantly influences the physical properties of ink coatings. Thus, the properties that promote the use of thiol-enes in pigmented inks are related to the variety of mechanical and physical properties. These properties result from high polymerization rate and high conversion and include enhanced flexibility and good substrate adhesion.

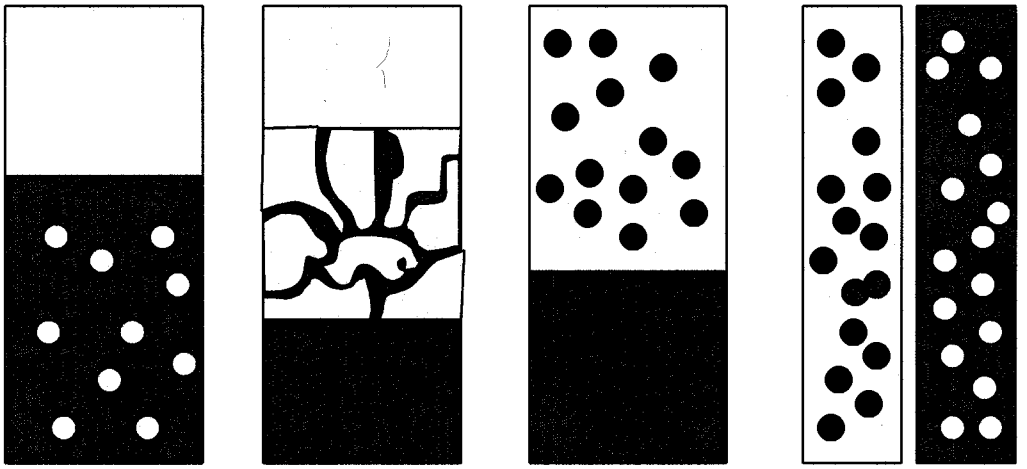

Figure 2.1. Winsor's classification of the water-amphiphile-oil mixtures adopted from (4).

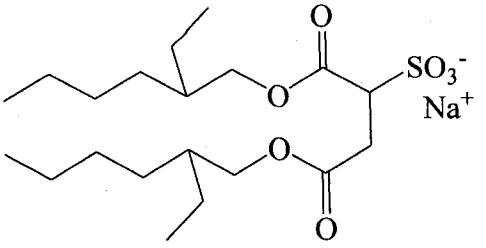

Figure 2.2. Structure of AOT.

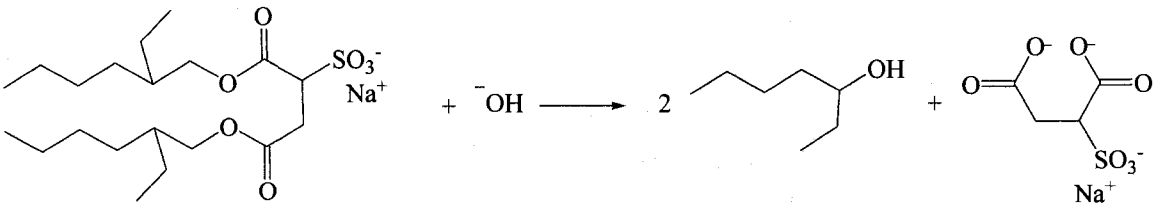

Figure 2.3. Hydrolysis of AOT in presence of base.

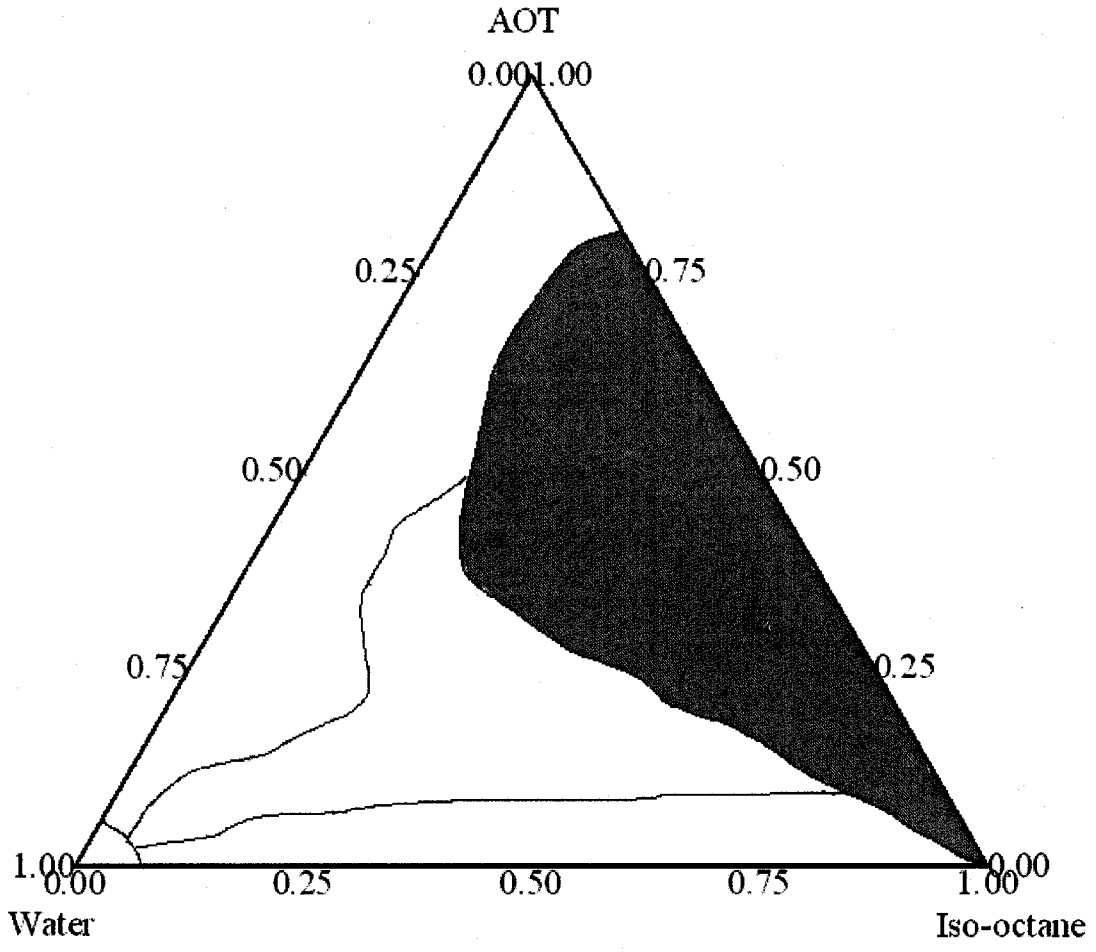

Figure 2.4. Ternary phase diagram adapted from (8).

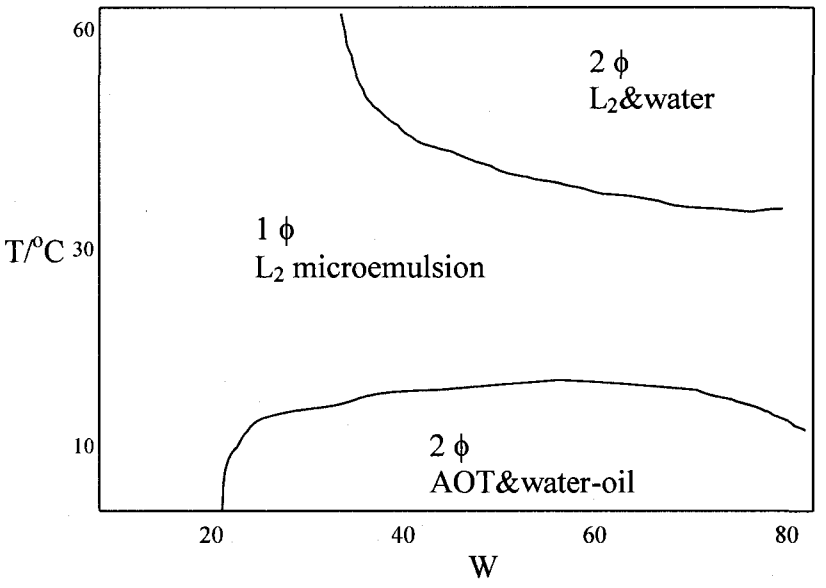

Figure 2.5. Water-in-oil microemulsion phase diagram for AOT-water-heptane system adapted form (15).

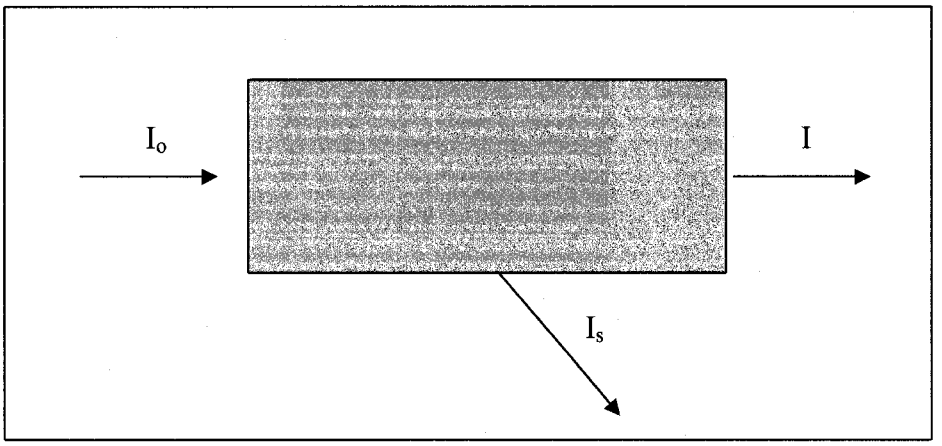

Figure 2.6. Light interfering with inhomogeneous scatterers.

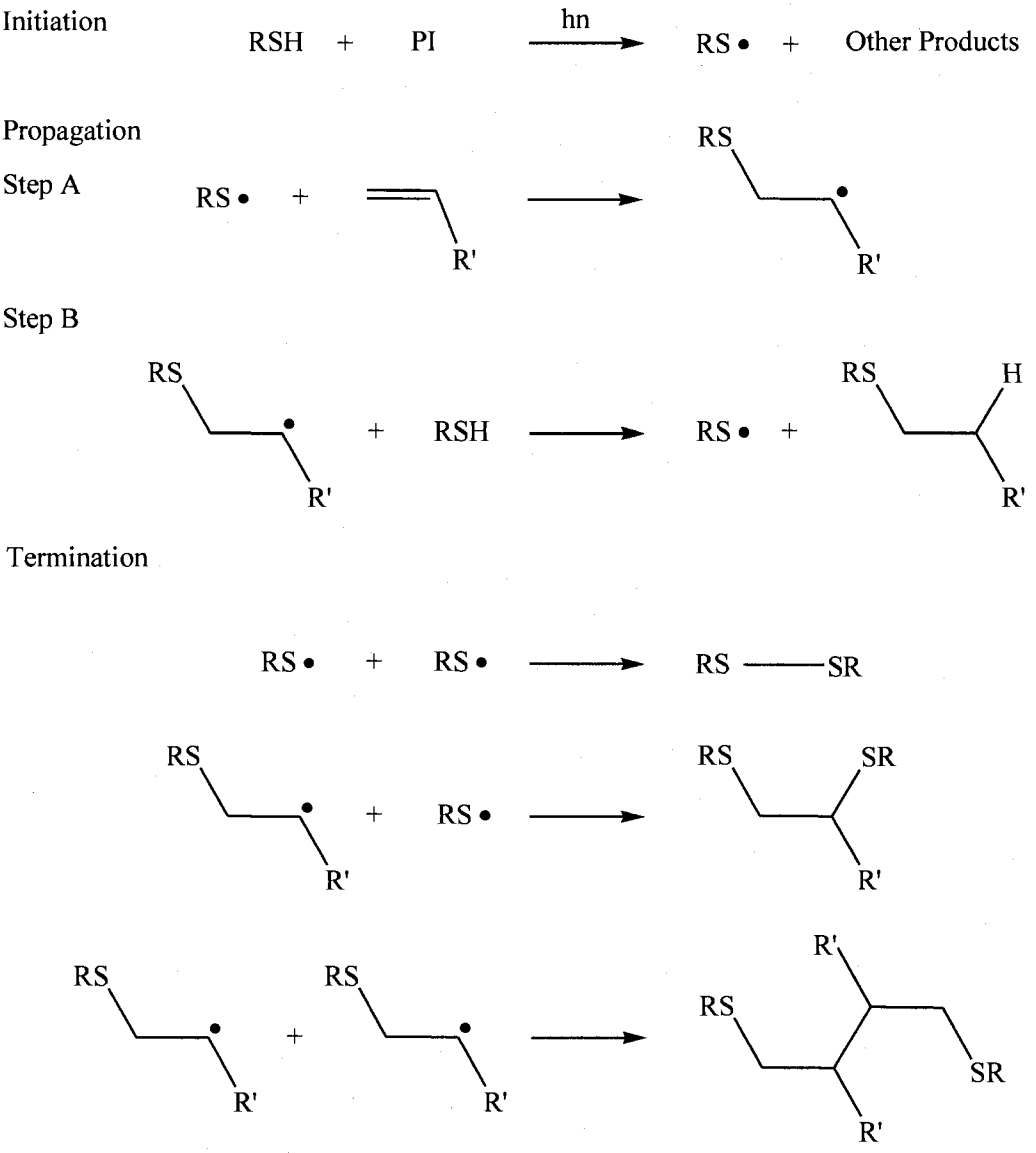

Figure 2.7. Thiol-ene photopolymerization mechanism.

Reference

(1) TP Hoar, JH Schulman: Transparent Water-in-oil dispersions: the oleopathic hydro-micelle. Nature 152 (1943) 102.

(2) RW Mattoon, MB Mathews: Micelles in non-aqueous media. The Journal of Chemical Physics 17 (1949) 496.

(3) PA Winsor: Hydrotropy, solubilisation and related emulsification processes. Transactions of the Faraday Society 44 (1948) 376.

(4) SP Moulik, BK Paul: Structure, dynamics and transport properties of microemulsion. Advances in Colloid and Interface Science 78 (1998) 99.

(5) TK De, A Maitra: Solution Behavior of Aerosol OT in Non-Polar Solvents. Advances in Colloid and Interface Science. 59 (1995) 95.

(6) H-F Eicke, M Zulauf: Inverted micelles and microemulsions in the ternary system H2O/Aerosol-OT/Isooctane as studied by photon correlation spectroscopy. Journal of Physical Chemistry 83 (1979) 480.

(7) L Magid, CA Martin: Carbon-13 NMR investigation of Aerosol-OT water-in-oil microemulsion. Journal of Physical Chemistry 85 (1981) 3938.

(8) B Tamamushi, N Watanabe: The formation of molecular aggregation structures in ternary system: Aerosol OT/water/iso-octane. Colloid & Polymer Science 258 (1980) 174.

(9) SL Yuan, GY Xu, ZT Cai: MesoDyn simulation study on phase diagram of Aerosol OT/isooctane/water system. Chinese Chemical Letters 13 (2002) 1025.

(10) A Maitra: Determination of size parameters of water-Aerosol OT-oil reverse micelles from their nuclear magnetic resonance data. Journal of Physical Chemistry 88 (1984) 5122.

(11) SP Moulik, K Mukherjee, DC Mukherjee: Thermodynamics of micellization of Aerosol OT in polar and nonpolar solvents. A clorimetric study. Langmuir 9 (1993) 1727.

(12) G Haandrikman, GJ Daane, FJ Kerkhof, NM van Os, LA Rupert: A microcalorimetric investigation of the solubilization of water in reversed micelles and water-in-oil microemulsions. Journal of Physical Chemistry 96 (1992) 9061.

(13) A D'Aprano, A Lizzio, V Turco Liveri: Enthalpies of solution and volumes of water in revesed AOT micelles. Journal of Physical Chemistry 91 (1987) 4749.

(14) K Kon-No, A Kitahara: Solubility behavior of water in nonaqueous solutions of oil-aoluble surfactants: effect of molecular structure of surfactants and solvents. Journal of Colloid and Interface Science 37 (1971) 469.

(15) J Eastoe, S Nave, RK Heenen, DC Steytler, I Grillo: What is so spacial about Aerosol-OT? Part III - Glutacone versus sulfosuccinate headgroups and oil-water interfacial tension. Langmuir 18 (2002) 1505.

(16) K Kon-No, A Kitahara: Secondary solubilization of electrolytes by di(2-ethylhexyl) sodium sulfosuccinate in cyclihexane solutions. Journal of Colloid and Interface Science 41 (1972) 47.

(17) J Carballido-Landeira, I Berenstein, P Taboada, V Mosquera, VK Vanag, IR Epstein, V Perez-Villar, A Munuzuri: Long-lasting dashed waves in a reactive microemusion. Physical Chemistry Chemical Physics 10 (2008) 1094.

(18) PE Zinsli: Inhomogeneous interior of Aerosol OT microemulsions probed by fluorescence and polarized decay. Journal of Physical Chemistry 83 (1979) 3223.

(19) G Onori, A Santucci: IR investigation of water structure in Aerosol OT reverse micellar aggregates. Journal of Physical Chemistry 97 (1993) 5430.

(20) TK Jain, M Varshney, A Maitra: Structural studies of Aerosol OT revese micellar aggregates by FT-IR. Journal of Physical Chemistry 93 (1989) 7409.

(21) PD Moran, GA Bowmaker, RP Cooney, JR Bartlett, JL Woolfrey: Vibrational spectroscopic study of the structure of sodium bis(2-ethylhexyl)sulfosuccinate revese micellar and water-in-oil microemulsions. Langmuir 11 (1995) 738.

(22) A Maitra: Determination of size parameters of water-Aerosol OT-oil reverse micelles from their Nuclear Magnetic Resonance Data. Journal of Physical Chemistry 88 (1984) 5122.

(23) A Maitra, H-F Eicke: Effect of rotational isomerism on the water-solubilizing properties of Aerosol OT as studied by H NMR spectroscopy. Journal of Physical Chemistry 85 (1981) 2687.

(24) CS Oliveira, EL Bastos, EL Duarte, R Itri, MS Baptista: Ion pairs of crystal violet in sodium bis(2-ethylhexyl)sulfosuccinate reverse micelles. Langmuir 22 (2006) 8718.

(25) H Hauser, G Haering, A Pande, PL Luisi: Interaction of water with sodium bis(2-ethyl-1-hexyl) sulfosuccinate in reversed micelles. Journal of Physical Chemistry 93 (1989) 7869.

(26) G Carlstrom, B Halle: Water dynamics in microemulsion droplets. A Nuclear Spin Relaxation Study. Langmuir 4 (1988) 1346.

(27) M Belletete, M Lachapelle, G Durocher: Dynamics of interfacial interactions between the molecular probe 2-(p-(dimethylamino)phenyl)-3,3-dimethyl-3H-indole and Aeroslo OT inverted micelles. Journal of Physical Chemistry 94 (1990) 7642.

(28) K Hamada, T Ikeda, T Kawai, K Kon-No: Ionic Strength Effects of Electrolytes on Solubilized States of Water in AOT Reversed Micelles. Journal of Colloid and Interface Science 233 (2001) 166.

(29) J Faeder, BM Ladanyi: Molecular Dynamics simulations of the interior of aqueous reverse micelles. Journal of Physical Chemistry B 104 (2000) 1033.

(30) S Barbaric, PL Luisi: Micellar solubilization of biopolymers in organic solvents. 5. Activity and conformation of a-chrymotrypsin in isooctane-AOT reverse micelles Journal of the American Chemical Society 103 (1981) 4239.

(31) T Hellweg: Phase structure of microemulsions. Current Opinions in Colloid & Interface Science 7 (2002) 50.

(32) I Javierre, F Nallet, A-M Bellocq, M Maugey: Structure and dynamic properties of a polymer-induced sponge phase. Journal of Physics: Condense Matter 12 (2000) A295.

(33) M Nagao, S Okabe, M Shibayama: Small-angle neutron-scattering study on a structure of microemulsion mixed with polymer network. The Journal of Chemical Physics 123 (2005) 144909.

(34) H-P Hentze, EW Kaler: Polymerization of and within self-organized media. Current Opinion in Colloids and Interface Science 8 (2003) 164.

(35) X Li, SP Xia, WJ Zeng, WY Zhang, SX Dong: Monitor of Polymerization of Inverse Microemulsion Containing Methyl Methacrylate and Acrylic Acid. Chinese Chemical Letters 17 (2006) 247.

(36) J Jang: Conducting Polymer Nanomaterials and their applications. Advance Polymer Science 199 (2006) 189.

(37) F Yan, G Xue: Journal of Material Chemistry 9 (1999) 3035.

(38) V Tasakova, S Winkels, JW Schultze: Electrochim Acta 46 (2000) 759.

(39) T Kawai, Y Usui, K Kon-No: Synthesis and growth mechanism of GeO_2 particles in AOT reversed micelles. Colloids and Surfaces A 149 (1999) 39.

(40) Z Chen, S Li, Y Yan: Synthesis of Template-Free Zeolite Nanocrystals by Reverse Microemulsion-Microwave Method. Chemistry of Materials 17 (2005) 2262.

(41) Y Yan, Z Chen, S Li: Synthesis of template-free zeolite nanocrystals by revese micreomulsion - microwave method. Chemistry of Materials 17 (2005) 2262.

(42) R Tang, Y Xue, W Yang, L Zha, S Fu: Rich-syndiotacticity of Poly(cyclohexyl methacrylate) prepared by modified microemulsion polymerization. Journal of Macromolecular Science Part A: Pure and Applied Chemistry 44 (2007) 569.

(43) HM Cheung, M Sasthav, WR Palani Raj: Polymerization of single-phase microemulsions: dependence of polymer morphology on microemulsion structure. Polymer 36 (1995) 2637.

(44) G Zhang, X Xu, J Tang, H Liu, H Ge, Z Zeng: Formation of Microporous Polymeric Materials by Microemulsion Radiation Polymerization of Butyl Acrylate. Journal of Applied Polymer Science 77 (2000) 1989.

(45) HM Cheung, M Sasthav: Characterization and Polymerization of Middle-Phase Microemulsion in Styrene/Water System. Langmuir 7 (1991) 1378.

(46) J Texter, F Yan: Solvent-Reversible Poration in Ionic Liquid Copolymers. Angewandte Chemie 46 (2007) 2440.

(47) J Texter, L Ge, TH Mourey, TG Bryan: Polymerizable Bis(2-ethylhexyl)sulfosuccinate: Application in Microemulsion Polymerization. Langmuir 20 (2004) 11288.

(48) B Tieke, W Pyckhout-Hintzen, M Dreja: Copolymerization behaviour and structure of styrene and polymerizable surfactants in three-component cationic microemulsion. Macromolecules 31 (1998) 272.

(49) CA Guymon, CL Lester, SM Smith, CC D.: Physical Properties of Hydrogels Synthesized from Lyotropic Liquid Crystalline Templates. Chemistry of Materials 15 (2003) 3376.

(50) A Guinier, G Fournet: Small-Angle Scattering of X-Rays, Wiley, New York, 1955.

(51) F Zernike, JA Prins: Z. Physics 41 (1927) 184.

(52) G Fournet: Diffusion des rayons X para les fluides. Acta Crystallographica 4 (1951) 293.

(53) M Kotlarchyk, N Quirke, JS Huang, SA Safran, MW Kim, GS Grest: Attractive Interactions in Micelles and Micreomulsions. Physical Review Letters 53 (1984) 592.

(54) R Strey, J Winkler, L Magid: Small-Angle Neutron Scattering from Diffuse Interfaces. 1. Mono- and Bilayers in the water-octane-C12E5 system. Journal of Physical Chemistry 95 (1991) 7502.

(55) G Capuzzi, F Pini, CMC Gambi, M Monduzzi, P Baglioni, J Teixeira: Small-Angle Neutron Scattering of Ca(AOT)2/D2O/Decane Microemulsion. Langmuir 13 (1997) 6927.

(56) CMC Gambi, R Giordano, M Laurati, L Lanzi, F Pini, P Baglioni: SANS analysis of perfluoropolyether water-in-oil microemulsions by hard sphere and adhesive hard sphere potentials. Applied Physics A 74 (2002) S377.

(57) BH Robinson, RK Heenen, J Eastoe, DC Steytler, G Fragneto: Small-angle neutron scattering from novel bis-2-ethylhexylsulphorosuccinate microemulsions: evidence for non-spherical structures. Physica B 180&181 (1992) 555.

(58) M Nagao, H Seto, D Okuhara, H Okabayashi, T Takeds, M Hikosaka: A small-angle neutron-scattering study of the effect of pressure on structures in a ternary microemulsion system. Physica B 241-243 (1998) 970.

(59) B Simmons, GC Irvin, S Li, V John, GL McPherson, N Balsara, V Agarwal, A Bose: Langmuir 18 (2002) 624.

(60) B Simmons, V Agarwal, GL McPherson, V John, A Bose: Small Angle Neutron Scattering Study of Mixed AOT + Lecithin Revese Micelles. Langmuir 18 (2002) 8345.

(61) SH Chen, J Rouch, F Sciortino, P Tartaglia: Static and dynamic properties of water-in-oil microemulsions near the critical and percolation points. Journal of Physics.: Condense Matter 6 (1994) 10855.

(62) M Kotlarchyk, SH Chen: Analysis of small angle neutron scattering spectra from polydisperse interacting colloids. Journal of Chemical Physics 79 (1983) 2461.

(63) M Kotlarchyk, SH Chen, JS Huang, MW Kim: Structure of 3-Component Microemulsions in the Critical Region Determined by Small-Angle Neutron-Scattering. Physical Review A 29 (1984) 2054.

(64) J Eastoe, KJ Hetherington, D Sharpe, J Dong, RK Heenen, DC Steytler: Films of di-chained surfactants in microemulsions. Colloids and Surfaces A: Physicochemical and Engineering Aspects 128 (1997) 209.

(65) M Nagao, S Okabe, M Shibayama: Small-angle neutron scattering study on a structure of microemulsion mixed with polymer networks. The Journal of Chemical Physics 123 (2005) 144909.

(66) JK Percus, GJ Yevick: Analysis of classical statistical mechanics by means of collective coordinates. Physical Review 110 (1958) 1.

(67) J Eastoe, WK Young, BH Robinson, DC Steytler: Journal of Chemical Society. Faraday Transactions 86 (1990) 2883.

(68) M Kotlarchyk, SH Chen, JS Huang: Temperature Dependence of Size and Polydispersity in a Three-Component Microemulsion by Small Angle Neutron Scattering. Journal of Physical Chemistry 86 (1982) 3273.

(69) M Kotlarchyk, SH Chen, JS Huang, MW Kim: Structure of dense sodium di-2-ehtylsulfosuccinate/D2O/Decane microemulsions. Physical Review Letters 53 (1984) 941.

(70) M Kotlarchyk, S-H Chen, JS Huang: Critical behavior of a microemulsion studied by small-angle neutron scattering. Physical Review A 28 (1983) 508.

(71) M Kotlarchyk, JS Huang, SH Chen: Structure of AOT Reversed Micelles determined by SANS. Journal of Physical Chemistry 89 (1985) 4382.

(72) E Gulari, B Bedwell, S Alkhafaji: Quasi-elastic light-scattering investigation of microemulsions. Journal of Colloid and Interface Science 77 (1980) 202.

(73) G Odian: Principles of Polymerization, 4th Ed., Wiley, New York, 2004.

(74) JG Kloosterboer: Network formation by chain crosslinking photopolymerization and its applications in electronics. Advances in Polymer Science 84 (1988) 1.

(75) AF Senyurt, H Wei, CE Hoyle, SG Piland, TE Gould: Ternary thiol-ene/acrylate photopolymers: effect of acrylate structure on mechanical properties. Macromolecules 40 (2007) 4901.

(76) CE Hoyle, TY Lee, T Roper: Thiol–Enes: Chemistry of the Past with a Promise for the Future. Journal of Polymer Science Part A. Polymer Chemistry 52 (2004) 5301.

(77) CE Hoyle, M Cole, M Bachemin, W Kuang, V Kalyanaraman, S Jonsson, in K.D. Belfield, J.V. Crivello (Eds.), Photoinitiated Polymerization: ACS Symposium Series No. 793. American Chemical Society, Washington, DC, 2003, p. 52.

(78) CE Hoyle, TY Lee, TM Roper: Thiol-enes: chemistry of the past with promise for the future. Journal of Polymer Science: Part A: Polymer Chemistry 42 (2004) 5301.

(79) TM Roper, T Kwee, TY Lee, CA Guymon, CE Hoyle: Photopolymerization of pigmented thiol-ene systems. Polymer 45 (2004) 2921.

CHAPTER III

HUMIDITY RESPONSIVE FILMS BASED ON DODECYL ACRYLATE MICROEMULSIONS

Introduction

From a previous study(1) we learned that it was feasible to form films from water-in-oil microemulsions. The films prepared from a reverse microemulsion based on an acrylate system exhibited a quasi-reversible response to the humidity of the environment. There are two characteristic parameters of interest to us, which determine the structure of the microemulsion: the amount of water in the system, and the water-to-surfactant ratio. In microemulsions, the water-to-surfactant ratio determines the size of water micelles, when the water content influences the packing of water domains. With this in mind, we wanted to determine the change in the films' appearance and humidity response as a function of these factors. We assumed that, if the aggregation of the aqueous phase (water and surfactant) was a result of phase separation, there would be significant differences in films with different compositions.

Microemulsions are thermodynamically stable mixtures of oil, water, and surfactant that consist of nanometer-sized micelles. The nanometer-sized micellar droplets are incapable of scattering visible light, and thus the mixtures are optically transparent. A surfactant is used to form a bridge between the two immiscible fluids, allowing the formation of a macroscopically homogeneous but microscopically heterogeneous system.(2) The spontaneous formation of a single-phase system from two otherwise immiscible components is a specific characteristic of microemulsions.

Microemulsions are thermodynamically stable because the surfactant sufficiently reduces the interfacial tension between the oil and water phases. This in turn, lowers the energy required to increase the surface area, allowing spontaneous droplet formation to occur.(3,4) Typically, microemulsions have an oil phase dispersed in a continuous aqueous phase. Reverse microemulsions are characterized by nanometer-sized drops of water distributed throughout an oil phase.(5-10) The most common water-in-oil (w/o) reverse microemulsions use the anionic surfactant sodium bis(2-ethylhexyl) sulfosuccinate (Aerosol-OT, AOT), which exhibits varied aqueous phase behavior, including the formation of: dense droplet, vesicular, lamellar, bicontinuous, cubic, hexagonal, and liquid crystalline.(11) AOT, with its double tail, forms stable reverse microemulsions (water in oil) with many different organic substances.(3)

Because of the stability and small droplet size of microemulsions, they are capable of producing coatings that overcome many of the shortcomings of traditional solvent-based processes.(12-14) Polymerization with use of a microemulsion is commonly used to produce high molecular weight polymer particles of small size (10-1000 nm) that are polymerized within the micelles of an aqueous or non-aqueous medium.(12,13) To date, investigations of polymerization involving inverse water-in-oil microemulsions have mainly been focused on synthesis of water-soluble monomers in an aqueous phase.(14)

In this chapter, we describe the formation of hydrophobic polymer films with an aqueous phase distributed throughout. The characterization of films prepared from microemulsions in which the oil phase contains dodecyl acrylate and 1,6-hexanediol diacrylate is presented. In particular, their response to humidity as a function of their water content is illustrated.

Experimental

Materials

The following chemicals were used as received: sodium bis(2-ethylhexyl) sulfosuccinate (AOT) (>96%) from Aldrich, dodecyl acrylate (DDA) (90%) from Sartomer, 1,6-hexanediol diacrylate (HDDA) (>99%) from Cytec Surface Specialties, and Irgacure 369 from Ciba Specialty Chemicals.

Preparation of Microemulsions

All microemulsions were prepared according to the following procedure. For the preparation of a microemulsion with 10% water relative to the monomers, 11.07 g (0.025 mol) of AOT was added to 50 mL of a monomer mixture, which consisted of 41.8 g (0.17 mol) of dodecyl acrylate (DDA) and 2.5 g (0.11 mol) of 1,6-hexanediol diacrylate (HDDA). The solution was mixed for up to 24 hours, or until all the AOT was fully dissolved. Next, deionized water was added (4.92 mL) to form microemulsions with a water-to-surfactant ratio (W) of 10. The composition of 5.7 wt % of crosslinker (HDDA) with respect to DDA was kept constant for most of the formulations; it will be indicated when a larger amount of crosslinker was added. Other microemulsions with different water contents were prepared in a similar manner. In each case, the amount of AOT was varied so that the water-to-surfactant ratio was kept constant to insure the same initial micellar size of the water droplets. Finally, a photoinitiator (Irgacure 369) was added, in the amounts necessary to achieve a 3 mM concentration relative to the monomers. The final compositions of the prepared microemulsions are listed in Table 3.1 and shown on Figure 3.1.

Polymerization of Films

The films were prepared between two glass microscope slides. It was decided that two thicknesses of films would be necessary: thinner films for visual observation under a microscope, and thicker films for the testing of other properties. The thicknesses of the formed films were determined either by placing a microscope cover glass (Fisher Scientific 12-540-B) placed between two glass slides (for thicker films), or by using 10-micron glass spacers (for thinner films). Samples were photopolymerized with a small handheld ultraviolet light source (365 nm) (light intensity 2.3 mW cm^{-2}). Exposure time was one minute on each side of the film. The films' names are derived from the amount of weight-percent water-content in relation to the monomers in the microemulsion they are formed from, for example, "25% film" refers to a film that was prepared from a microemulsion containing 25% water relative to the oil phase. Films used for experiments with UV-Vis were prepared between two quartz slides from ChemGlass (CGQ-0640-02); before the experiment was started one of the slides was removed.

Humidity Measurements

Humidity measurements were made using an Omegaette HH314 humidity/temperature meter. The following conditions were used in the experiments: *open*, *desiccator*, and *saturated* atmospheres. A condition designated as an *open* atmosphere refers to a lab atmosphere with a relative humidity ranging from 50% to 55%. The relative humidity for a *desiccator* atmosphere was achieved through use of a drying agent ($CaCl_2$) and was approximately 12%. A closed jar with few milliliters of water

created 100% relative humidity and is referred to as a *saturated* atmosphere. All experiments were carried out at ambient temperatures and pressure. Images of the films were taken with digital camera and processed with BTV Pro Carbon software.

Instruments and Methods

Thermal gravimetric measurements were obtained using a TGA 2050 Thermogravimetric Analyzer from TA Instruments. Thermal stability was evaluated through temperature ramp, and composition was evaluated using the quasi-isothermal (stepwise) method. Both of the methods were performed over a temperature range from room temperature (about 15° C) to 500° C, with a heating rate at 5° C min^{-1}. However, in the stepwise method, an isothermal method was applied whenever the sample's rate of weight change exceeded 0.5 % min^{-1}; the heat ramp was re-employed whenever the rate of weight change fell below 0.05 % min^{-1}.

The percentage transmission of 500 nm light was recorded on a UV-2401PC Shimadzu double-beam instrument in time-acquisition mode. ATR FT-IR spectra were obtained using a Nicolet Nexus 470 FT-IR spectrometer with Omnic computer software.

All measurements were repeated three times, with standard deviations of less than 10%.

Phase Diagrams

Samples of known AOT concentrations in the DDA/HDDA mixture were prepared. DI water was added in a step-wise manner until a clouding point was reached. The cloud point refers to turbid solutions, which do not become clear even after long and vigorous shaking and mixing. At cloud point the composition of a sample was

recalculated. This process resulted in defining the transition border shown in the tertiary phase diagram (Figure 3.1). The phase change as function of temperature was also evaluated. Microemulsions with W = 10 and water concentration between 0.5 – 20 wt% wrt monomers were prepared. The microemulsions were placed in jacketed beaker on a magnetic stir. The beaker was connected to a heating immersion circulator (Julabo4) filled with water. The microemulsions were observed between 2 to 70 °C. The sample was allowed to equilibrate at lower temperatures for at least 15 minutes, after which time the temperature was raised stepwise by five degrees. Table 3.3 contains the composition of the microemulsions tested.

Results and Discussion

Polymerization-induced aggregation

The microemulsions are optically transparent solutions. The solutions contained: dodecyl acrylate (DDA), and 1,6-hexanediol diacrylate (HDDA), a photoinitiator (Irgacure 369), AOT as the surfactant, and deionized water. The water content was at 5, 10, 15, 20, 25, and 30 wt % with respect to monomers. The compositions of the microemulsions used in this investigation are presented in Table 3.1. All of the microemulsions fall within the w/o microemulsion (phase L_2) as illustrated on Figure 3.1.

When the solutions were exposed to UV light, a photopolymerization occurred producing opaque films. This change in appearance indicates that the nanometer-sized drops of water in the microemulsions aggregate when the polymeric films are formed.

The optical clarity of the solutions is due to the size of formed water droplets, which are between 5 and 50 nm in radius. Even though the microemulsion formation and

the structure of the phases strongly depend on surfactant type; the main role of the surfactant is to reduce interfacial tension between oil and water. Reduction of the interfacial tensions, lowers the energy, which forces increase in the surface area. This leads to spontaneous dispersion of water or oil droplets.(15) The system becomes thermodynamically stable. With dispersion of one of the phases into very small droplets the configurational entropy changes ΔS_{conf} according to equation 3.1.

$$\Delta S_{conf} = -nk_B\left[\ln\phi + \frac{1-\phi}{\phi}\ln(1-\phi)\right] \qquad \text{Equation 3.1}$$

where n is the number of droplets of dispersed phase and ϕ is dispersed phase volume fraction.

If the change in interfacial area is ΔA, and the interfacial tension between phases 1 and 2 is γ_{12}, the free energy of droplets formation (dispersion ΔG_d) is then:

$$\Delta G_d = \Delta A\gamma_{12} - T\Delta S_{conf} \qquad \text{Equation 3.2}$$

Upon dispersion, the number of droplets increases and thus the configurational entropy becomes positive. The presence of surfactant in the system reduces the interfacial tension to a lower value, and the energy term $\Delta A\gamma_{12}$ becomes small and positive. These two parts result in a favorable negative change in free energy and the spontaneous microemulsification of the system. In other words, $\Delta A\gamma_{12} \leq T\Delta S_{conf}$. The interfacial tension needs to be very low, on the order of 10^{-2} to 10^{-4} mN m^{-1}.

The components of the microemulsion droplets rapidly exchange on the scale of milliseconds. They diffuse and undergo collisions, which if sufficiently forceful may rupture the surfactant layer. Therefore, the droplets are kinetically unstable. Still, when the droplets size is less then 50 nm, the tendency to coalesce will be balanced by an

energy barrier. Consequently, the system will remain dispersed and transparent for a long time in a kinetically stable emulsion.

When we consider thermodynamic changes that occur during the polymerization of the oil phase, the entropy term, ΔS, from equation 3.2 is reduced. This occurs because the number of possible combinations for the droplets' arrangements is reduced. When the monomer, in the liquid phase is present, there is a constant dynamic exchange between water droplets.(11) Thus, the entropy of mixing is large. Upon polymerization the monomers form solid phase, as with a polymer-dispersed liquid crystal,(16) and the entropy of mixing is greatly reduced. This results in an overall free energy increase. The only way to reduce free energy is by reduction of the surface area through the aggregation of the water droplets. We assume that the surface energy of the AOT-water interface between the polymer-monomer solution is the same as for the pure monomer. In another words, when the monomer polymerizes, the polymer molecules force the water droplets to combine.(17)

Xia et al. showed that adding a polymer to decane in a reverse microemulsion causeed phase separation.(18) However, in our systems, the organic phase itself is polymerizing. Therefore, the aggregation of the initially nanometer-sized water drops to domains larger than the wavelength of visible light, could be caused by the polymerization, which shifts the size distribution of the microemulsion to larger sizes. It is likely that both a perturbation of the microemulsion and phase separation are occurring simultaneously. The rapid polymerization could be trapping the water into large domains before complete phase separation occurs. This changes the morphology of the system.

Small Angle Neutron Scattering studies were performed to determine the morphology and will be discussed in later parts of this work.

Immediately after the polymerization, the films were opaque, which can be seen in part (a) of Figures 3.2, 3.3, and 3.4. The films formed from microemulsion with lower amounts of water (5% and 10% films) were more transparent then the ones formed with higher water contents. It would be expected that with higher water amounts in the microemulsions, the aggregation forces more water in each pool in the polymerized system. However, the microemulsions were designed to have the same W of 10 (W=[water]/[AOT]). Kotlarchyk at el.(19) showed for series of different oils, that there is a linear correlation between the water-to-surfactant ratio and the radius of the micelles in the microemulsions. Thus, the microemulsions with the same W should have micelles with the same size distribution. Similarly, one would expect to see the same size aggregates formed in the polymerized films. The difference in transparency of films seen in part (a) of Figures 3.2, 3.3 and 3.4, can be understood through the fact that with higher water content (higher concentration of AOT to sustain W = 10) there is less polymerizable oil phase. For the 5% film the monomer concentration is 85 wt%, which decreases to 45 wt% for the 30% film. With this change in composition, the continuous polymer matrix is more frequently disturbed by the aqueous phase (water and AOT). As it will be explained later, the excess of AOT places itself not only on the outside of water pools but also within the polymer matrix.

Opacity as a Function of Humidity

Upon polymerization the films have an opaque, milky-white appearance (Figure 3.2a). When the polymerized films were exposed to environments with humidity less

than 100%, they began to lose opacity and eventually became transparent (see Figure 3.2b and 3.3b). Films exposed to the open atmosphere and kept in the desiccator became equally transparent. However, if the films were kept in the saturated atmosphere they absorbed water. As demonstrated for the films in Figure 3.4b, the opacity actually exceeds that of the film right after polymerization. The pictures in Figure 3.4b show films after 40-hour exposure to saturated atmosphere, which allows demonstration in the difference in opacity. It needs to be stated that the films start gaining water even after short exposure to saturated atmosphere; however, it is difficult to discern the distinction in opacity on the picture of the films exposed to one-hour saturation.

The change in opacity of the films was followed by the change in transmittance of visible light (Figure 3.5). The films were prepared in a controlled manner, with the same thickness and time of polymerization. The films were placed in the spectrometer immediately after polymerization and transmittance in the open atmosphere was recorded as a function of time. At zero time the films showed significant difference in the transmittance (Figure 3.5), which can also be seen as variation in opacity in Figure 3.2a. For example, the 10% film is transparent (44% transmittance) whereas the 25% film has a transmittance of about 1%. This film also shows an induction period, where the transmittance does not change for several minutes. This variation of the two films' transmittances has to do with different water amounts and possibly different water aggregation sizes. The films reach a plateau in transmittance after about 120 minutes; however, they still showed different final transmittances, which relates to the films initial compositions. When all films prepared from all microemulsions are compared, they demonstrate trends falling in logical transmittance response, meaning the film with the

highest water content 30% film exhibited the lowest transmittances (0.6% at the beginning and 65% at the end), and the 5% film had the highest transmittance (right after polymerization 74 %, and a final value of 88%). All other films fall in-between these limits. In addition, the 30% film showed the longest induction period, where the transmittance changed very little over about 20 minutes.

Thermal gravimetric analysis (TGA) plots presented in Figure 3.6 confirm that the transparent films from the desiccator and open atmospheres still contained a significant amount of water. For example, immediately after polymerization the 25% film (Figure 3.2a) showed 11% water content (Figure 3.6, plot c). The TGA plot of the same film exposed for 40 hours in the open atmosphere indicated that there was still 2% water remaining (Figure 3.6, plot a). The same result was obtained for the film kept in the desiccator atmosphere for 40 hours (Figure 3.6, plot b). It was also found that the film exposed to the saturated atmosphere gained water. Immediately after polymerization the 25% film was exposed to the saturated atmosphere for 40 hours (Figure 3.4b). This film had gained water as shown in plot d in Figure 3.6; the mass fraction of water increased from 11% to about 19%.

Mass Loss of Water as a Function of Water Content

It has been shown that in reverse (w/o) microemulsions, water is present in three solubilized states.(20) Below $W < 4$, water associates with the ionic head groups of the surfactant. Swollen micelles are formed when W is between 4 and 12. In that state the extra water hydrogen bonds to the hydrated head groups of the surfactant. Finally, when $W > 12$ the excess water builds up in the core of the micelles and is referred to as *bulk* water. Thus, we propose that in our films, after they become transparent, the water left in

the films is associated with the surfactant's ionic head groups. Interestingly, the films with higher initial water content (25 and 30 %) lose water with higher rates than films with lower initial water content.

To further investigate the loss of water with time, films containing different amounts of water, but with the same water-to-AOT ratio (W = 10), were weighed immediately after photopolymerization and exposed to the atmosphere. Each film was then weighed as a function of time to construct a graph of mass percent of water lost as a function of time at 25 °C (Figure 3.7). The films became transparent within 80 minutes. The data demonstrate that the films lose up to 80 % of the total water present within 80 minutes, suggesting that a significant amount of water exists unbound to the surfactant and is able to leave the film. However, there is trapped water strongly associated with the surfactant. For example, the film prepared from 25% microemulsion lost 77 % of its water. The residual 23 % of water represents 2.2 % of total mass of sample, which is seen in the TGA analysis of the transparent 25 % films (Figure 3.6, traces a and b).

In addition, there is a relationship between the initial water content and the fraction of water lost (Figure 3.8). Even though the microemulsions were prepared with the same water-to-surfactant ratio we believe that polymerization-induced aggregation forms aggregates with different water content. The water leaving the film at room temperature is the *free* water of the droplets, which is loosely bound to the AOT. The films initially containing more water must form water aggregates with larger fractions of such water. It also shows that 20 to 40 % of the total water stays bound to the surfactant.

Quasi-Reversible Hydration

Films prepared from the microemulsions were allowed to "dry" in the *open* atmosphere for 48 hours followed by an exposure to the *saturated* atmosphere for various times. The appearance of films changed from transparent to opaque as they regained water (Figure 3.2). The cyclic process of drying and re-hydrating exhibited in Figure 3.2 and 3.3 can be performed many times.

Figure 3.9 shows plots of the re-saturation process for the 25% film. When the transmittance of the film had reached a plateau (at least 180 minutes), the film was removed from the spectrometer and placed in the *saturated* atmosphere for different periods of time (10, 20, 30 or 80 minutes). The sample was then removed from the *saturated* atmosphere and immediately repositioned in the spectrometer. The change in transmittance was then recorded in the *open* atmosphere as a function of time. The re-saturated films show the initial transmittance values of 56 %, 49 %, 44 %, and 36 % corresponding to times in the *saturated* environment of 10, 20, 30, and 80 minutes, respectively. As expected, when the sample was exposed to the longest saturation time it became the most opaque with an initial transmittance of only 36 % and exhibited the longest time to reach the final transmittance (~70 %). In each case, after the film was removed from the saturated atmosphere and placed in the spectrometer (i. e., the open environment) the film eventually attained a transmittance of 70 %.

Presence of Water

Infrared spectra of the films under several conditions were recorded to aid the interpretation of the results from the previous section. IR spectra were recorded for an

opaque film immediately after polymerization prepared from the microemulsion with 10% water, for the same film in a transparent state after 24 hours of exposure to the open atmosphere, and for a film prepared from the same microemulsion that was allowed to completely dry in the desiccator (Figure 3.10). The decrease in the peak at 3500 cm^{-1} indicates that the amount of water in the initially hydrated film decreased with time. The most water is present in the freshly photocured film (Figure 3.10, trace a) as demonstrated by the peak in the water region with the highest absorbance. When the film had been allowed to dry for a very long time, the IR spectrum for the film shows no water present (Figure 3.10, trace c). However, if the film was allowed to become transparent, the water peak in IR spectrum (Figure 3.10, trace b) was smaller than for the freshly polymerized, but still shows the presence of water in the film, as confirmed by TGA (Figure 3.6, plot a and b). Such films could be re-saturated.

Determination of Water Content by TGA

We attempted to determine amounts of water in films prepared from microemulsions containing different water contents ranging from 5 to 30 % by TGA. Samples were analyzed immediately after polymerization to minimize evaporation of water from the films. First, a dynamic temperature ramp with heating rate of 5 °C/min from room temperature to 500 °C was used. The resulting mass loss-versus-temperature plots are presented in Figure 3.11. The results in Figure 3.11 show that water is present in each of the films after the polymerization. The trends are consistent with the initial composition of the microemulsions. The water loss occurs from the starting temperature to above 100° C. Unfortunately, the determination of the water content was complicated because at about 130° C the unreacted monomers leave the film (confirmed by TGA

analysis of a pure film prepared from 5%HDDA/95%DDA mixture Figure 3.13). For films with higher water contents of 25 % and 30 % (plots e and f in Figure 3.10, respectively), these two events overlap without giving a well-defined plateau for water loss. In addition, kinetic effects associated with the heating rate make the evaluation of the precise amount of water difficult. Changing the heating rate to 1 °C min^{-1} shifted the final plateau to 150 °C (Figure 3.12) from 200 °C for the sample heated at 5 °C min^{-1}. For the lower heating rate, water leaves at a very low temperature (below 80 °C); however, the unreacted monomer evaporation occurs also at lower temperatures and extends over a 40 degree range (between 80 and 120° C) possibly overlapping with the remaining water evaporation.

Next, in each of the films, the surfactant decomposition occurs. In addition, for scans at 1° C min^{-1} the decomposition of sodium bis(2-ethylhexyl) sulfosuccinate (AOT) occurred at lower temperatures. For example, for the freshly polymerized films from 25% microemulsion the AOT decomposes at 198° C for 1° C min^{-1} in contrast to 229 ° C for a heating rate of 5° C min^{-1}.

To evaluate the origin of the weight loss at temperatures greater than 350° C, a film of 5%HDDA/95%DDA (Figure 3.13) was tested. For a pure film without surfactant or water, the network decomposes at 380 °C. It is clear from the results in Figure 3.10 that depending on the water content, the onset of the network decomposition occurs at different temperatures. This may be due to acrylate hydrolysis or a change in network structure thus morphology.

In a second approach we used quasi-isothermal (stepwise) TGA method, which allows determination of components in a more controlled way. Again, we used the temperature range from room temperature (about 15° C) to 500° C, and the heating rate of 5° C min^{-1}. However, in the stepwise method whenever the sample's rate of weight change exceeded 0.5 % min^{-1} an isothermal heating is applied. Whenever the rate of weight change falls below 0.05 % min^{-1}, the heat ramp is re-employed. As can be seen in Figure 3.14, the degradation steps are clearly visualized for each film. The water leaves the films at low temperature, below 50 ° C, and the mass reaches a plateau. When the temperature reaches 130 ° C additional decrease can be seen, which appears as an actual step for film formed from 30% microemulsion. As mentioned above, this mass decrease is due to evaporation of unreacted monomers (Figure 3.15). The composition determined from the stepwise method is summarized in Table 3.2. The amounts of water in the films right after polymerization, although they follow a logical trend, do not reflect the actual composition of the microemulsions. In addition, large amounts of unreacted monomers can be seen leaving the films (from 3 to 13 total wt%). This result is surprising since a semi-quantitative test was carried out (Figure 3.16) to determine the required time for full conversion. From the TGA decomposition traces in the Figure 3.16, the lack of monomer-leaving-step for the film prepared at 90-second-exposure we concluded, that 90 seconds was a sufficient time for film formation.

Higher Crosslinker Content

Microemulsions with different monomer composition were prepared in order to improve the mechanical properties of the films. The compositions were 10:90, 15:85, 30:70, 0:100 monoacrylate (DDA) to diacrylate (HDDA). The films with 10:90

composition exhibited similar behavior to the 5:95 films described above. However, when more than 15 vol% of crosslinker was added, the films were in a quasi-stable state and became white upon mechanical disturbance. The white color remained even when water was removed from the film. It was recognized that the persistent white color is caused by surfactant crystallization in the polymerized medium (Figure 3.17).

Microemulsion Phase Diagram

The set of microemulsions with increasing water and surfactant amount was tested for thermal stability. The compositions of these are presented in Table 3.3. We expected to observe phase separation at lower temperatures and at temperatures higher than 60 °C due to differences in surfactant layer rigidity as described in chapter 2. The microemulsions were prepared at room temperatures (close to 25 °C) and placed in a jacketed beaker which was stirred magnetically. Next, the temperature was lowered to 2 °C, at which the microemulsion was kept for at least 15 minutes. The temperature was increased every 5 degrees and microemulsion was allowed to reach each temperature and remained at it for approximately 10 minutes. For all microemulsions listed in Table 3.4 there was no phase separation observed.

Evaluation of Diffusion Coefficient, D

The transport rate of diffusants is usually expressed in terms of permeability, P, or a diffusion coefficient, D. The permeability is related to the diffusion coefficient and equilibrium solubility, S:

$$P = S \cdot D \qquad \text{Equation 3.3}$$

One of the simplest methods for the determination of the diffusion coefficient is the weighing method.(21,22) The weight gain or loss of a sample of known shape and size, kept in an atmosphere of constant diffusant vapor pressure, is measured with time. The diffusion coefficient can be then calculated from the weight variation of the sample as shown in the equation:

$$D = \frac{\pi}{16}\left[\frac{d\left(\frac{M_t}{M_\infty}\right)}{d\left(\frac{\sqrt{t}}{l}\right)}\right]^2 \qquad \text{Equation 3.4}$$

The diffusion coefficients of the water molecules can be determined from the initial slope of M_t/M_∞ as a function of $t^{1/2}/l$ (Figure 3.18, 3.19, and 3.20). The set of diffusion coefficients for water molecules for the films prepared from microemulsions with increasing water content but constant water-to-surfactant ratio are summarized in Tables 3.4, 3.5 and 3.6. There were three sets of microemulsions with values of W equal to 5, 10, and 13. The values for the water diffusion coefficient are on the similar value scale found in the literature for hydrophobic polymer networks.(21) As expected, the films prepared with larger water content (25%, 30%) show larger values for the diffusion coefficient. This confirms the hypothesis about the presence of *free* water in these films.

In addition, the films prepared from microemulsions with W = 13, thus the largest micellar size, have the largest values of diffusion coefficient for corresponding water contents of 15, 20, and 25%. The amount of the surfactant that is present in these films forces formation of bigger domains in the polymerized films, than is the case for the films formed from microemulsions with W = 5. The films from microemulsions with the

smallest micellar size (W = 5) contain a large amount of the surfactant in the polymer network, thus are able to form smaller water domains. From this simple experiment we can conclude that, as predicted, the initial micellar size has an influence on the water domains in the polymerized films. Further discussion and a conformation of this finding will be elaborated on in Chapter 4.

Conclusions

Films prepared from reversed microemulsions were characterized. The organic phase consisted of dodecyl acrylate and 1,6-hexanediol diacrylate with water drops in a separate phase stabilized with the anionic surfactant sodium bis(2-ethylhexyl) sulfosuccinate (Aerosol-OT, AOT). The solution before polymerization was clear, but upon photopolymerization the films formed were opaque. The opacity is a result of water droplet aggregation from nano-sized micelles in the microemulsion into micron-sized aggregates in the film.

The films become clear upon exposure to less than 100% relative humidity, and the films could be re-saturated by exposure to 100% humidity. Even when the film is clear, water remains in the film for an extended period of time. This suggests that water exists in two states. In the first state *bulk* or *free* water is loosely bound and leaves the film at room temperature. In the second state, water is bound to the surfactant's head groups. The AOT-bound water represents 20 to 50 % of the initial water. The amount of bulk water is related to the initial composition of the microemulsion; the highest amount is found in the films formed from microemulsions with the highest water content.

Table 3.1. Compositions of microemulsions used for the formation of films

Water concentration wrt monomer (%)		**5**	**10**	**15**	**20**	**25**	**30**
Weight composition	**Water (%)**	4.51	8.13	11.35	14.26	16.93	19.52
	AOT (%)	10.57	18.35	24.27	28.75	32.26	34.90
	DDA (%)	80.01	69.26	60.57	53.68	47.83	42.89
	HDDA (%)	4.84	4.17	3.73	3.25	2.92	2.64
	Initiator (%)	0.06	0.09	0.08	0.07	0.06	0.05

Table 3.2. Films' compositions determined through Stepwise Isothermal TGA

Amount of water in microemulsion (% wrt monomers)	Water (wt%) in microemulsion	Water (wt%)	Unreacted monomers (wt%)	AOT (wt%)	Network (wt%)
5%	4.51	4.47	2.64	11.93	74.37
10%	8.13	6.23	7	19.7	61.95
15%	11.35	5.87	9.76	23.1	55.22
20%	14.26	8.19	8.41	27.37	49.26
25%	16.93	9.7	7.7	29.82	45.37
30%	19.52	14.4	13.16	31.51	33.63

Table 3.3. Compositions of microemulsions tested for thermal stability

DDA (wt %)	HDDA (wt %)	AOT (wt %)	Water (wt %)	% Water wrt DDA+HDDA	Calculated W
92.68	5.60	1.22	0.49	0.50	9.9
91.12	5.50	2.41	0.97	0.99	9.9
88.06	5.32	4.71	1.90	2.00	9.9
83.78	5.06	7.96	3.20	3.48	9.9
79.75	4.82	10.99	4.45	5.00	10.0
74.78	4.52	14.74	5.96	7.00	10.0
68.06	4.11	19.81	8.02	10.00	10.0
64.02	3.87	22.86	9.25	11.99	9.9
58.47	3.53	27.03	10.97	15.04	10.0
50.58	3.06	33.12	13.25	19.81	9.9

Table 3.4. Diffusion coefficients of water from films prepared from microemulsions with W=10

Film	Slope* ($cm\ s^{-1/2}$)	D* ($cm^2\ s^{-1}$)	D** ($cm^2\ s^{-1}$)
5%	-1.8×10^{-4}	3.4×10^{-8}	5.6×10^{-8}
10%	-1.8×10^{-4}	3.3×10^{-8}	7.5×10^{-8}
15%	-3.9×10^{-4}	1.5×10^{-7}	2.1×10^{-7}
20%	-4.6×10^{-4}	2.2×10^{-7}	6.4×10^{-7}
25%	-7.1×10^{-4}	5.0×10^{-7}	8.9×10^{-7}
30%	-9.2×10^{-4}	8.5×10^{-7}	1.5×10^{-6}

* Data from experiment presented in Figure 3.18

**Average value of D for four runs experimental error $\approx \pm 0.7 \times 10^{-8}$

Table 3.5. Diffusion coefficients of water from films prepared from microemulsions with W=5

Film	**Slope*** **($cm\ s^{-1/2}$)**	**D*** **($cm^2\ s^{-1}$)**
5%	-1.5×10^{-4}	2.3×10^{-8}
10%	-2.6×10^{-4}	6.8×10^{-8}
15%	-4.1×10^{-4}	1.7×10^{-7}
20%	-6.0×10^{-4}	3.5×10^{-7}
25%	-5.7×10^{-4}	3.2×10^{-7}

* Data from experiment presented in Figure 3.19

Table 3.6. Diffusion coefficients of water from films prepared from microemulsions with W=13

Film	**Slope*** **(cm $s^{-½}$)**	**D*** **(cm^2 s^{-1})**
5%	-1.6×10^{-4}	2.7×10^{-8}
10%	-2.4×10^{-4}	5.8×10^{-8}
15%	-6.4×10^{-4}	4.1×10^{-7}
20%	-7.5×10^{-4}	5.6×10^{-7}
25%	-1.1×10^{-3}	1.2×10^{-6}

* Data from experiment presented in Figure 3.20

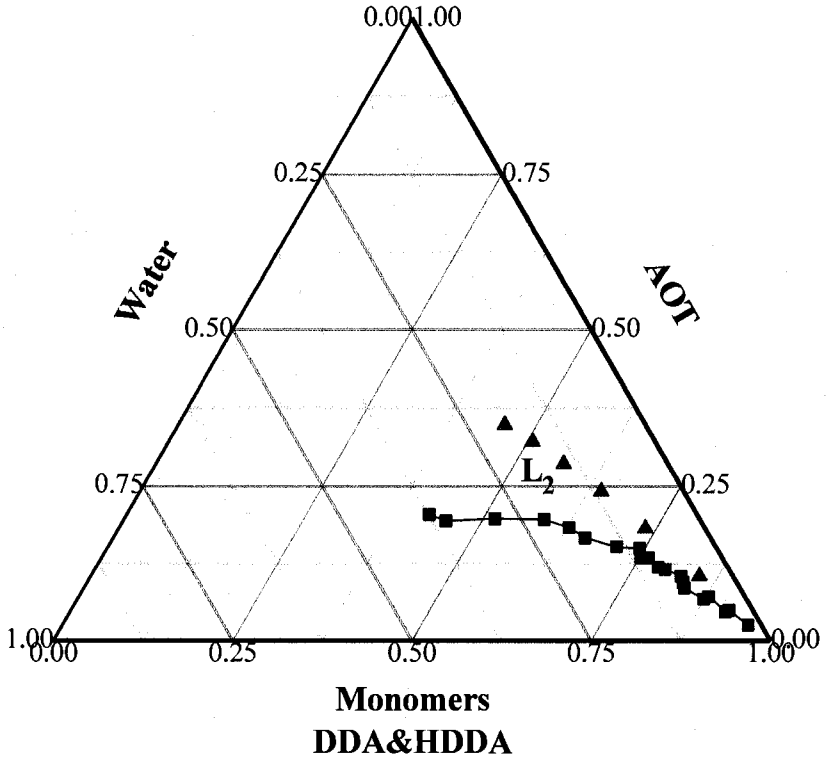

Figure 3.1. Ternary phase diagram of Water/AOT/Monomers. (■) indicates cloud points above which phase L_2 represents a reverse microemulsion region on the diagram, (▲) the microemulsions used in this research fall within L_2 phase.

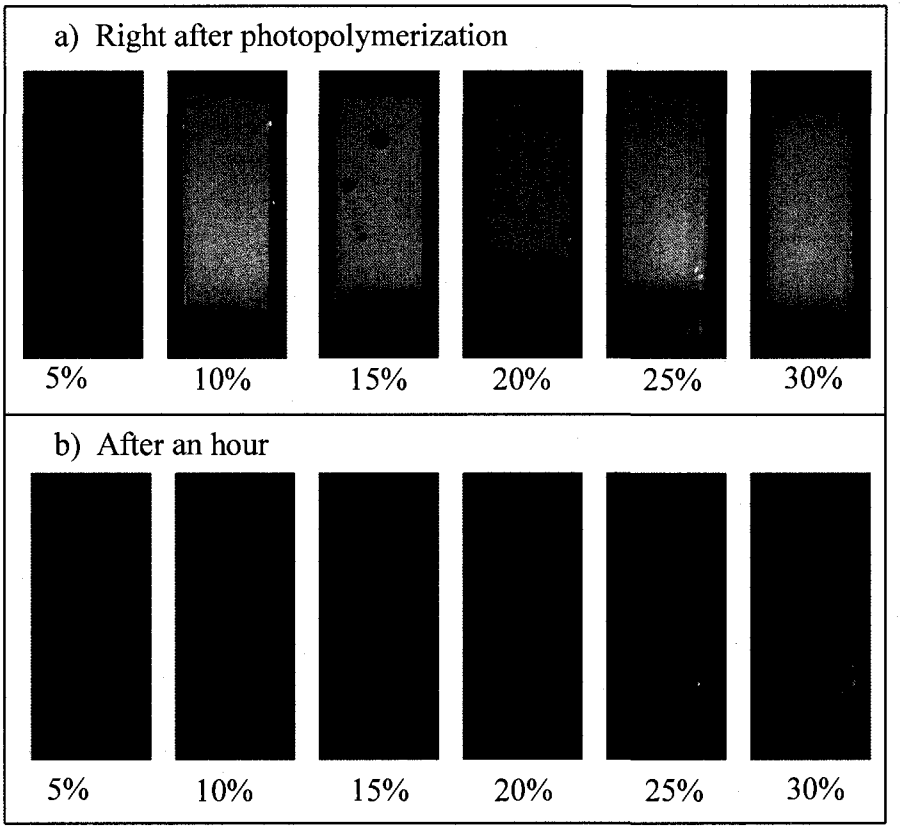

Figure 3.2. Pictorial illustrations of the films prepared from microemulsions with varying amounts of water relative to monomers (indicated in the figure) and W = 10. (a) the opaque films immediately after polymerization; (b) the same films after 1-hour exposure to the *open* atmosphere.

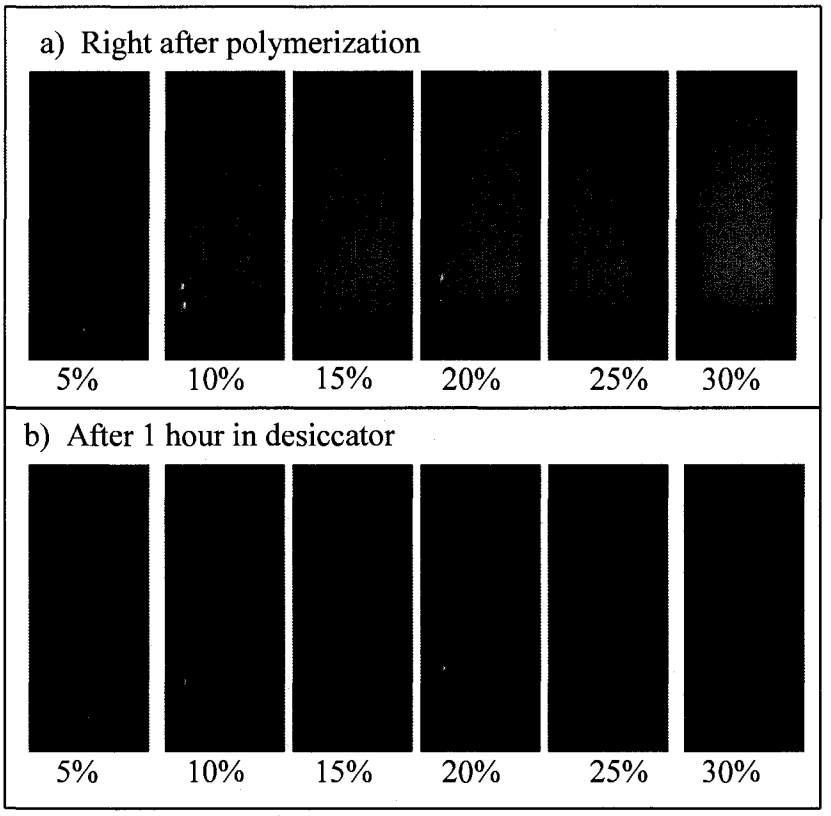

Figure 3.3. Pictorial illustrations of the films prepared from microemulsions with varying amounts of water relative to monomers (indicated in the figure) and W = 10. (a) the opaque films immediately after polymerization; (b) the same films after 1-hour exposure to the *dry* atmosphere of the desiccator.

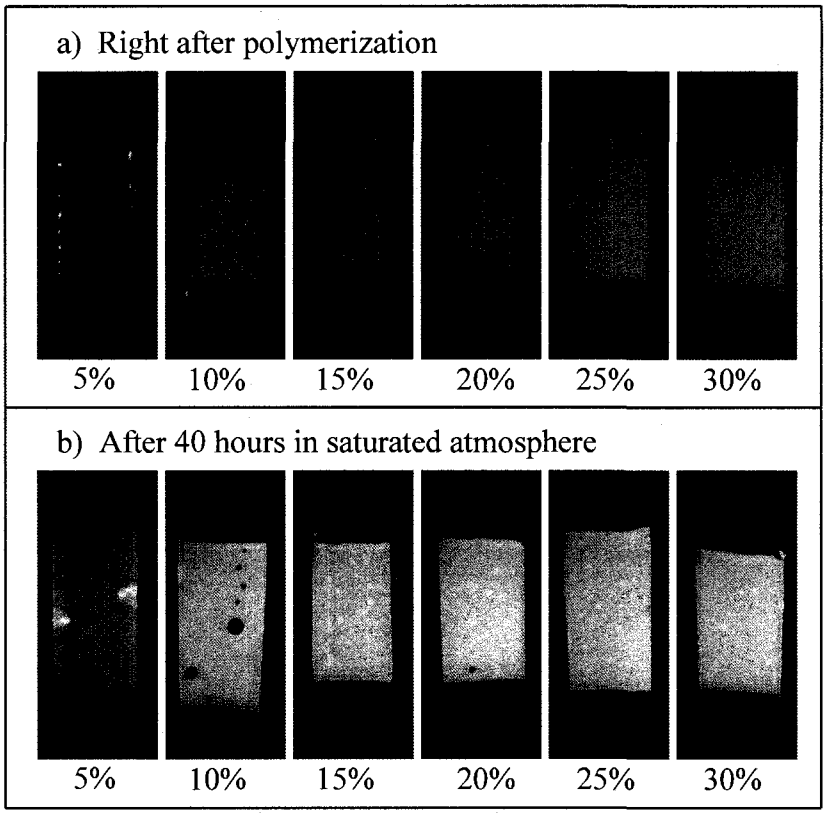

Figure 3.4. Pictorial illustrations of the films prepared from microemulsions with varying amounts of water relative to monomers (indicated in the figure) and W = 10. (a) the opaque films immediately after polymerization; (b) the same films after 40-hour exposure to the *saturated* atmosphere.

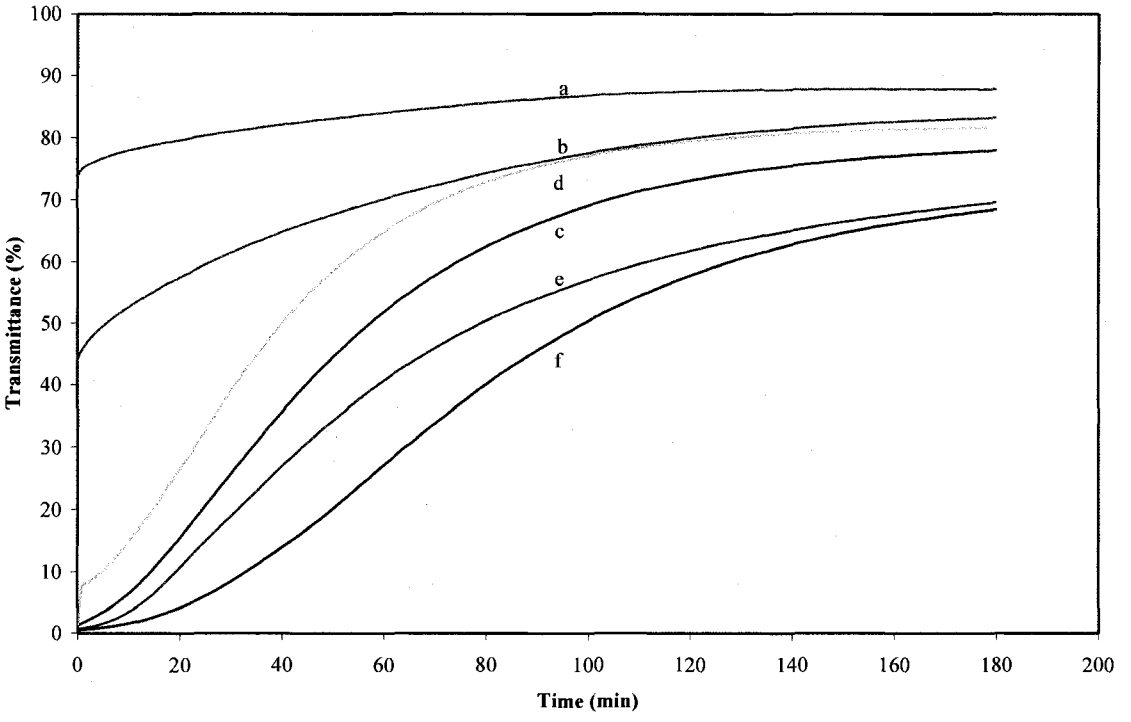

Figure 3.5. Change in transmittance of the light at 500 nm wavelength after polymerization for films prepared from (a) 5%, (b) 10%, (c) 15%, (d) 20%, (e) 25%, and (f) 30% microemulsions in the *open* atmosphere.

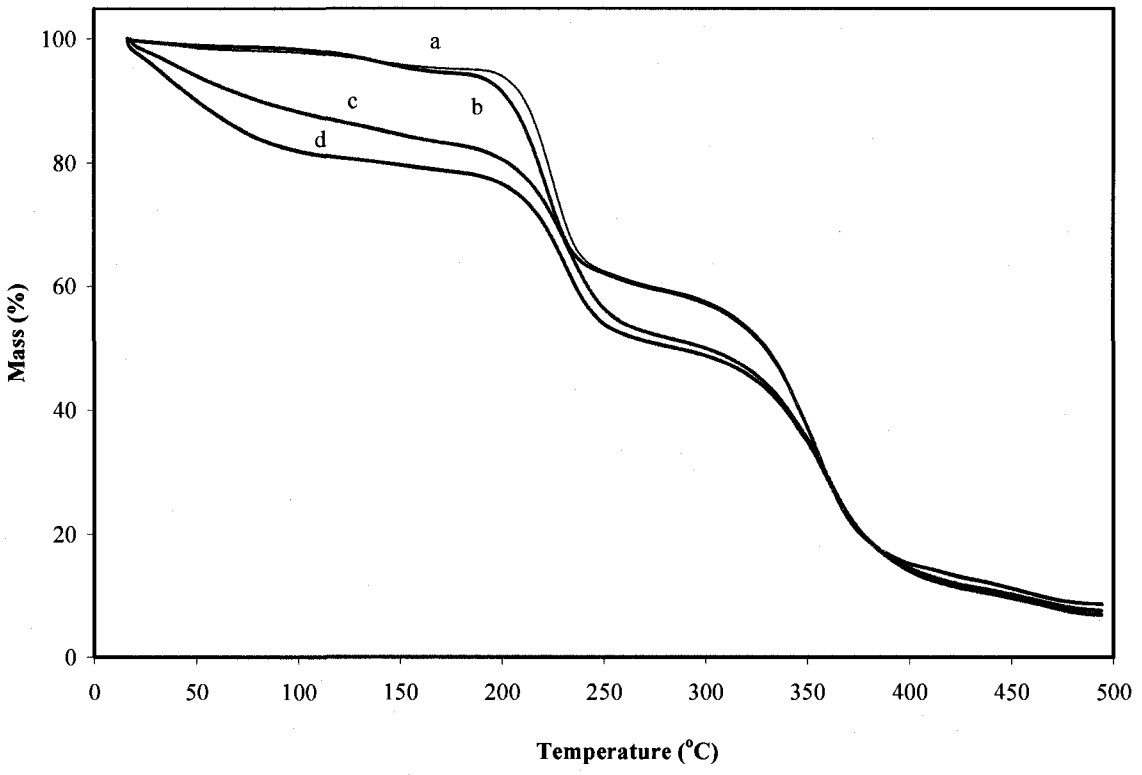

Figure 3.6. TGA analysis of films kept at different humidity conditions and prepared from the microemulsion with 25 % of water content relative to monomers (water is 18 % relative to total mass); (a) film exposed to the *open* atmosphere for 40 hours, (b) film kept in the desiccator for 40 hours, (c) film immediately after polymerization, (d) film kept in the *saturated* atmosphere for 40 h.

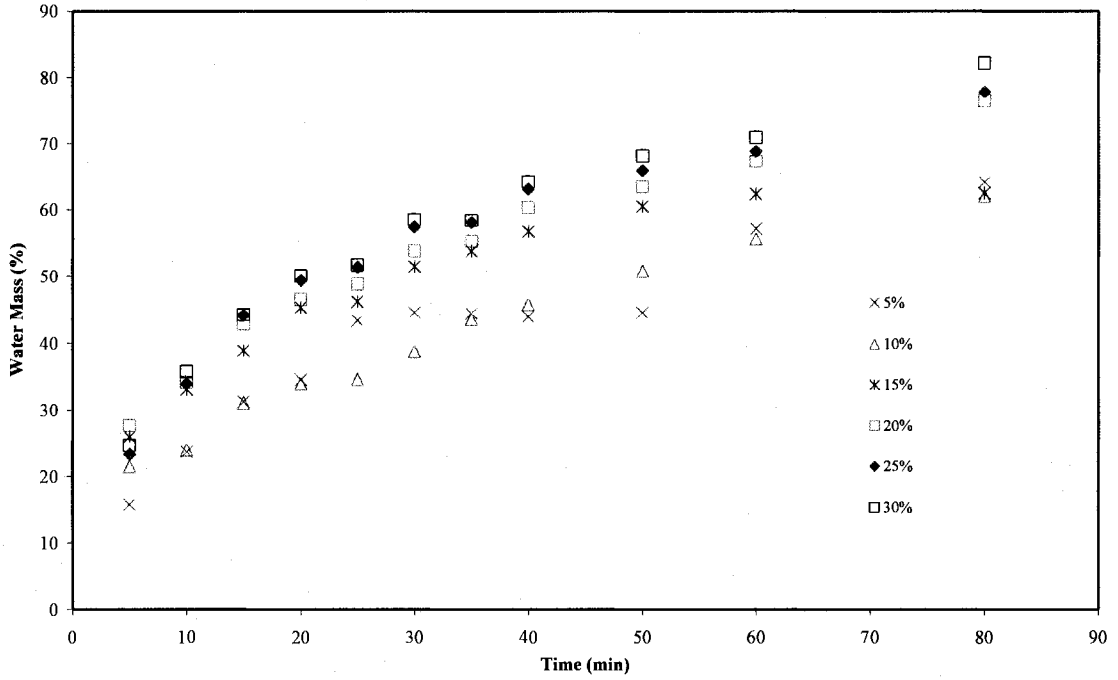

Figure 3.7. Loss of water as a function of time for films at room temperature and in the *open* atmosphere with 50 - 55% relative humidity.

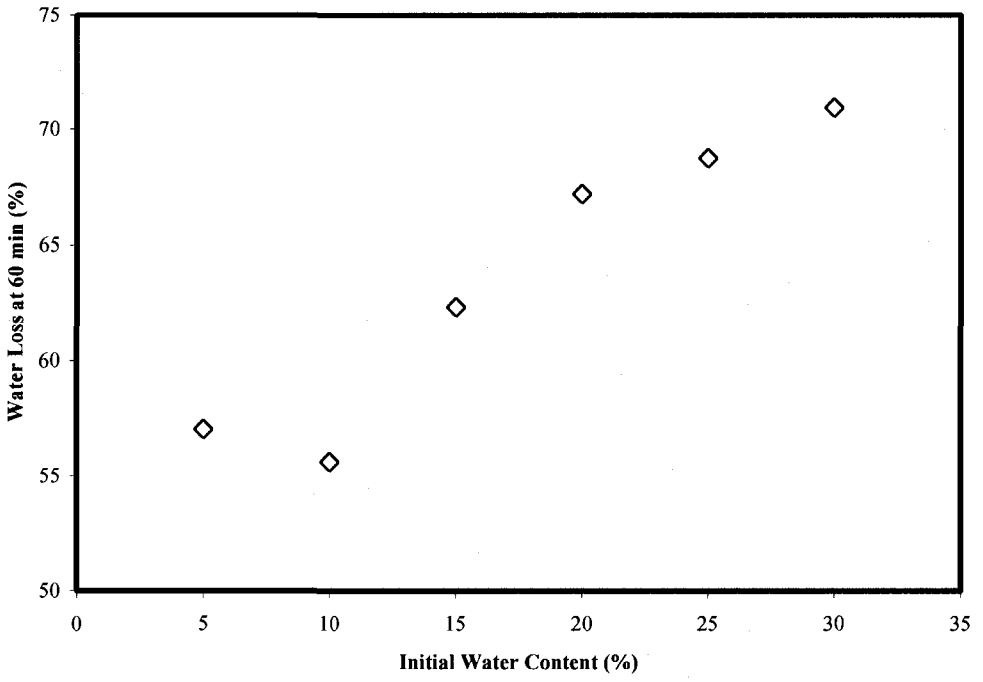

Figure 3.8. Mass fraction of water loss as a function of the initial percentage of water at room temperature after 60 minutes.

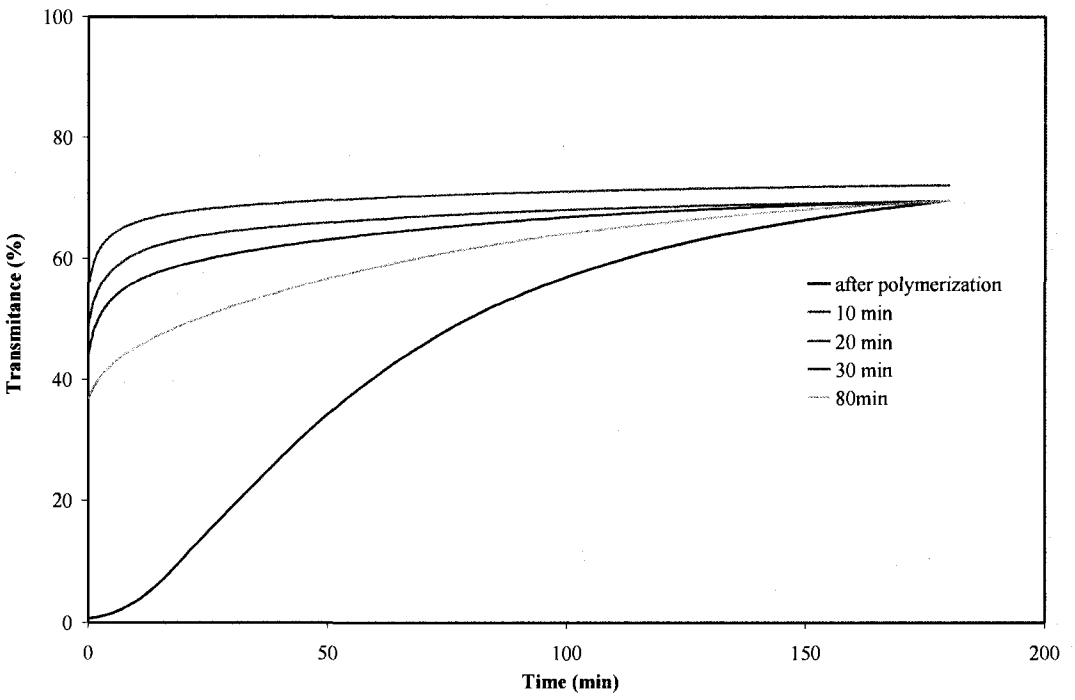

Figure 3.9. Change in transmittance of the light at 500 nm wavelength for 25% film: (e) right after polymerization and after exposure to different times in the *saturated* atmosphere: (a) 10 min, (b) 20 min, (c) 30 min, and (d) 80 min.

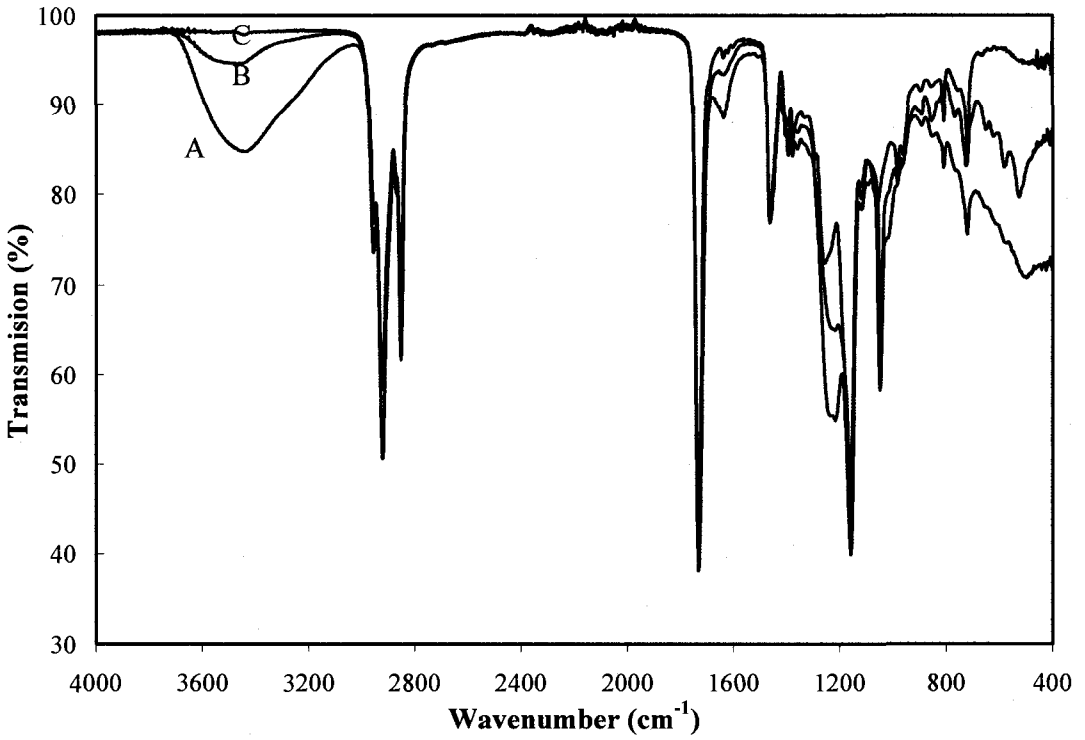

Figure 3.10. IR spectra comparing opaque and transparent films prepared from microemulsion with 10% water:

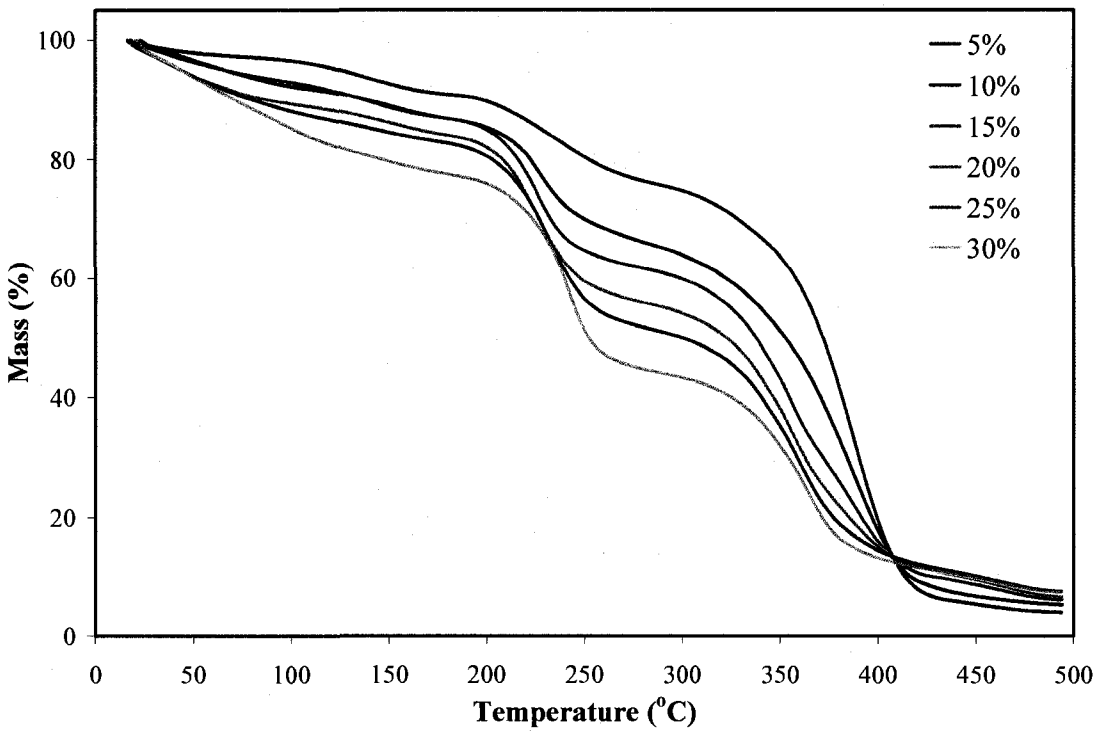

Figure 3.11. TGA of films prepared from microemulsions with different water content but the same water-to-AOT ratios; each ramped at 5°C/min from room temperature to 500 °C. Percent water in the initial microemulsions (with respect to monomers) shown on the figure.

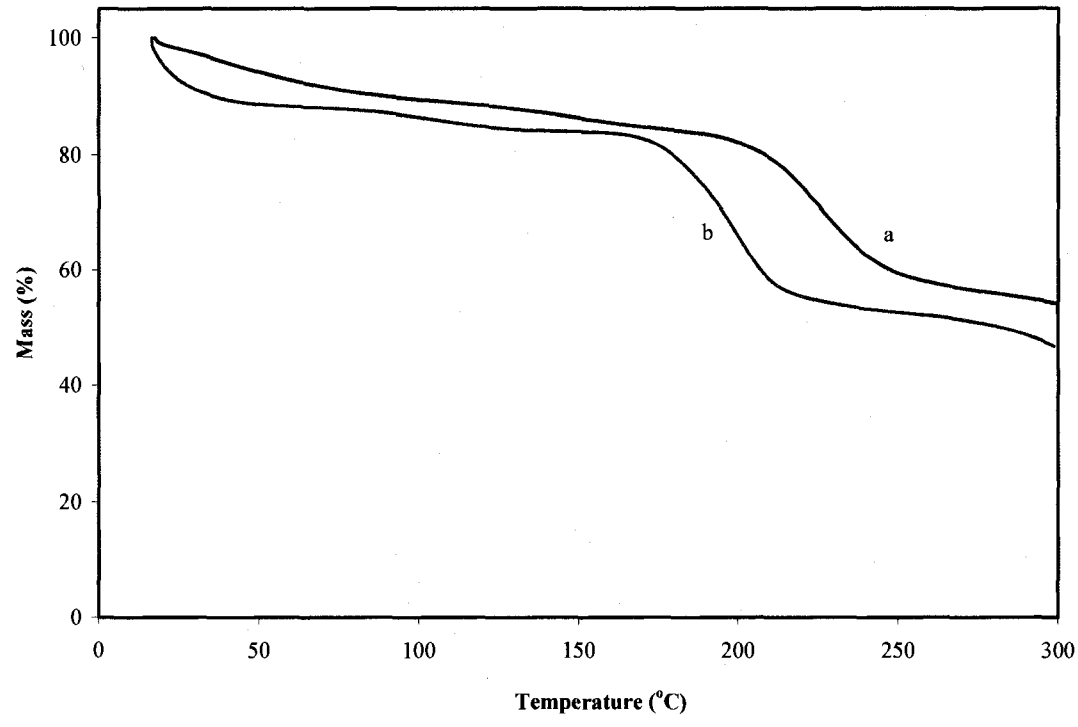

Figure 3.12. TGA of films prepared from microemulsion with 25% water (wrt monomers) at different heating rates from room temperature to 300 °C; (a) 5 °C/min, (b) 1 °C/min.

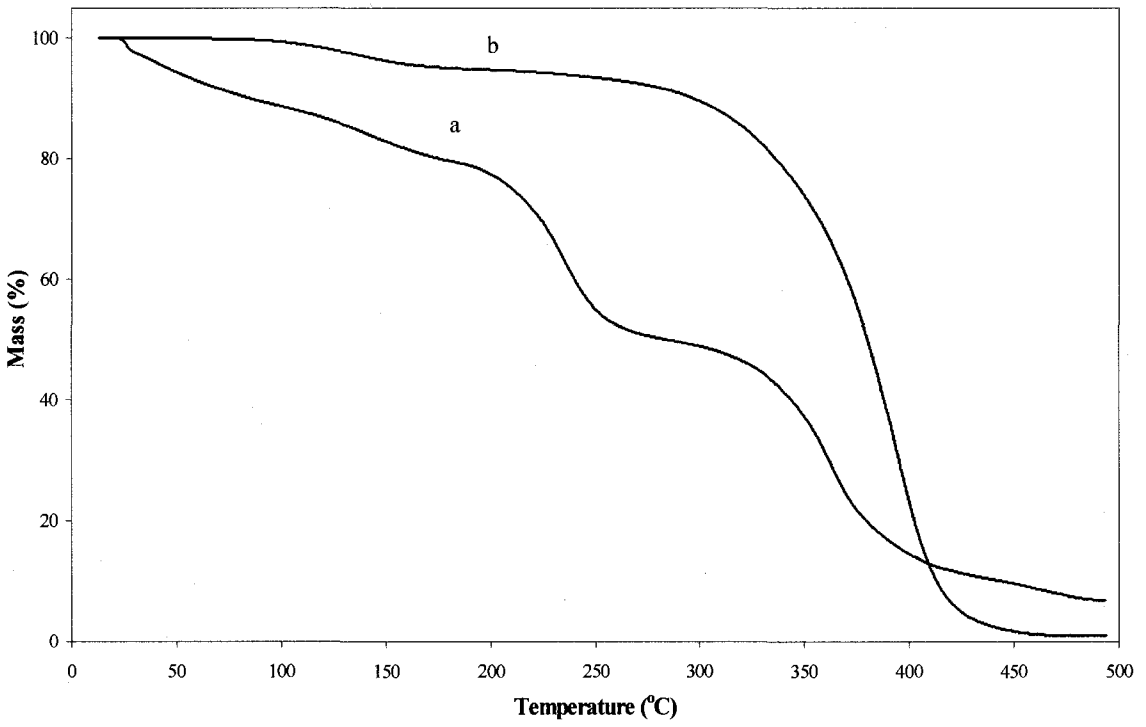

Figure 3.13. TGA of two films; (a) 25% film immediately after polymerization, (b) film prepared only from the monomers (DDA and HDDA, 0 % of water).

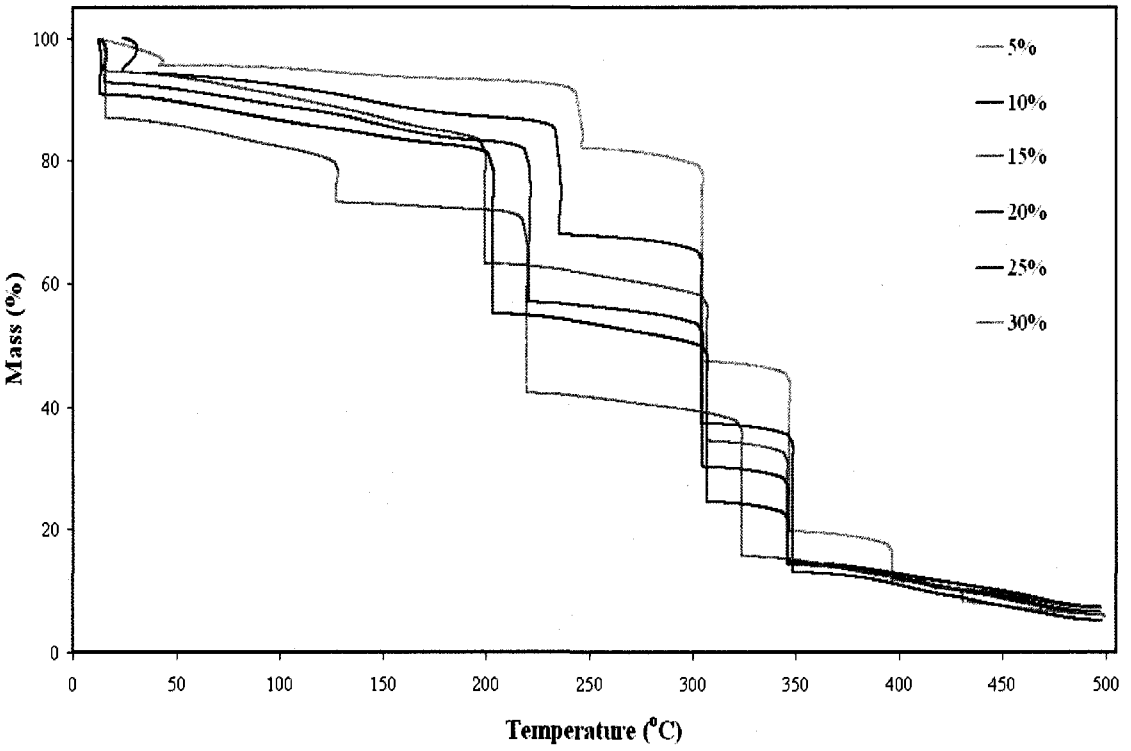

Figure 3.14. Stepwise Isothermal TGA analysis of films right after polymerization.

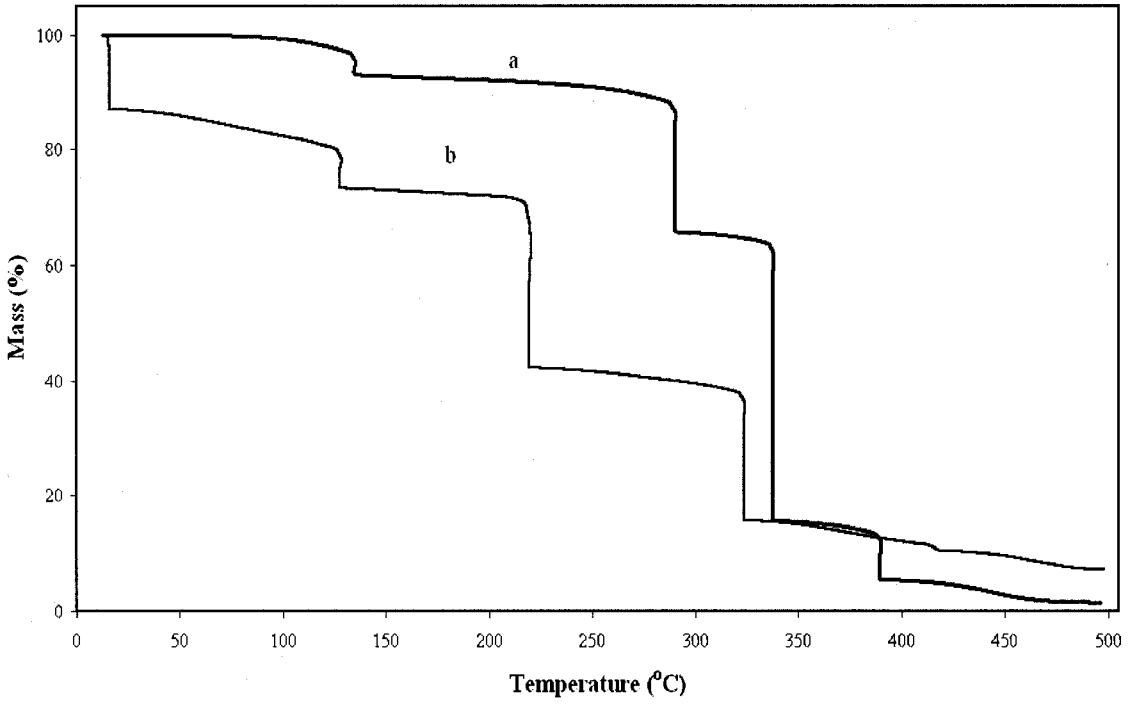

Figure 3.15. Stepwise Isothermal TGA analysis of two films right after polymerization (a) film photopolymerized from DDA crosslinked with 5.7 wt% HDDA, (b) film prepared form microemulsion design to have 30 wt % of water wrt monomers (W = 10).

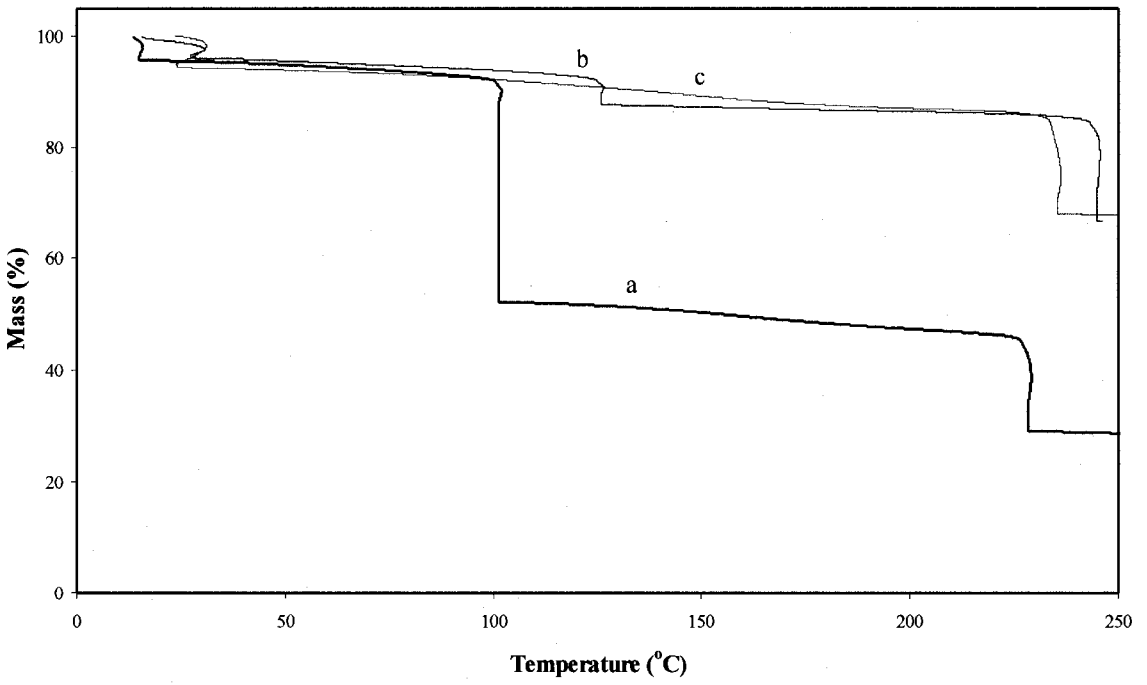

Figure 3.16. Stepwise TGA analysis of film prepared from 10% microemulsion polymerized under different exposures times: (a) 30 sec, (b) 60 sec, and (c) 90 sec.

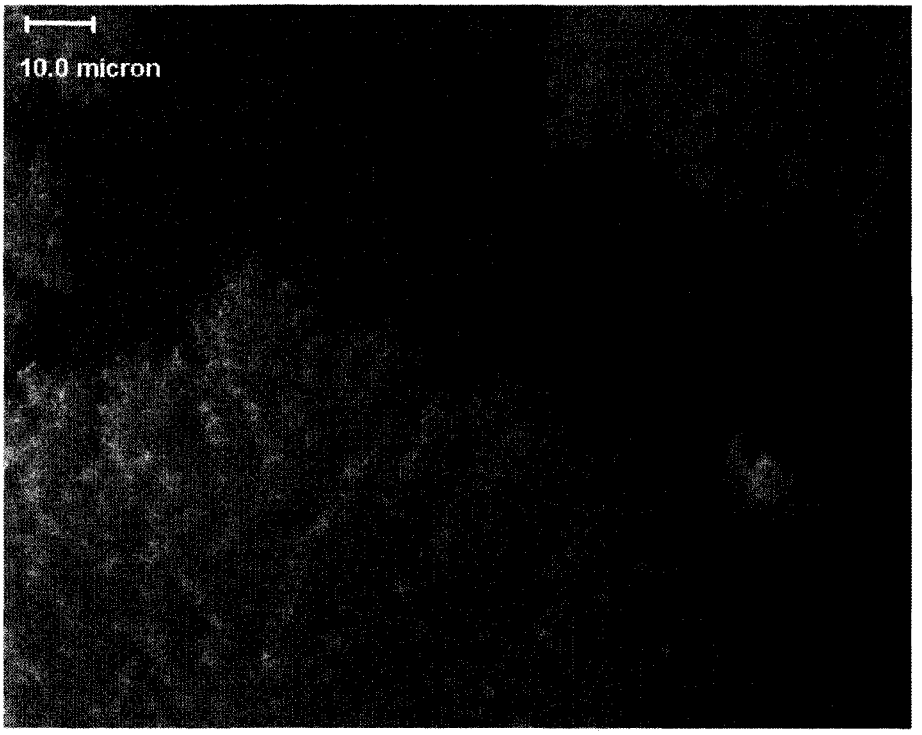

Figure 3.17. Microscope picture of crystallization of the surfactant in the film formed from microemulsion with 15 vol% of diacrylate (HDDA), W = 10, and 10% water with respect to monomers.

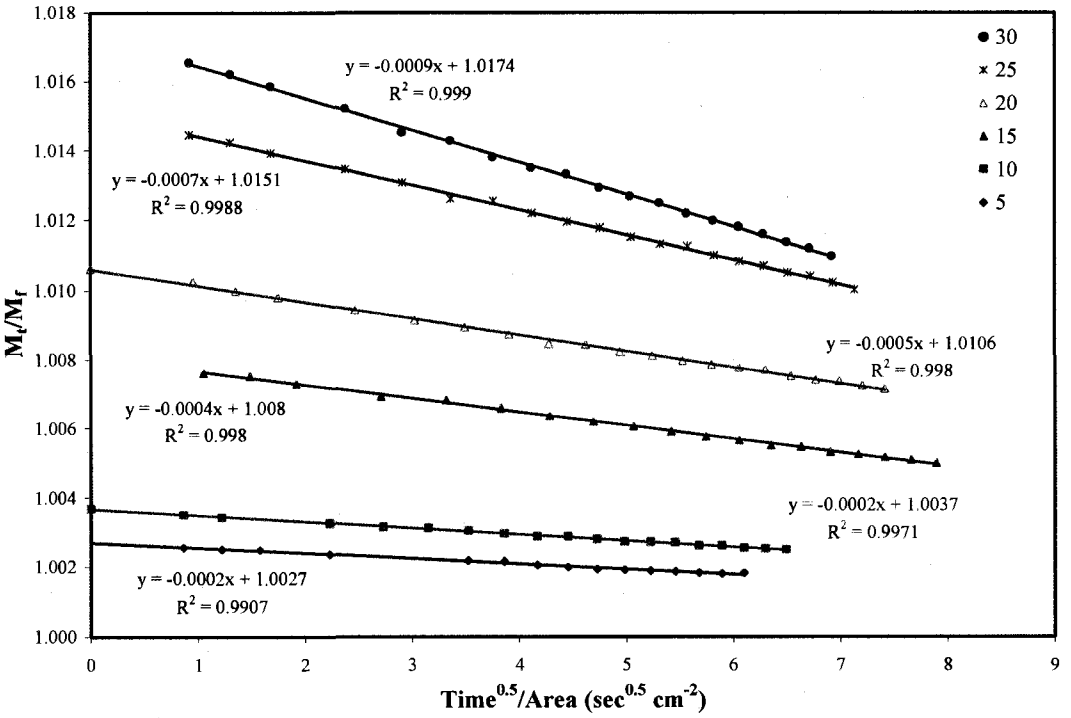

Figure 3.18. The determination of the diffusion coefficient for a set of films prepared from (◆) 5%, (■) 10%, (▲) 15%, (▲) 20%, (∗) 25% and (●) 30% microemulsion with W = 10. Lines represent linear fit to the data.

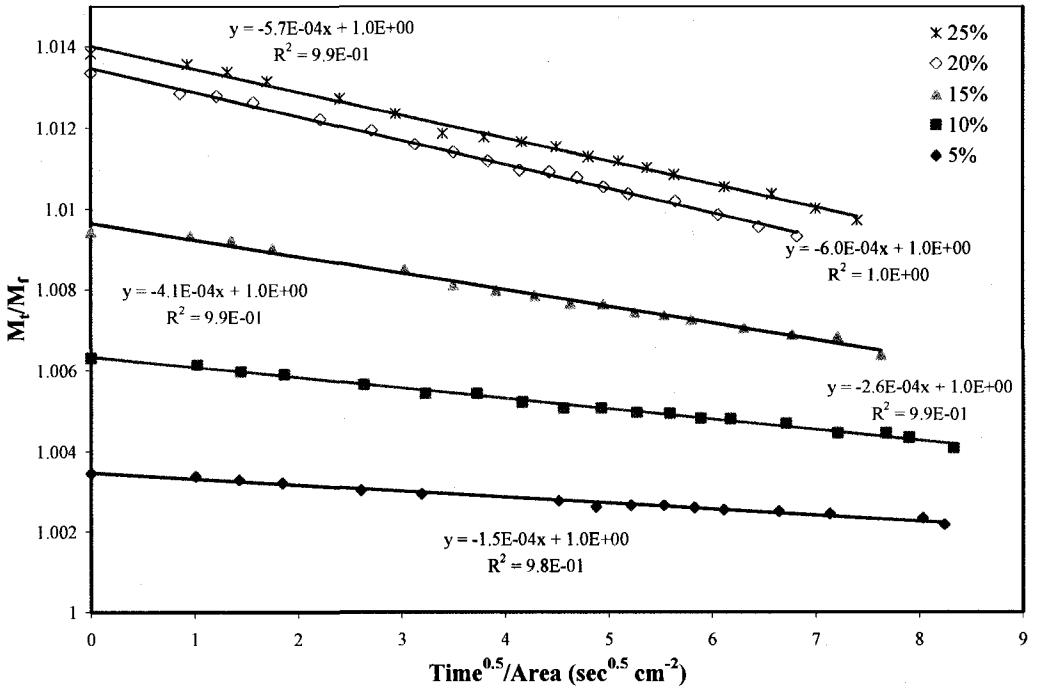

Figure 3.19. The determination of the diffusion coefficient for a set of films prepared from (◆) 5%, (■) 10%, (▲) 15%, (◇) 20%, and (✳) 25% microemulsion with W = 5. Lines represent linear fit to the data.

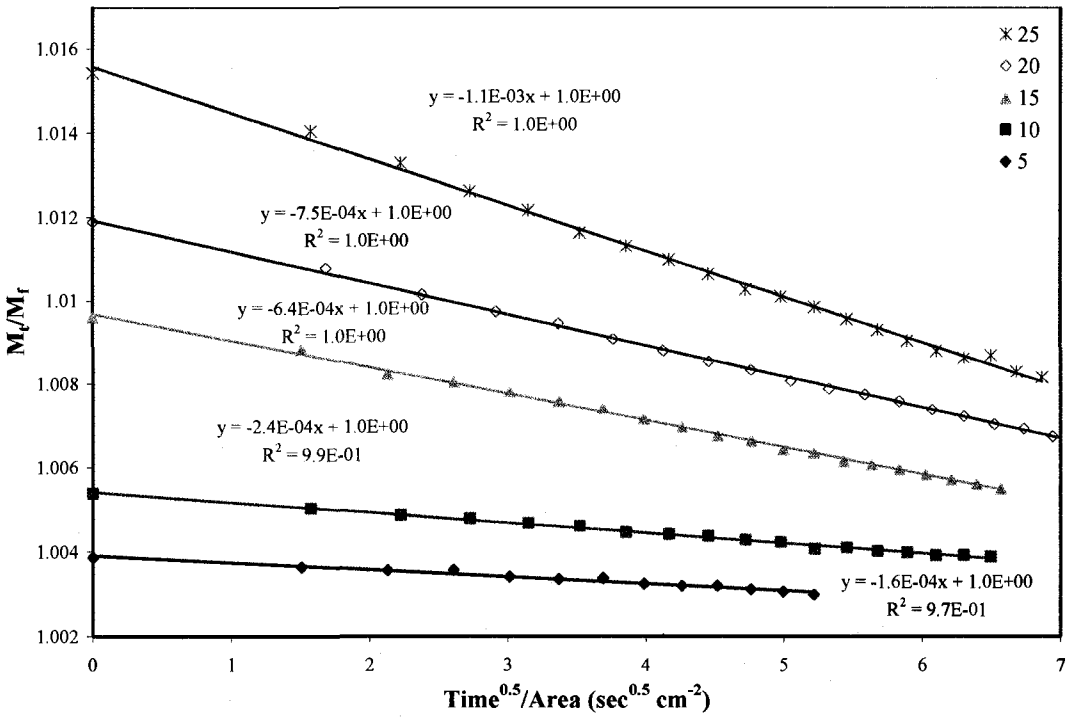

Figure 3.20. The determination of the diffusion coefficient for a set of films prepared from (◆) 5%, (■) 10%, (▲) 15%, (◇) 20%, and (∗) 25% microemulsion with W = 13. Lines represent linear fit to the data.

References

(1) KC Leard: Determining Effective Techniques For Investigating Polymer-Dispersed Aqueous Materials, The University of Southern Mississippi, Hattiesburg, 2005.

(2) J Eastoe, BH Robinson, DC Steytler, D Thorn-Leeson: Structural Studies of Microemiulsions Stabilised by Aerosol-OT. Advances in Colloid and Interface Science 36 (1991) 1.

(3) J Eastoe, S Nave, J Penfold: What Is So Special about Aerosol-OT? 1. Aqueous Systems. Langmuir 16 (2000) 8733.

(4) P Alexandris, JE Holzwarth, TA Hatton: Thermodynamics of Droplet Clustering in Percolating AOT Water-in-Oil Microemulsions. Journal of Physical Chemistry 99 (1995) 8222.

(5) VK Vanag, DV Boulanov: Behavior of the Belousov-Zhabotinskii Oscillator in Reverse Micelles of AOT in Octane. Journal of Physical Chemistry 98 (1994) 1449.

(6) VK Vanag, I Hanazaki: Frequency-Multiplying Bifurcation in the Oscillatory Belousov-Zhabotinskii Reaction Proceeding in Interacting Water Droplets of the Reverse Microemulsions of Aerosol OT in Octane. Journal of Physical Chemistry 99 (1995) 644.

(7) VK Vanag, I Hanazaki: pH Dependence of the Belousov-Zhabotinsky Reaction in Water-in-Oil Reverse Microemulsion of AOT in Octane. Journal of Physical Chemistry 100 (1996) 10609.

(8) VK Vanag, I Hanazaki: Effect of Light on the Belousov-Zhabotinsky in Water-in-Oil Microemulsions of Aerosol OT in Octane. Journal of Physical Chemistry A. 101 (1997) 2147.

(9) VK Vanag, IR Epstein: Physical Review Letters 87 (2001) 228.

(10) VK Vanag, IR Epstein: Dash waves in a reaction-diffusion system. Physical Review Letters 90 (2003) 098301.

(11) SP Moulik, BK Paul: Structure, dynamics and transport properties of microemulsion. Advances in Colloid and Interface Science 78 (1998) 99.

(12) X-M Xie, T-J Xiao, Z-M Zhang, A Tanioka: Effect of Interfacial Tension on the Formation of the Gradient Morphology in Polymer Blends. Journal of Colloid and Interface Science 206 (1998) 189.

(13) J Texter, LE Oppenheimer, JR Minter: Microemulsion Polymerization in the Water, Aerosol-OT Tetrahydrofufuryl Methacrylate System. Polymer Bullelin 27 (1992) 487.

(14) J Barton: Free-Radical Polymerization in Inverse Microemulsions. Progress in Polymer Science 21 (1996) 399.

(15) CA Miller, T Nishimi: Spontaneous emulsification of oil in Aerosol-OT/Water/hydrocarbon systems. Langmuir 16 (2000) 9233.

(16) F Roussel, J-M Buisine, U Maschke, X Coqueret: Photopolymerization kinetics and phase behaviour of acrylate based polymer dispersed liquid crystals. Liquid Crystals 24 (1998) 555.

(17) J Barrajo, CC Riccardi, RJJ Williams, HM Sidiqui, M Dumon, JP Pascault: Thermodynamic Analysis of Reaction-Induced Phase Separation in Epoxy-Based Polymer Dispersed Liquid Crystals (PDLC). Polymer 39 (1998) 845.

(18) K-Q Xia, Y-B Zhang, P Tong, C Wu: Interactions in mixtures of a microemulsion and a polymer. Physical Review E 55 (1997) 5792.

(19) M Kotlarchyk, SH Chen, JS Huang: Temperature Dependence of Size and Polydispersity in a Three-Component Microemulsion by Small Angle Neutron Scattering. Journal of Physical Chemistry 86 (1982) 3273.

(20) K Hamada, T Ikeda, T Kawai, K Kon-No: Ionic Strength Effects of Electrolytes on Solubilized States of Water in AOT Reversed Micelles. Journal of Colloid and Interface Science 233 (2001) 166.

(21) J-S Yoon, H-W Jung, M-N Kim, E-S Park: Diffusion Coefficient and Equilibrium Solubility of water molecules in biodegrable polymers. Journal of Applied Polymer Science 77 (2000) 1716.

(22) DJT Hill, MC Lim, AK Whittaker: Water diffusion in hydroxyethyl methacrylate (HEMA)-based hydrogels formed by g-radiolysis. Polymer International 48 (1999) 1046.

CHAPTER IV

STRUCTURAL CHANGE INDUCED BY PHOTOPOLYMERIZATION OF AOT/D_2O/DODECYL ACRYLATE INVERSE MICROEMULSIONS STUDIED BY SMALL AND ULTRA-SMALL ANGLE NEUTRON SCATTERING

Introduction

As discussed in chapter 2, there are a variety of methods that allow characterization of the self-assembled structures in microemulsions. Light and neutron scattering methods are most widely used for this type of analysis, because of the similar length scale of the method and tested subjects make them convenient. The size of the microemulsions structures ranges from 10 to 1000 Å. The wavelengths used for light and neutron scattering are 400-700 nm and 1-10 Å, respectively. In this chapter, a relation between the structure and size of the microemulsions' micelles and the structures in the formed films is analyzed with the aid of neutron scattering methods.(1)

Microemulsion systems display a rich phase behavior (2) that can include morphologies as varied as spherical droplets, 'sponge' phases,(3) and lamellar phases,(4) all of which can have structures on the nanometer scale.(5-10) Therefore, the use of a polymerizable oil phase in inverse microemulsion systems provides an opportunity to create well-designed, nanostructured, polymeric materials for a variety of potential applications (functional membranes, separation membranes, fuel cells, etc...). By controlling the formulation of the microemulsions, one has a large degree of control over the size and shape of the resulting phase structures. This is likely to have a large impact on the relevant physical properties of the films (i.e., transport) for given applications. An

insight into these structure-property relationships provides a sound basis for the designing of systems with tailored properties. It is, therefore, crucial to develop a fundamental understanding of the relationship between the 'solution' microemulsion structure and the resulting structure in the polymerized microemulsion film. By understanding this structural relationship, it should be possible to rationally design high-performance, nanostructured films for targeted applications.

We addressed this interesting problem through the use of small-angle and ultra-small-angle neutron scattering (SANS/USANS). In this chapter, we present analysis of SANS and USANS data for a series of microemulsions that reveal significant changes in structure upon polymerization. Based on the analysis of these data, we propose a model to describe the scattering behavior for these materials. As noted in the previous Chapter, the structures in the films based on the acrylate microemulsions were too small for observation under an optical microscope. Therefore, hoping to determine the surfactant's organization in the polymerized material, we chose USAN for the film analysis.

In the previous chapter, we demonstrated the ability to form films composed of a hydrophobic polymer matrix with an aqueous phase distributed throughout. (11) Clear microemulsions of monomers, surfactant, and water were photopolymerized into opaque materials. The initially clear state of the w/o microemulsion indicates that the aqueous component is dispersed on a nanometer scale. After photopolymerization, the opacity of the films indicates the aggregation of the aqueous phase into structures whose size exceeds the wavelength of visible light, viz. 500 nm.

Polymerization reactions in microemulsions have been explored in attempts to produce latexes with bead sizes below those generated through emulsion polymerization,

or to preserve the microstructure of the microemulsion template.(12) Typically, microemulsion polymerizations are used in the synthesis of well-defined, nanometer-sized polymer particles with a narrow size distribution. The inherent properties of microemulsion systems give a large degree of control over the polymerization process, and, ultimately, the types of polymer particles that can be synthesized.(13) Specifically, inverse-microemulsion polymerization is an attractive approach to synthesis of high-molecular-weight water-soluble polymers,(13,14) as well as difficult to dissolve polymers(15) such as polyaniline(16) and polythiophene(17). It has also been shown that the synthesis of various types of colloidal particles of inorganic solids can be carried out within microemulsions (e.g. metals, metal carbonates, semiconductors).(18-20)

As outlined in Chapter 2, there has been little work on polymerizations that occur throughout the continuous phase of the microemulsion.(21-23) These works were concerned with polymerization of a monomer in a bicontinuous microemulsion to form porous polymers to be utilized as membranes.(24) Because the resulting polymers often did not reflect the original microstructure, polymerizable surfactants were introduced.(25,26) In another attempt to preserve the lamellar nanostructure of the microemulsion, a small amount of crosslinking throughout the oil phase resulted in nanostructured polyacrylamide hydrogels.(27)

Experimental

Materials

The dioctyl sulfosuccinate sodium salt (AOT) surfactant (>96% purity) and the deuterium oxide, D_2O, (99.9 6 atom % D) were purchased from Aldrich; the monomer, dodecyl acrylate (DDA) at 90 % purity, was purchased from Sartomer; the crosslinker hexanediol diacrylate (HDDA) at >99% purity, was purchased from Cytec Surface Specialties; the photoinitiator, Irgacure 369, was obtained from Ciba Specialty Chemicals. All materials were used as received.

Preparation of Microemulsions

All microemulsions were prepared according to the following procedure: A stock solution (5.7 wt % mixture HDDA crosslinker with the respect to DDA monomer) was prepared and used for all microemulsion formulations. A predetermined amount of AOT surfactant was added to the monomer/crosslinker formulation, and the solution was allowed to stir until all the AOT surfactant was fully dissolved. In order to prepare microemulsions with a range of water-to-surfactant ratios, W, a predetermined amount of D_2O was added to the AOT/monomer mixture and stirred vigorously. The photoinitiator was then added to the microemulsion at a concentration of 7×10^{-3} M relative to the monomer volume present. The water-to-surfactant ratio, W, was varied from 5 to 13, and the water content ranged from 5 to 30 wt % wrt monomers. A list of the different microemulsion formulations can be found in Table 4.1.

Preparation of Films

The films were prepared by placing approximately 2 mL of the microemulsion formulation between two glass microscope slides (using glass spacers of 0.8 mm thickness). Samples were photopolymerized with a small handheld ultraviolet light source (365 nm) with an intensity of 2.3 mW/cm^2 as measured by an International Light (IL1400A) radiometer. The exposure time was 2 minutes on each side of the film.

Small-Angle and Ultra-Small-Angle Neutron Scattering (SANS & USANS)

The SANS and USANS measurements were carried out on beamlines NG7 and BT5, respectively, at the National Institute of Standards and Technology (NIST) Center for Neutron Research (NCNR), Gaithersburg, MD. The liquid-phase microemulsions were placed in 1.0 mm path length SANS liquid sample holders. Circular shapes were cut out of the films and also placed in 1.0 mm path length SANS sample holders. The NG7 beamline includes a high-resolution 2D detector (65 x 65 cm^2) and focusing refractive lenses. The instrument employs a mechanical velocity selector as a monochromator and a circular pinhole collimator. The SANS intensity, I, was recorded as a function of the magnitude of the scattering vector Q ($Q = \frac{4\pi \sin\frac{\theta}{2}}{\lambda}$), where θ is the scattering angle and λ is the neutron wavelength, equal to 6 Å. The detector angle was set at 0^o, and the sample-to-detector distance was set to 1 m, 4.5 m, and 13 m to cover the Q range of 0.003 to 0.6 $Å^{-1}$. This setting enables the probing of materials' structural features ranging from roughly 1 nm to over 500 nm. The USANS measurements were performed using the BT5 double-crystal diffractometer at the NCNR.(28) Samples were each run for 6-8 hours. 1 mm samples were placed in quartz cells. The wavelength of the

incident neutrons, λ, was set at 2.38 Å, and data were collected over a Q-range from $2.5x10^{-5}$ $Å^{-1}$ to $5.3x10^{-3}$ $Å^{-1}$. For both SANS and USANS, the measured intensity was converted to absolute intensity by correcting for transmission and background scattering. All SANS and USANS data were reduced and modeled using software developed at the NIST Center for Neutron Research.(29)

Definition of Parameters

It is necessary to define several of the parameters that we will use in the data analysis. The first of these parameters, W, is the molar ratio of D_2O to the surfactant in the system. In some instances it has been useful to examine the data using a parameter that we define as $\phi_{w/s}$, which is the ratio of the total volume fraction of the water in the system, ϕ_w , to that of the surfactant, ϕ_s. A last parameter that has proven to be useful in discussions of the structure of microemulsions(30) is that of the droplet density, which is given by

$$\phi_d = \frac{(\phi_w + \phi_s)}{(\phi_w + \phi_s + \phi_m)} \qquad \text{Equation 4.1}$$

where ϕ_w, ϕ_s, and ϕ_m are the total volume fraction of water, surfactant, and monomer in the microemulsion.

Scattering Theory

Over the past three decades, small-angle neutron scattering (SANS) has proven to be a useful tool in examining the structure of water-in-oil (and oil-in-water) microemulsion systems.(31-38) Although a complete review of that literature is beyond the scope of this work, it is necessary to discuss a few of the seminal contributions to this

area of research. Studies by Kotlarchyk and coworkers(39-44) used SANS to elucidate the structure in pure three-component AOT-D_2O-alkane systems. Their results have shown that the droplets in such systems are polydisperse, weakly-interacting spheres at room temperature. Furthermore, they demonstrated that the droplet radius increased linearly with an increase in the molar ratio of D_2O to AOT ($W=[D_2O]/[AOT]$). In particular, they found, empirically, that the mean droplet radius <r> could be expressed in terms of W using the following equation(40)

$$\langle r \rangle = \frac{3v_{D_2O}}{a_0} W + \frac{3V_H}{a_0} \qquad \text{Equation 4.2}$$

where v_{D2O} is the specific volume of a D_2O molecule, V_H is the volume of the water-penetrated portion of a single AOT head group, and a_o is the area per AOT head group on the water-core surface. In related work by Kotlarchyk and coworkers,(41) modeling of the SANS data was accomplished using a form factor for polydisperse hard spheres and a structure factor taking into account contributions from inter-particle interactions and density fluctuations.

The total scattering function, I(Q), of a microemulsion system can be described by the product of the contributions from the shape of the scattering particle (i.e., the form factor), F(Q), and the spatial distribution of the these scattering particles, or structure factor, S(Q) given by the following relation

$$I(Q) = n\left|\langle F(Q)\rangle\right|^2 \langle S(Q)\rangle \qquad \text{Equation 4.3}$$

where n is the number density of the scattering particles and the brackets, $\langle\rangle$, represent the ensemble average due to thermal fluctuations. Our present work uses a core-shell model

for spherical droplets for F(Q) that considers the core to be polydisperse and the shell to consist of a monolayer of the surfactant molecules. Polydispersity is taken into account by weighting the form factor by a probability function described with the Schulz distribution.(40,41,45) This is a common technique used to describe the polydispersity of droplet sizes in microemulsions. The form factor, F(Q), for a spherical core-shell particle can be expressed by

$$F(Q) = V_c \cdot (\rho_c - \rho_s)\ F_o(QR_c) + V_s \cdot (\rho_s - \rho_{solvent})\ F_o(QR_s) \qquad \text{Equation 4.4}$$

where V_c and V_s are the volumes of the particles with radii of the core R_c and of the shell, R_s.(46) Neutron-scattering length densities of the core, shell, and the solvent are ρ_c, ρ_s, $\rho_{solvent}$, respectively. The function $F_o(x)$ is a first-order spherical Bessel function of the first kind and is given by

$$F_o(x) = 3\frac{\sin x - x\cos x}{x^3} \qquad \text{Equation 4.5}$$

The contribution to I(Q) from the structure factor, S(Q), for the spherical core-shell particles has been modeled assuming hard-sphere interactions. This approach has been found to describe scattering from micoremulsions quite well.(40,47) The model structure factor employed here is based on the Percus-Yevick approximation.(48)

Results and Discussion

Microemulsions

Scattering patterns for a series of microemulsions with increasing $\phi_{w/s}$ (between 0.4 and 0.6) are presented in Figure 4.1. As $\phi_{w/s}$ increases, there is a qualitative change in the scattering behavior. At low $\phi_{w/s}$ (0.44) the microemulsion has a low total volume fraction of water, ($\phi_w = 0.037$), and W is approximately 9.4. Under these conditions, scattering is most likely due to spherical core-shell droplets that are not correlated with one another; therefore, the scattering represents the form factor described by Equation 4.4. However, there is an obvious structure peak that develops with an increase in $\phi_{w/s}$. Also, the peak intensity increases and the maximum shifts to higher Q values with an increase in $\phi_{w/s}$. This peak is due to inter-droplet correlations and will be discussed in greater detail.

For a set of microemulsions with the same water content, fitting of the scattering curves was done using a global fitting procedure where the scattering length density of the solvent (monomers), core (D_2O), and shell (AOT) were fixed to values of $\rho_{monomer}=2.75\text{x}10^{-7}$ Å^{-2}, $\rho_{D2O}=6.36\text{x}10^{-6}$ Å^{-2}, and $\rho_{shell}=1.78\text{x}10^{-7}$ Å^{-2}, respectively. It was assumed that the shell thickness consisted of a monolayer of AOT surfactant (44) and that this shell thickness should be constant among the different microemulsions. The value of the scattering length density was calculated for the surfactant (excluding the sodium sulfonate head group) using group parameters found in the literature.(49) It should be noted that several values of ρ_{shell} were systematically chosen to determine which part of the surfactant shell was contributing to the overall scattering intensity. The value given

above was found to give the best fits. The fitting parameters for the particle volume fraction, the polydispersity, and the particle radius were left as free parameters to be fit.

Figures 4.2A and 4.2B show fitting results for a series of samples containing 10 and 25 mass fraction of D_2O with respect to the monomers, and values of W of 5, 10, and 13. As can be seen, the model is in excellent agreement with the experimental scattering data. It should be pointed out, however, that at lower water contents, the fits are much better over the entire Q range when compared to higher water content microemulsions. This is likely due to the fact, that, at lower water contents, the particles are less densely packed; therefore, there is little distortion in the shape of the particles. However, at higher water contents the particles' shape could be slightly distorted because of their size and close packing. Several other models were systematically investigated; but none represented the data better than the one chosen for this study.

The shell thickness that simultaneously fits all the data most appropriately was found to be approximately 5 Å. One would assume that the shell thickness should be comparable to the length of the AOT molecule, which has been reported in the range of 12.9 Å – 13.3 Å.(50,51) We propose that the smaller thickness of the surfactant layer can be attributed to low contrast between the surfactant and the monomer phase. In addition, the head of the surfactant is hydrated, and its scattering is mixed with the scattering of the D_2O phase. This is consistent with the picture presented by Chen and co-workers.(44) In their model of the structure of inverse AOT micelles (Figure 4 of (44)), they show the tail of the surfactant to be approximately 8 Å in length with the oil phase penetrating the tail by ca. 2.4 Å. This would leave 4.6 Å of the surfactant to act as its own phase without being effectively diluted by another phase. Taking this into consideration, it is likely that

only about 5 Å of the surfactant in the present systems contribute to the scattering form factor. Furthermore, others(33,52) have showed the AOT chain is penetrated by the oil to a depth of 3 Å, which contributes to decreasing the contrast of the shell.

We have found that the total droplet core radius is determined by both the total water volume fraction as well as $\phi_{w/s}$. By plotting the total droplet radius (including the shell) as a function of ϕ_w (Figure 4.3), one can clearly see that there are three regimes governing the growth of the droplet size with increasing water content. By extrapolating the data from the regime II to ϕ_w=0, we obtain a value of ca. 16 Å for the radius of a "dry" droplet, or micelle. Although there are not enough data to do a legitimate extrapolation in regimes I and III, a fit to the two data points in each regime taken together with the fit from regime II, yield a dry micelle value of 16 Å ± 1 Å. This is an excellent agreement with values reported in the literature.(44,53,54) It is interesting, however, that the predicted dry micelle radius is considerably larger than the shell thickness chosen to model the data. This shows that the incorporation of the hard-sphere structure factor into our model properly accounts for inter-particle interactions. While we have not taken into consideration the "true" thickness of the AOT monolayer in the form factor, this is compensated for by the chosen hard-sphere structure factor that accounts for how the droplets interact with one another.

Photopolymerized Microemulsions

Upon photopolymerization of the microemulsions, the optically clear dispersions are transformed into opaque films.(11) This could be explained by a major reorganization of the nanoscale microemulsion structure into structures large enough to

scatter visible light. Evidence of this structural change is revealed in the SANS/USANS scattering profiles in Figure 4.4 for the microemulsion with $\phi_{w/s} = 0.5$. The SANS profile is shown to go from the representative scattering of the microemulsion, to a scattering profile for the film which shows a well-defined peak in the high Q range of 0.15 $Å^{-1}$ to 0.25 $Å^{-1}$ and a scattering feature in the USANS range of 10^{-4} to 10^{-3} $Å^{-1}$ which is due to much larger structures. This behavior was observed for all samples. The position of the high Q peak and the nature of low Q scattering is clearly influenced by both ϕ_w and $\phi_{w/s}$.

Figure 4.5A shows the position of the high Q peak as a function of $\phi_{w/s}$. In order to relate this peak to a real-space size scale, the d-spacing was calculated from Q_{max} using Bragg's law given by

$$D_{Bragg} = \frac{2\pi}{Q_{max}} \qquad \text{Equation 4.6}$$

and is plotted in Figure 4.5A. It is apparent that the position of the high Q peak, and subsequently D_{Bragg}, is clearly dependent on $\phi_{w/s}$. Again, there are three noticeable regimes to the scattering behavior. In the range of $0.4 < \phi_{w/s} < 0.6$ there is little change in D_{Bragg} associated with the scattering peak. However, above and below this regime, D_{Bragg} strongly dependents on $\phi_{w/s}$. In order to gain a deeper insight into the effect of $\phi_{w/s}$ on the structure, we have chosen to plot the data for two sets of samples (Figure 4.5B), where ϕ_w is held relatively constant while W assumes values of 5, 10, and 13. The D_{Bragg} data from both sets of samples appear to fall on the same line. A linear fit to these data yields an intercept, at $\phi_{w/s}=0$, of approximately 26 Å. This spacing is equal to roughly twice the reported length of the surfactant molecule. This is a verification that the structure giving

rise to the high-Q peak is likely coming from lamellar-like bilayers of the surfactant molecule, in which the bilayers are swollen with water.

Moving along the scattering curve towards lower values of Q, one first finds that in the Q range from 10^{-3} $Å^{-1}$ to 10^{-2} $Å^{-1}$ the scattering follows a Q^{-4} dependence. This is true for all the polymerized microemulsions and indicates that the large structures, or domains, responsible for the low-Q scattering are distinct domains characterized by a sharp interface.(55,56) There is also a structure peak in the range of $2x10^{-4}$ $Å^{-1}$ to $7x10^{-4}$ $Å^{-1}$ indicating a correlation between the large-scale inhomogeneities and, finally, a leveling off of the scattering intensity at ultra-low scattering vectors. The smeared USANS data for the films within the range of $0.4<\phi_{w/s}<0.6$ are shown in Figure 4.6. Above a $\phi_{w/s}$ value of approximately 0.45, there is little change in the scattering behavior. Although it is not discernable in the log-log plot of intensity versus Q, there is a distinct maximum in each scattering curve located in the region just before the scattering begins to follow a Q^{-4} power-law dependence. This maximum indicates a structural correlation between the large inhomogeneities. This gives rise to the ultra-low Q scattering and characteristic length scale, ξ, which was calculated from the maximum using Bragg law.

In order to get a clear picture of the role that water content plays in the development of this structure, we have chosen to plot the ξ data for films prepared from the microemulsions in which W remains relatively constant (10.6 ± 1) (this corresponds to $0.4< \phi_{w/s} <0.6$). These data, along with the d-spacing for the corresponding high-Q peak in the same films, can be seen in Figure 4.7. As the water volume fraction increases, so does the characteristic length scale between the large domains. However, above a value of $\phi_w \approx 0.10$ there is little change in the dimension associated with the correlation

distance between the large domains. It is apparent that the d-spacing starts to increase, albeit miniscully, for the bilayer structure. It should be noted that this value of the water content corresponds to a droplet density of ca. 0.30. This indicates that, above a critical droplet density, the large domains remain relatively unchanged in their structure, while the smaller structures are capable of swelling with water. The implications of these data on the proposed morphology for these systems will be discussed in greater detail.

The Morphology Model

Several models for these systems' morphology could be chosen to explain the scattering observed for the polymerized microemulsion films. We were interested in differentiating whether or not polymerization simply induced phase separation, or led to an actual rearrangement of the water and surfactant, thus altering the shape and size distribution of the microemulsion droplets.(11) Moreover, another likely scenario is that phase separation occurs simultaneously with an altering of the nanostructure of the microemulsion droplets. It is known. that by adding a polymer to the oil phase in an inverse microemulsion, one can induce phase separation. Xia and coworkers found that, above a critical concentration of the polymer in the oil phase, microemulsions transition from clear to turbid, indicating phase separation.(57) In the current study, the entire oil phase is polymerizable, making it certain that the polymer concentration is high enough to induce phase separation. Although the results from Xia et al. can explain, in large part, the qualitative observations made in the current system,(11) their experimental results were solely based on turbidity measurements, which do not give any insight into the role that phase separation plays in the rearrangement of the surfactant.

It is apparent that the high-Q peak is indeed caused by scattering from a bilayer of the surfactant molecules with water located between the layers. Furthermore, the Q^{-4} power-law behavior indicates a sharp interface between the polymer matrix and the large heterogeneities. We propose that, upon polymerization, the change in volume as the monomer mixture shifts into a polymer network causes phase separation via aggregation of the surfactant which stabilizes water droplets into larger water droplets. As explained in the previous Chapter, the driving force for this aggregation can be understood by examining the various contributions to the free energy associated with the formation of the microemulsion droplets (ΔG_{form}). The expression for ΔG_{form} is given by

$$\Delta G_{form} = \Delta A \gamma_{1,2} - T\Delta S \qquad \text{Equation 4.7}$$

where ΔA is the change in the interfacial area between the water and the continuous phase, $\gamma_{1,2}$ is the interfacial tension between the two phases, ΔS is the overall change in entropy of the system, and T is the temperature.(11) As the polymerization occurs, the entropy term is reduced significantly because the number of possible conformations of the droplets is reduced. Water can no longer freely exchange between droplets, thus the entropy of mixing decreases. As a result, the overall free energy of the system is increased. The only viable means to lower the free energy is to decrease the total surface area, which is achieved through droplet aggregation. The larger droplets of water are likely stabilized by some fraction of the surfactant, whereas the rest of the surfactant is partitioned in the matrix as bi-layer structures swollen with water. In order to determine the plausibility of this explanation, the entire scattering curve for the film ($\phi_{w/s}$=0.5) was fit with a simple polydisperse spherical droplet model with hard-sphere interactions

where the contrast factor was based on the contrast between D_2O and the polymer matrix. The results of this fit to the data can be seen in Figure 4.8. In Figure 4.8, the USANS data has not been desmeared. As result, it does not blend seamlessly with the SANS data. However, the data in this form gives much more reliable fit results. The USANS and SANS data were fit simultaneously using a model that accounts for instrument smearing of the data. The volume fraction of droplets in the corresponding microemulsion was assumed to be very similar to the droplet density (≈ 0.38) calculated for this system based on the formulation. With this minor assumption, the model describing the morphology in this way represents the data quite well.

Discrepancies can be explained by considering that the model is not very detailed and does not take into consideration (1) the surfactant shell surrounding the larger water droplets, or (2) how much of the water and surfactant are located in the bi-layer structures. This explanation is further supported by the data in Figure 4.7. The characteristic length-scale increases until $\phi_w \approx 0.10$ ($\phi_d \approx 0.30$), after which there is little change. The bilayer structures, however, show a different behavior. The d-spacing is unchanged until $\phi_w \approx 0.10$, after which there appears to be an increase. This means that the large droplets can only support a certain amount of water, probably dictated by the amount of surfactant in the system, and that the "excess" water is contained in the bi-layer structures present in the matrix of the film. Once the larger droplets are "saturated", the bilayers compensate by swelling with water. Although the exact morphology of the bi-layer structures is not known, it is likely that these structures resemble the self-assembled fibular structures observed by John and coworkers in AOT-based organogels.(50,58) It is also likely that these bilayer structures could contribute to the

low-Q scattering if they undergo a large degree of aggregation. However, in order to refine our model and determine the exact nature of the different levels of organization and self-assembly present within these systems, further systematic investigations must be carried out.

Conclusions

SANS and USANS have been employed to investigate the effects of photopolymerization on the structure of inverse microemulsion systems formed from AOT-water-monomer systems. The SANS profiles for the microemulsions were shown to be sensitive to the total amount of water, as well as $\phi_{w/s}$, and were successfully fit with a model for spherical, core-shell droplets with hard-sphere interactions. From this model, the droplet core and shell size were determined for each microemulsion system. These data revealed that the droplet growth, with increasing water content, was highly dependent upon $\phi_{w/s}$. The SANS/USANS profiles of the photopolymerized films reveal that the nanometer size water droplets in the microemulsions rearrange upon polymerization to form two different structures. Large droplet structures are formed from the aggregation of the nanometer size droplets in the microemulsion. These droplets are large enough to scatter visible light and give the films their opacity. Secondly, some portion of the surfactant self-assembles into a bilayer structure characterized by a peak in the high-Q range of 0.15 $Å^{-1}$ to 0.25 $Å^{-1}$.

Light scattering was also conducted. Surprisingly, the microemulsions based on dodecyl acrylate did not efficiently scatter light. Consequently, decay profiles were not easily observed, and when they were detected there was a question of their correctness.

Thus, neither the transnational diffusion coefficient nor the effective hydrodynamic radius could not be calculated from DLS.

Table 4.1. Parameters for microemulsion formulations used in this study

$\phi_{w/s}$	$W = \frac{[AOT]}{[H_2O]}$	**Monomers** ϕ_m	**AOT** ϕ_s	**D_2O** ϕ_w
0.23	4.9	0.67	0.27	0.07
0.26	5.7	0.44	0.44	0.12
0.44	9.4	0.88	0.086	0.037
0.45	9.7	0.78	0.15	0.069
0.48	10.3	0.69	0.21	0.099
0.50	10.7	0.62	0.25	0.13
0.53	11.3	0.56	0.29	0.15
0.56	12.0	0.51	0.31	0.18
0.59	12.8	0.81	0.12	0.072
0.69	14.8	0.60	0.24	0.16

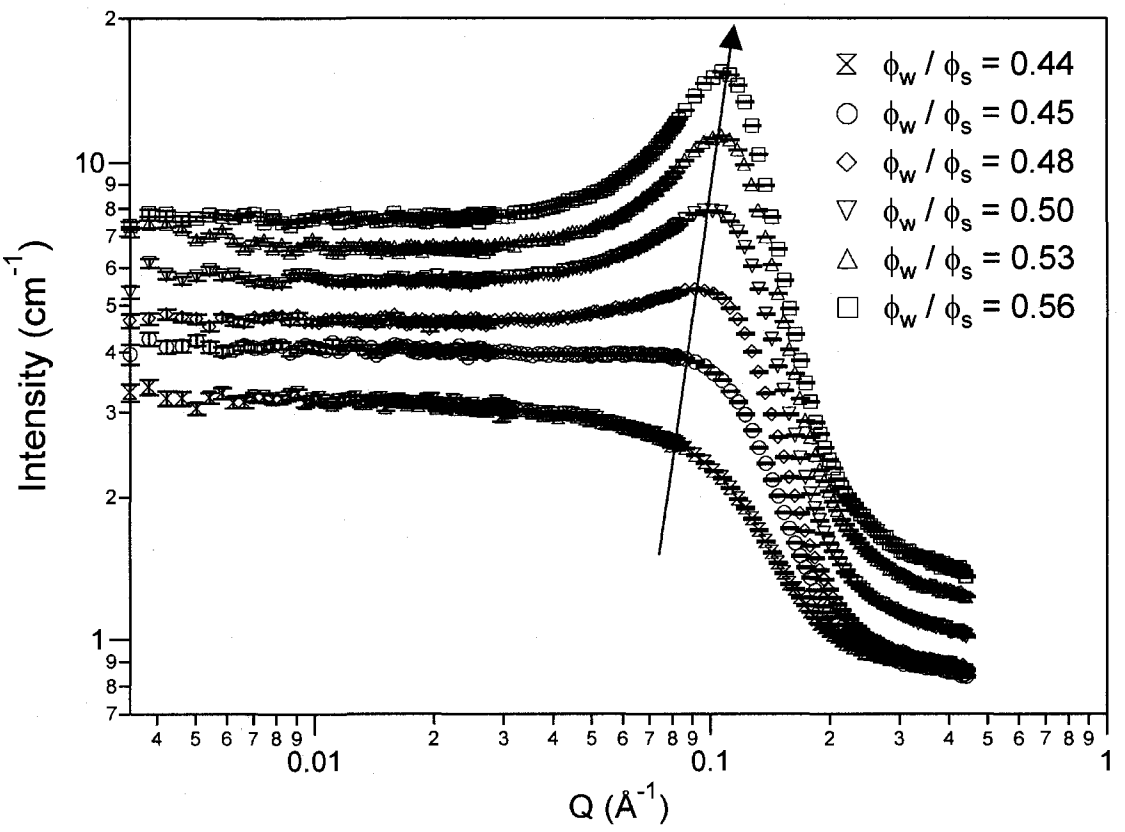

Figure 4.1. Absolute scattering intensity versus scattering vector, Q, for a set of microemulsions with $\phi_{w/s}$ ranging from 0.4 to 0.6. The scattering curves have been offset vertically for comparison.

a)

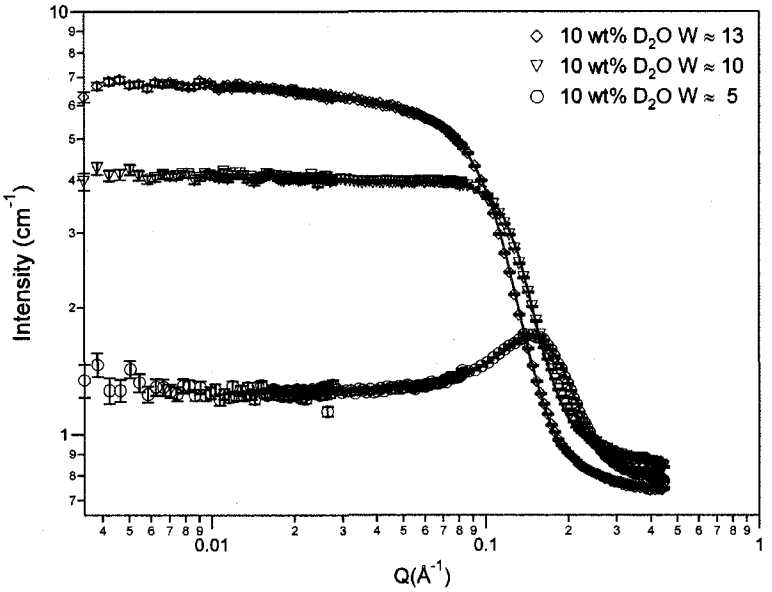

b)

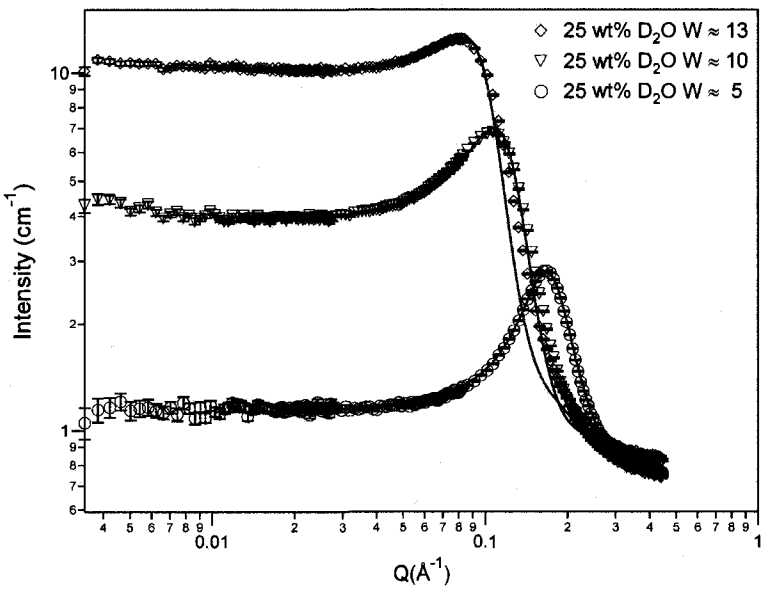

Figure 4.2. Scattering patterns of two sets of microemulsion: a) microemulsions with $\phi_w \approx 0.067(\pm 0.006)$ and changing W, b) microemulsions with $\phi_w \approx 0.14(\pm 0.02)$ and changing W. Lines represent fits of scattering model to the data.

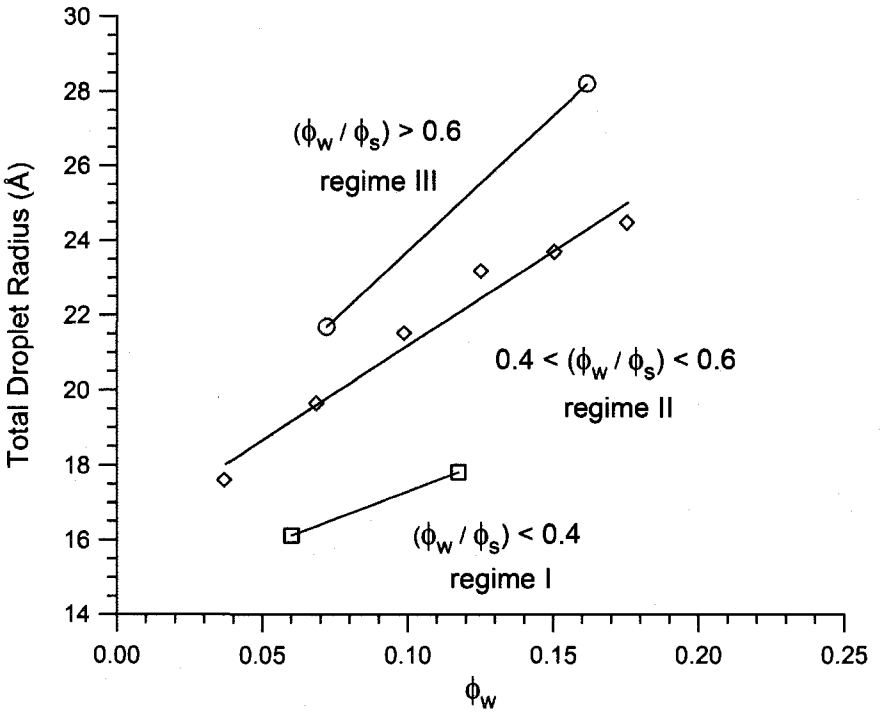

Figure 4.3. Total droplet radius in Å versus the water volume fraction (ϕ_w). Lines are present to guide the eye.

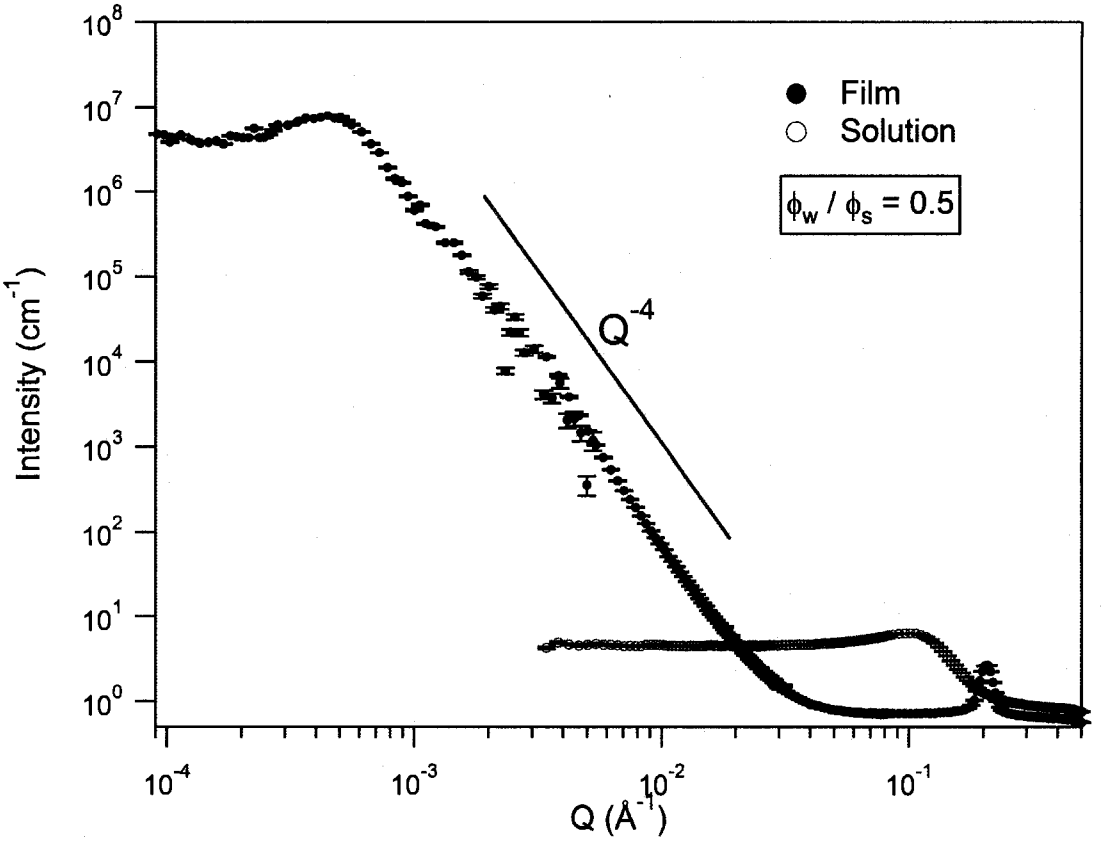

Figure 4.4. SANS and USANS data showing the structural change of a microemulsion with $\phi_{w/s}$=0.5 upon polymerization.

a)

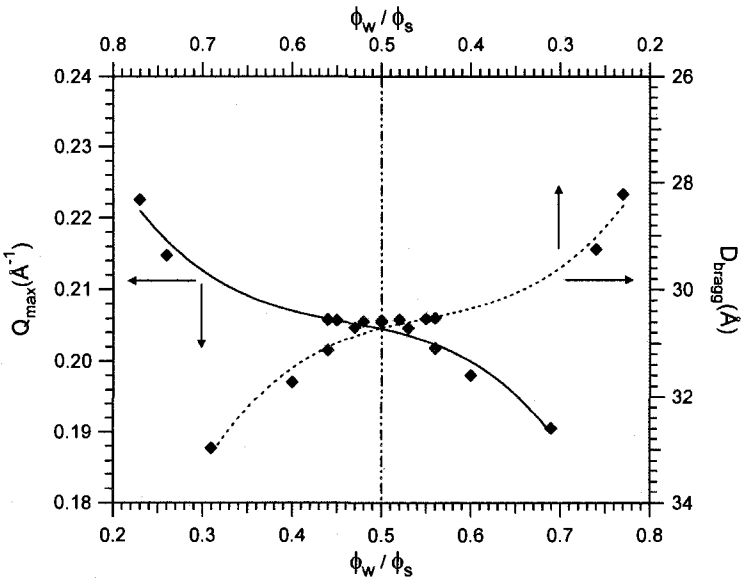

b)

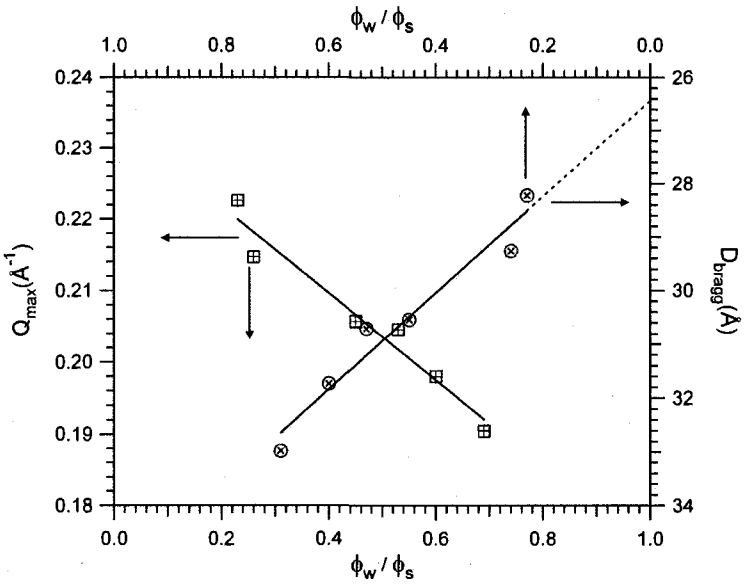

Figure 4.5. a) Position in Q and corresponding D-spacing for the high-Q peak in the polymerized microemulsion films. Lines are present to guide the eye. b) Position in Q and corresponding D-spacing for films containing $\phi_w \approx 0.067(\pm 0.006)$ and $\phi_w \approx 0.14(\pm 0.02)$ over a range of W (i.e., varying $\phi_{w/s}$). The line represents a linear fit to the data and extrapolation to the y-intercept.

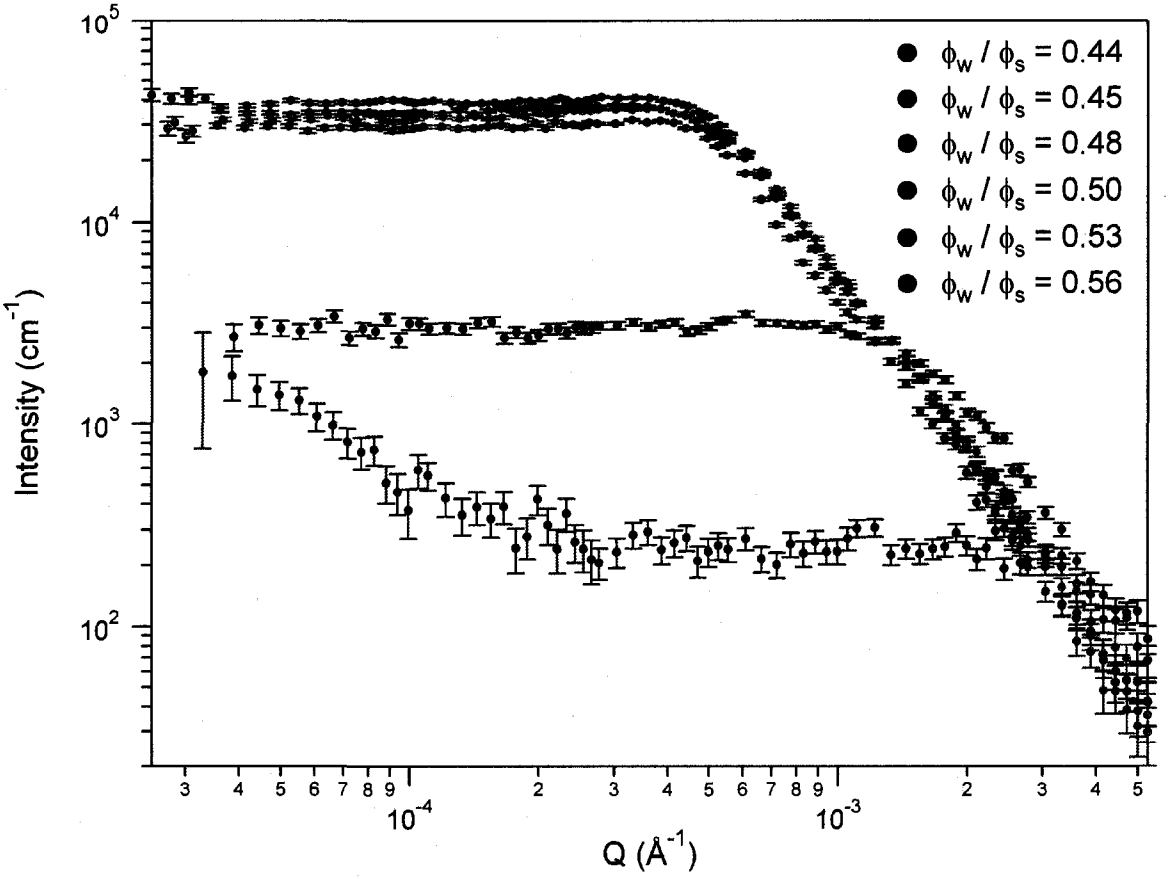

Figure 4.6. USANS data for films with $\phi_{w/s}$ ranging from 0.4 to 0.6.

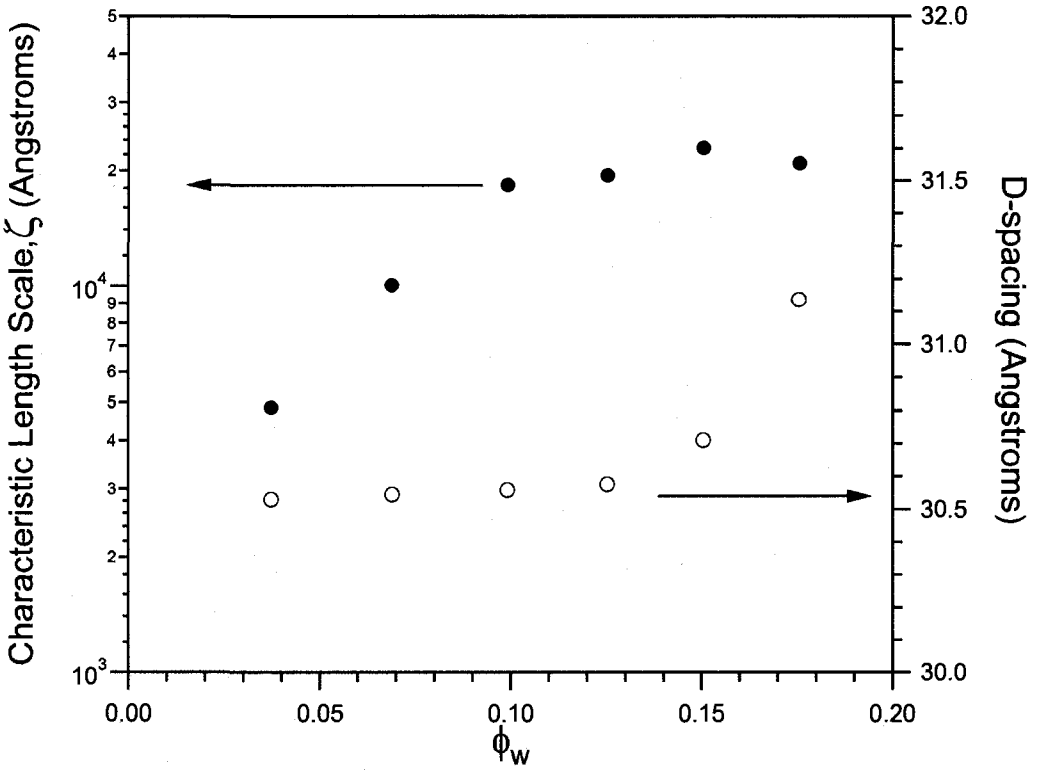

Figure 4.7. Characteristic length scale, ξ (determined from USANS), and D-spacing associated with high-Q peak (determined from SANS) versus ϕ_w for films with $\phi_{w/s}$ ranging from 0.4 to 0.6.

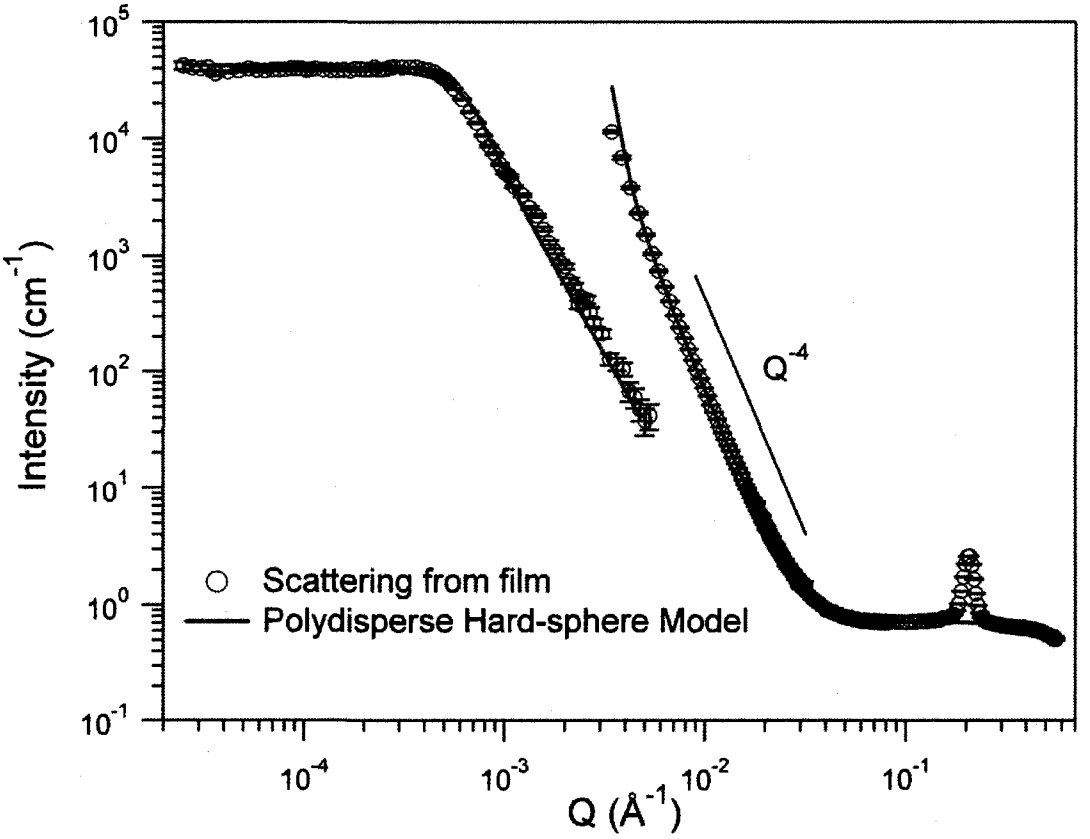

Figure 4.8. Fit of a polydisperse hard-sphere model to the SANS and USANS scattering data of a polymerized film with $\phi w/s=0.5$.

References

(1) EW Kaler, R de Vries, CC Co: Microemulsion Polymerization. 1. Small-Angle Neutron Scattering Study of Monomer Partitioning. Macromolecules 34 (2001) 3224.

(2) T Hellweg: Phase structures of microemulsions. Current Opinions in Colloid & Interface Science 7 (2002) 50.

(3) I Javierre, F Nallet, A-M Bellocq, M Maugey: Structure and dynamic properties of a polymer-induced sponge phase. Journal of Physics: Condensed Matter 12 (2000) A295.

(4) M Nagao, S Okabe, M Shibayama: Small-angle neutron-scattering study on a structure of microemulsion mixed with polymer network. The Journal of Chemical Physics 123 (2005) 144909(1-8).

(5) J Eastoe, S Nave, J Penfold: What Is So Special about Aerosol-OT? 1. Aqueous Systems. Langmuir 16 (2000) 8733.

(6) H Saito, K Shinoda: The effect of temperature on the phase sequilibria and the typispersions of the ternary systems composed of water, cyclohexane, and nonionic surfactant. Journal of Colloid and Interface Science 26 (1968) 70.

(7) M Harada, A Shioi, K Matsumoto: Phase equilibrium of Sodium Bis(2-ethulhexyl) Phosphate/water/n-heptane/sodium chloride microemulsion. Journal of Physical Chemistry 95 (1991) 7495.

(8) H-F Eicke, M Borkovec, B Das-Gupta: Conductivity of water-in-oil microemulsions: a quantative change fluctuation model. Journal of Physical Chemistry 93 (1989) 314.

(9) H Kunieda, K Shinoda: Solution behavior of Aerosol OT/Water?Oil System. Journal of Colloid and Interface Science 70 (1979) 577.

(10) SP Moulik, BK Paul: Structure, dynamics and transport properties of microemulsion. Advances in Colloid and Interface Science 78 (1998) 99.

(11) JE Marszalek, JA Pojman, KL Aultman, CE Hoyle, JB Whitehead: Humidity-Responsive Polymeric Films Based on AOT-Water Reverse Microemulsions. Journal of Applied Polymer Science 106 (2007) 1957.

(12) EW Kaler, KV Schubert, KM Lusvardi: Polymerization in nonaqueous microemulsions. Colloid & Polymer Science 274 (1996) 875.

(13) H-P Hentze, EW Kaler: Polymerization of and within self-organized media. Current Opinion in Colloids and Interface Science 8 (2003) 164.

(14) X Li, SP Xia, WJ Zeng, WY Zhang, SX Dong: Monitor of Polymerization of Inverse Microemulsion Containing Methyl Methacrylate and Acrylic Acid. Chinese Chemical Letters 17 (2006) 247.

(15) J Jang: Conducting Polymer Nanomaterials and their applications. Advance Polymer Science 199 (2006) 189.

(16) F Yan, G Xue: Journal of Material Chemistry 9 (1999) 3035.

(17) V Tasakova, S Winkels, JW Schultze: Electrochim Acta 46 (2000) 759.

(18) T Kawai, Y Usui, K Kon-No: Synthesis and growth mechanism of GeO 2 particles in AOT reversed micelles. Colloids Surf A 149 (1999) 39.

(19) Z Chen, S Li, Y Yan: Synthesis of Template-Free Zeolite Nanocrystals by Reverse Microemulsion-Microwave Method. Chemistry of Materials 17 (2005) 2262.

(21) HM Cheung, M Sasthav, WR Palani Raj: Polymerization of single-phase microemulsions: dependence of polymer morphology on microemulsion structure. Polymer 36 (1995) 2637.

(22) G Zhang, X Xu, J Tang, H Liu, H Ge, Z Zeng: Formation of Microporous Polymeric Materials by Microemulsion Radiation Polymerization of Butyl Acrylate. Journal of Applied Polymer Science 77 (2000) 1989.

(23) HM Cheung, M Sasthav: Characterization and Polymerization of Middle-Phase Microemulsion in Styrene/Water System. Langmuir 7 (1991) 1378.

(24) J Texter, F Yan: Solvent-Reversible Poration in Ionic Liquid Copolymers. Angewandte Chemie 46 (2007) 2440.

(25) J Texter, L Ge, TH Mourey, TG Bryan: Polymerizable Bis(2-ethylhexyl)sulfosuccinate: Application in Microemulsion Polymerization. Langmuir 20 (2004) 11288.

(26) B Tieke, W Pyckhout-Hintzen, M Dreja: Copolymerization behaviour and structure of styrene and polymerizable surfactants in three-component cationic microemulsion. Macromolecules 31 (1998) 272.

(27) CA Guymon, CL Lester, SM Smith, CC D.: Physical Properties of Hydrogels Synthesized from Lyotropic Liquid Crystalline Templates. Chemistry of Materials 15 (2003) 3376.

(28) JG Barker, CJ Glinka, JJ Moyer, MH Kim, AR Drews, M Agamalian: Journal of Applied Crystallography 38 (2005) 1004.

(29) SR Kline: Reduction and analysis of SANS and USANS data using IGOR Pro Journal of Applied Crystallography 39 (2006) 895.

(30) M Nagao, H Seto, M Shibayama, NL Yamada: small-angle neutron scattering of droplet density dependence of the water-in-oil droplet structure ina ternary microemulsion. Journal of Applied Crystallography 36 (2003) 602.

(31) M Kotlarchyk, N Quirke, JS Huang, SA Safran, MW Kim, GS Grest: Attractive Interactions in Micelles and Micreomulsions. Physical Review Letters 53 (1984) 592.

(32) R Strey, J Winkler, L Magid: Small-Angle Neutron Scattering from Diffuse Interfaces. 1. Mono- and Bilayers in the water-octane-C12E5 system. Journal of Physical Chemistry 95 (1991) 7502.

(33) G Capuzzi, F Pini, CMC Gambi, M Monduzzi, P Baglioni, J Teixeira: Small-Angle Neutron Scattering of Ca(AOT)2/D2O/Decane Microemulsion. Langmuir 13 (1997) 6927.

(34) CMC Gambi, R Giordano, M Laurati, L Lanzi, F Pini, P Baglioni: SANS analysis of perfluoropolyether water-in-oil microemulsions by hard sphere and adhesive hard sphere potentials. Applied Physics A 74 (2002) S377.

(35) BH Robinson, RK Heenen, J Eastoe, DC Steytler, G Fragneto: Small-angle neutron scattering from novel bis-2-ethylhexylsulphorosuccinate microemulsions: evidence for non-spherical structures. Physica B 180&181 (1992) 555.

(36) M Nagao, H Seto, D Okuhara, H Okabayashi, T Takeds, M Hikosaka: A small-angle neutron-scattering study of the effect of pressure on structures in a ternary microemulsion system. Physica B 241-243 (1998) 970.

(37) B Simmons, GC Irvin, S Li, V John, GL McPherson, N Balsara, V Agarwal, A Bose: Langmuir 18 (2002) 624.

(38) B Simmons, V Agarwal, GL McPherson, V John, A Bose: Small Angle Neutron Scattering Study of Mixed AOT + Lecithin Revese Micelles. Langmuir 18 (2002) 8345.

(39) M Kotlarchyk, SH Chen, JS Huang: Temperature Dependence of Size and Polydispersity in a Three-Component Microemulsion by Small Angle Neutron Scattering. Journal of Physical Chemistry 86 (1982) 3273.

(40) M Kotlarchyk, SH Chen: Analysis of small angle neutron scattering spectra from polydisperse interacting colloids. Journal of Physical Chemistry 79 (1983) 2461.

(41) M Kotlarchyk, SH Chen, JS Huang, MW Kim: Structure of 3-Component Microemulsions in the Critical Region Determined by Small-Angle Neutron-Scattering. Physical Review A 29 (1984) 2054.

(42) M Kotlarchyk, SH Chen, JS Huang, MW Kim: Structure of dense sodium di-2-ehtylsulfosuccinate/D2O/Decane microemulsions. Physical Review Letters 53 (1984) 941.

(43) M Kotlarchyk, S-H Chen, JS Huang: Critical behavior of a microemulsion studied by small-angle neutron scattering. Physical Review A 28 (1983) 508.

(44) M Kotlarchyk, JS Huang, SH Chen: Structure of AOT Reversed Micelles determined by SANS. Journal of Physical Chemistry. 89 (1985) 4382.

(45) SH Chen, J Rouch, F Sciortino, P Tartaglia: Static and dynamic properties of water-in-oil microemulsions near the critical and percolation points. Journal of Physics: Condensed Matter 6 (1994) 10855.

(46) J Eastoe, KJ Hetherington, D Sharpe, J Dong, RK Heenen, DC Steytler: Films of di-chained surfactants in microemulsions. Colloids and Surfaces A: Physicochemical and Engineering Aspects 128 (1997) 209.

(47) M Nagao, S Okabe, M Shibayama: Small-angle neutron scattering study on a structure of microemulsion mixed with polymer networks. The Journal of Chemical Physics 123 (2005) 144909-1-8.

(48) JK Percus, GJ Yevick: Analysis of classical statistical mechanics by means of collective coordinates. Physical Review 110 (1958) 1.

(49) E Caponetti, D Chillura-Martino, F Ferrante, L Pedone, A Ruggirello, VT Liveri: Structure of Urea Clusters Confined in AOT Reverse Micelles. Langmuir 19 (2003) 4913.

(50) B Simmons, C Taylor, F Landis, VT John, G McPherson, D Schwartz, RB Moore: Microstructure Determination of AOT+ Phenol Ogranogels Utilizing Small Angle X-Ray Scattering and Atomic Force Microscopy. Journal of American Chemical Society 123 (2001) 2414.

(51) M Kotlarchyk, S-H Chen, JS Huang, MW Kim: Structure of dense Sodium Di-2-ethylsulfosuccinate/D2O/Decane Microemulsions. Physical Review Letters 53 (1984) 941.

(52) S-H Chen, T-L Lin, JS Huang: Physics of Complex and Supermolecular Fliuds, Safran and Clark, Eds.; Wiley Interscience Publication: J. Wiley & Sons, New York, 1987.

(53) A Maitra: Determination of size parameters of water-Aerosol OT-oil reverse micelles from their Nuclear Magnetic Resonance Data. Journal of Physical Chemistry 88 (1984) 5122.

(54) H-F Eicke, M Zulauf: Inverted micelles and microemulsions in the ternary system H2O/Aerosol-OT/Isooctane as studied by photon correlation spectroscopy. Journal of Physical Chemistry 83 (1979) 480.

(55) M Teubner, R Strey: Origin of the scattering peak in microemulsions. Journal of Chemical Physics 87 (1987) 3195.

(56) R-J Roe: Methods of X-ray and Neutron Scattering in Polymer Science, Oxfod University Press, New York, 2000.

(57) K-Q Xia, Y-B Zhang, P Tong, C Wu: Interactions in mixtures of a microemulsion and a polymer. Physcal Review E 55 (1997) 5792.

(58) M Singh, G Tan, V Agarwal, G Fritz, K Maskos, A Bose, V John, G McPherson: Strucrual evolution ofa two-component organogel. Langmuir 20 (2004) 7392.

CHAPTER V

INTERACTIONS OF MICROEMULSIONS WITH POLYMERS

Introduction

The main challenge we were facing was the question of what causes the aggregation of the aqueous phase in the film. As discussed in the previous chapter, the polymerization of the microemulsion caused an aggregation of the aqueous phase. It was not clear if this phenomenon was caused by a phase separation or an exclusion process. If it was a phase separation, we wanted to establish the point in the reaction at which it occurred. To solve this problem, we examined how the microemulsion was changed by the presence of a polymer formed from the same monomer as the oil part of the microeulsions. We wanted to learn how the size distribution of the micelles in the microemulsions was affected by the presence of the polymer. This analysis would provide a snapshot of a specific conversion of polymerization and would simulate the effect of a reversibly performed reaction. We aimed to evaluate the kinetic influence of the polymerization process by adding polymers with different molecular weights to microemulsions with varying water content and micellar size.

Colloid-polymer mixtures have wide-ranging applications, both academically and industrially.(1,2) Since a large number of commercial products contain both colloids and polymers, a thorough understanding of the structure and interactions of such mixtures is essential. There also exists an interest in studying the phase behavior of various binary mixtures of colloidal particles and polymer molecules.

The microemulsions are used as model systems to study and examine colloid-polymer systems. For mixtures of a colloid and a non-absorbing polymer, it has been assumed(3,4) that the colloidal particles are hard spheres and that the polymer molecules behave as hard spheres towards the colloidal particles. The hard-sphere-like interaction between the colloidal particles and the polymer molecules results in a spherical shell around each of the colloidal particles, within which the center of mass of the polymer molecules is excluded. The free energy of the mixture can be reduced by grouping the colloidal particles together. In that way they share depletion volumes. This gives rise to an effective attraction between the colloidal particles. Depletion attraction controls the phase stability of many colloid-polymer mixtures, which are of direct interest to industries.(5) Thus, in a mixture of a colloid and a non-adsorbing polymer, the potential U(r) can develop an attractive well because of the depletion effect. The polymer chains are expelled from the region between two colloidal particles when their surface separation becomes smaller than the size of the polymer chains. The exclusion of polymer molecules from the space between the colloidal particles leads to an unbalanced osmotic pressure difference. This pushes the colloidal particles together and results in an effective attraction between the two colloidal particles. If the attraction is large enough, phase separation occurs in the colloid-polymer mixture.

Neutron(6,7) and light scattering(8) measurements have shown that the bare interaction potential between the droplets can be described by hard-core repulsion plus an attractive square well.(9)

An effective interaction potential U(r) for the colloidal particles in a non-absorbing polymer solution was derived in late 1950s. It assumed that the colloidal particles are

hard spheres, and that the polymer molecules behave as hard spheres towards the colloidal particles but are able to freely penetrate each other. Under this approximation, U(r) takes the form (3,10)

$$U(r)=\begin{cases} +\infty, & r \le \sigma \\ -\Pi_p V_0(r), & \sigma < r \le \sigma + 2R_g \\ 0, & r > \sigma + 2R_g \end{cases} \qquad \text{Equation 5.1}$$

where σ is the particle diameter, Π_p is the osmotic pressure of the polymer molecules, and R_g is their radius of gyration. The volume of the overlapping depletion zones, $V_0(r)$, is given by

$$V_0(r) = v_p\left(\frac{\delta}{\delta-1}\right)^3\left[1-\frac{2r}{3\sigma\delta}+\frac{1}{2}\left(\frac{r}{\sigma\delta}\right)^3\right] \qquad \text{Equation 5.2}$$

where v_p is the volume occupied by a polymer chain and

$$\delta = 1+\frac{2R_g}{\sigma} \qquad \text{Equation 5.3}$$

When potential U(r) is composed by a hard core plus a weak attractive tail, the direct correlation function, C(r), can be obtained under the mean spherical approximation, which is a perturbative treatment to the Percus-Yevick equation.(11)

$$C(r)=\begin{cases} C_{HS}(r), & r \le \sigma \\ -\dfrac{U(r)}{k_B T}, & r > \sigma \end{cases} \qquad \text{Equation 5.4}$$

In the Equation 5.4, k_BT is the thermal energy and $C_{HS}(r)$ is a known direct correlation function for a simple hard-sphere system.

In the following equation, the polymer volume fraction is expressed relative to the overlap concentration:

$$\Phi_p = \frac{c}{c^*} \text{ with } c^* = \frac{3MW}{4\pi R_g{}^3 N_A} \qquad \text{Equation 5.5}$$

The volume fraction occupied by the monomers of the chain is Φ, and the monomer volume fraction at c* is Φ^*.

Mutch et al.(12) looked at partial structure factors derived from SANS data for a mixture of a non-absorbing polymer and a microemulsion. They presented a plausible physical model that explained the increase in the polymer correlation length upon the addition into a microemulsion. In the model, the colloidal particles are beginning to cluster and the polymer is wrapping around these clusters. This results in an overall worsening of the polymer dissolution.

When a block copolymer is mixed with a w/o microemulsion it can induce an ordering of the microemulsion's structure. Vollmer et al.(13) showed that the addition of copolymer was an efficient method to stabilize the organization of a microemulsion into a large inter-lamellar spacing. They assumed that the observed ordering was closely related to the connecting of the microdomains via polymer chains. The addition of the polymer results in an increase in the viscosity of the system. The increase in viscosity is related to the formation of a connected network, especially when part of the polymer dissolves in the aqueous phase.(14)

Water-in-oil microemulsions are used as "complex solvents" for ABA triblock copolymers. When copolymers which contain hydrophilic poly(oxyethylene), POE,

blocks and a hydrophobic midblock (ex. polyisoprene) are dissolved in a microemulsion, such polymers so-called mesophases can be formed. The hydrophilic POE blocks incorporate into the aqueous cores of the micelles while the oil-soluble midblocks bridge the water domains.(15)

Nagaran(16) predicted the structural transitions in microemulsion systems induced by nonionic polymers. According to this author, the polymer induced transitions because it can associate with the surfactant aggregates. Through theoretical calculations, he predicted five potential phase transitions in polymer-microemulsion systems: (1) o/w droplet microemulsions in the presence of a polymer will remain o/w droplet microemulsions, but the number density of the droplets will increase. (2) bicontinuous microemulsions will transform into o/w droplet-microemulsion systems. (3) w/o droplet microemulsions phase invert to o/w droplet microemulsions, and droplet radius and the number of surfactant molecules in the film region of a droplet will decrease. (4) w/o droplet microemulsion systems can also transform into bicontinuous microemulsions. (5) w/o droplet microemulsions can remain w/o microemulsions; however, the amount of water that is solubilized per unit volume of the surfactant, the radius of the water core of the droplet, and the number of surfactant molecules in the film region of a droplet will all increase noticeably.

Polymer molecular weight can be evaluated by the addition of the polymer to a microemulsion. This method was introduced as a quick and easy evaluation method for a known polymer-microemulsion system, and as a replacement for the more costly and complicated traditional methods.(17) The microemulsion method gives the weight-average molecular weight of the polymer.

Experimental

Materials

The following chemicals were used as received: sodium bis(2-ethylhexyl) sulfosuccinate (AOT) (>96%) from Aldrich, dodecyl acrylate (DDA) (90%) from Sartomer, and 1,6-hexanediol diacrylate (HDDA) (>99%) from Cytec Surface Specialties. The poly(dodecyl acrylate)s, polyDDAs, were prepared, purified and characterized by Brian Zoltowski(18). Characteristics of the polymers are presented in Table 5.1.

Preparation of Microemulsions

Two sets of microemulsions were prepared. The first set had a constant water-to-surfactant ratio (W) of 10 and water content from 5 to 30 wt% with respect to monomers. The composition of this set is presented in Table 5.2. In the second set of microemulsions, the aqueous fraction was kept at 30 wt%, and W was varied between 3.5 and 20. The aqueous fraction is also called mass fraction of droplets, δ_d, and is defined as

$$\delta_d = \frac{(\delta_w + \delta_s)}{(\delta_w + \delta_s + \delta_m)} \qquad \text{Equation 5.1}$$

where δ_w, δ_s, and δ_m are the total mass fraction of water, surfactant, and monomer in the microemulsion. The composition of these microemulsions is presented in Table 5.3.

All of the microemulsions were prepared according to the following procedure: To prepare a microemulsion with 10% water relative to the monomers, 5.48 g (0.012 mol) of AOT was added to 22.48 mL of a monomer mixture, consisting of 18.87 g (0.08 mol) of

dodecyl acrylate (DDA) and 1.15 g (5 10^{-3} mol) of 1,6-hexanediol diacrylate (HDDA). The solution was allowed to mix for up to 24 hours, or until all the AOT was fully dissolved. Next, the deionized water was added (2.22 mL) to form a microemulsion with a water-to-surfactant ratio, W, of 10. The composition of 5 vol % of crosslinker (HDDA) with respect to DDA was kept constant for all of the formulations.

Cloud Point Determination

To determine a cloud point for each microemulsion, a small amount of poly(dodecyl acrylate) was added in a step-wise manner to a known mass of a given microemulsion. PolyDDA samples are thick liquids with viscosity ranging from 0.3 X 10^3 to 4.3 X 10^3 mPa·s at 80 °C; thus, the size of the added polymer droplet was limited to 0.01±0.005 g. The change in the clarity of the microemulsion was determined by visual observation. When the microemulsion became turbid, it was shaken vigorously and left to sit for a few hours. If, after that time, it was still turbid, the amount of added polymer was recorded as the critical concentration for that specific composition of the microemulsion.

Instruments and Methods

Thermal gravimetric measurements were obtained using a TGA 2050 Thermogravimetric Analyzer from TA instruments. The composition evaluation was done using the quasi-isothermal (stepwise) method. The method used a temperature range from room temperature (about 15° C) to 600° C, and a heating rate of 5° C min^{-1}. Whenever the rate of mass change of the sample exceeded 0.5 % min^{-1}, an isothermal

method was applied; the heat ramp was employed again whenever the rate of weight change fell below 0.05 % min^{-1}.

Results and Discussion

Since we were interested in the processes occurring during the polymerization of microemulsions, we added a polymer in a step-wise manner to a microemulsion of polymerizable monomers. The microemulsions used in the study had an oil phase composed of dodecyl acrylate (DDA) with 5.7 wt% of 1,6-hexandiol diacrylate. The polymer of choice was poly(dodecyl acrylate), polyDDA. A set of polymers with varying weight-average molecular weights was available in our lab.(18) A list of the polymers chosen for this study can be seen in Table 5.1. PolyDDA is a viscous liquid, thus in this study, it was used without additional solubilization.(19) DDA is a good solvent for polyDDA. The addition of a small amount of diacrylate had no effect on the solubility of the polyDDA.

There were two sets of microemulsions prepared for this study. In the first set, the size of the water micelles was kept constant by designing the microemulsions with a water-to-surfactant ratio of 10. Using equation 2.17, from the previous chapter, we estimated the radius of the water micelles to be close to 2.6 nm. The parameter that was varied was the amount of water; from 5 to 30 wt% with respect to the oil phase. The composition of the set is listed in Table 5.2. The second set had an aqueous phase, consisting of water and surfactant, kept at constant value of 30 wt %. The W was varied, which should have resulted in the size of water radii between 1.7 and 3.9 nm (Table 5.3).

All the microemulsions were prepared at least a day before the experiment of cloud point detection was carried out. The formulations with W of 17, 18, 19, and 20 did not form clear microemulsions, the solution remained turbid even upon vigorous, extended mixing. As can be seen in Figure 5.1, the last ▲ points, representing these three microemulsions, are on the border and beyond of the L_2 region in the phase diagram. These microemulsions were used in the cloud point experiment to examine the polymer influence on stabilization of the microemulsions.

The addition of polymer was done in a step-wise manner and after each addition the sample was shaken and examined visually. The microemulsion-polymer mixture samples were found to become turbid when the polymer concentration exceeded a critical concentration. The critical concentration was expressed in g/cm^3. The turbidity of the sample represented phase separation of the microemulsion. In this setting, the phase separation means a transition from a droplet microemulsion, which is a clear, optically one-phase solution, into a mixture of two phases that are not compatible, and are cloudy when shaken. If the turbid solution was left resting it separated, with aid from gravity, into two distinct layers of liquids.

The composition of the two layers that appeared upon phase separation was evaluated with quasi-isothermal TGA. The resulting plots are presented in Figure 5.2 and Figure 5.3. An addition of 1.15 g of the polymer (entry #2 from Table 5.1) to 5.51 g of the 10%-microemulsion (W = 10) resulted in 0.16 g cm^{-3} polymer concentration, and phase separation into two unequal layers. The top layer was only a very small part of the whole sample. As a result, the separation of the two was difficult. Nevertheless, it can be seen that the bottom layer (plot b in Figure 5.2) had less polymer and more surfactant

then the top stratum (plot c in Figure 5.2). The difference in the composition of the two layers is apparent in Figure 5.3. The bottom stratum from a phase-separated microemulsion (W = 19) had 13 % water, 50 % monomers, 24 % AOT and 7 % polymer. In comparison, the top layer had 4 % water, 66 % monomers, 12 % AOT and 15 % polymer. The overall composition at the cloud point was the following: 12 % water, 65 % monomers, 16 % AOT and 7 % polymer. The compositional shift upon phase separation is rather drastic. Most of the water and surfactant was excluded from the polymer-rich top layer. Only a small fraction of the polymer stayed in the bottom stratum.

We assume that the bottom layer consists of a droplet microemulsion structure with the small amount of polyDDA dissolved in the oil-continuous phase. It is believed that the water micelles grow considerably upon polymer addition as seen in the literature.(14) Moreover, the presence of the bicontinuous phase, with its characteristic appearance, supports our assumption. It is also in agreement with 4^{th} and 5^{th} type of Nagaran(16) transitions described earlier.

With increasing water-to-surfactant ratio, the amount of the polymer required to induce phase separation steeply decreased. A phase diagram as a function of polymer concentration is shown in Figure 5.4. The polyDDA used for this analysis had a molecular weight of 31,000. Many of the microemulsions exhibited an additional transition, which we recognize as the bicontinuous phase. It emerged between the droplet microemulsion phase and the two-phase region. The appearance of the microemulsion in the bicontinuous phase can be described as hazy with bluish tone. Left for an extended time, a microemulsion with this appearance would not separate into distinct layers.

When the water amount was favorable, the bicontinuous phase existed over a larger range of polymer concentrations. The phase boundary between the bicontinuous phase and the two-phase region can be compared to the phase boundary in pure microemulsion systems. This boundary is called the solubilization limit. It has been shown that at the composition of the solubilization limit the inter-droplet attractions are at a minimum.(20) Thus we deduce that the presence of the polymer decreases the inter-droplet attractions or even introduces "repulsive" interactions. The polymer dissolves in the oil-continuous phase without associating with the droplets.

The formulation with 15 wt% of water with respect to monomers and W = 17 was an unstable microemulsion. When stirred it had an opaque color that disappeared when allowed to settle. When a small amount of the polymer was added it became a clear microemulsion. The polymer induced the formation of a microemulsion. The increase in the microemulsion's ordering was previously observed upon addition of amphiphilic block copolymers.(7,13,21) In our case, the polymer was a hydrophobic homopolymer, most likely with a linear structure of the chain. In the literature, when a hydrophobic polymer is added to a microemulsion (ex. poly(dodecyl methacrylate) to AOT/water/isooctane)(8) it caused phase separation. To our knowledge, there is no indication in the literature of a microemulsion-structure promotion upon including a non-adsorbing polymer to the system.

From Figure 5.4 it can be seen that the segregation, a result of the "repulsive" interactions, for the polymer and micelles is stronger for larger droplets. To induce phase separation, microemulsions with large droplets (W = 15 and 16), required a polymer concentration that is four times smaller than the polymer concentration necessary for the

microemulsions with the smallest droplets (W = 3). For this microemulsion with 4.5 % of water and W = 3, the polymer concentration inducing the phase separation was equal to 0.4 g/cm^3. We understand that the high critical concentration is related to the following facts: the small water droplets are "diluted" in the "sea" of monomer-AOT mixture; the surfactant is compatible with the polymer and its presence does not cause immediate unfavorable interactions. In other words, the polyDDA is readily dissolved to high concentrations in the monomer-AOT "soup", and not affecting the state of the micelles. In addition, the droplets radius is predicted to be on order of 1.7 nm, thus even upon coalescence of the micelles, as seen in literature,(14) they do not scatter light.

Figures 5.4 and 5.5 present the critical polymer concentration for microemulsions, which have the same micellar size, as a function of the polymer molecular weight, and water concentration, respectively. The molecular weight of the polymer had a strong influence on the critical concentration of the polymer. However, that influence was strictly related to the water amount in the microemulsion. Again, the microemulsion with the smallest water content needs the highest polymer load to induce phase separation. Microemulsions with higher water content, 20, 25 and 30 wt%, were sensitive to the polyDDA chain length. As explained in Chapter 4 at higher water loads the droplets are densely packed and strongly interact with each other. The addition of the polymer introduced the "repulsions" between polymer chains and water droplets. In response, the micelles effectively attracted each other and separated out to form a polymer-poor phase. Large length polymer chains were more successful in this process. With longer chains they have larger radii of gyration, thus filling the monomer volume between micelles and pushing the water droplets together more easily. Similarly, Lynch et al.(22) saw an

increase in the two-phase area of the phase diagram with an increase in molecular weight of the added polymer (polystyrene in AOT/water/cyclohexane microemulsions).

If we consider other possibility, namely that the polyDDA adsorbs to the surface of the micelles, we need to look into the theory of polymeric dispersants.(23,24) We think about the free energy of interaction between two approaching particles. Both are bearing polymer adsorbed on the surface of the hard-sphere. Next, we assume that the polymeric layer around the particle is interpenetrable whereas the particles are impenetrable. The total change in free energy per unit area, when the two particles approach each other, is given by the sum of three terms: an attractive term due to van der Waals attraction between the surfaces; a repulsive term due to the loss of configurational entropy; a repulsive term due to the osmotic pressure effect. The osmotic pressure effects, caused by the change in free energy of mixing between the polymer and the solvent, result as the variation in the density of chain segments. For high surface coverage and high molecular weight of the adsorbed chains, the "repulsive" forces are dominant. This steeply increases the interaction energy which decreases the separation distance to near $2R_g$ of the unperturbed chains.

In this approach, the high molecular polymer would also have a higher impact on the microemulsion with high droplet density. Likewise, the addition of polymers with an increasing molecular weight would affect the microemulsion with a low water concentration. In other words, in the framework of this theory, if the polymer were to be adsorbed on the surface of the micelles, there would be less long-chain polymer required than shorter-chain polymer to cause phase separation in all of the microemulsions. However, our results show that approximately the same concentration of the polymer,

regardless of molecular weight, triggers the phase transition in the water-poor formulation.

Conclusions

In this chapter we looked at the interactions between acrylate based microemulsions and the added polymer, poly(dodecyl acrylate). The addition of the polymer to the stable microemulsions induces phase transition into a bicontinuous phase and then into a two-phase system. The newly formed system consists of a polymer-rich top phase and a microemulson-rich bottom phase.

This two-phase separation occurred in all of the microemulsions studied. Depending on the composition of the microemulsion, there was a difference in the polymer load necessary to cause phase separation. For microemulsions with a low water content a high concentration of the polymer was required to induce the separation. In contrast, only a small amount of polymer was needed to disrupt the one-phase droplet arrangement in microemulsions with a high water load.

The polymer chains do not adsorb to the surface of the micelles. They are freely dissolved in the oil-continuous media of the microemulsions. Their presence, however, introduces repulsions that cause the exclusion of the micelles into a separate phase.

Now we need to connect this conclusions with the findings described in Chapter 2. The films formed from the microemulsions with large water content had larger aqueous domains than the films formed from water-poor microemulsions. This occurrence can be understood with the knowledge that the water-rich microemulsions are more sensitive to the polymer's presence. In these microemulsions, the phase separation, which is an

exclusion of the aqueous part from the system, appears at very small polymer loads. As a result, the water phase aggregates into larger domains. This occurs not only due to the favorable lowering of the energy as viewed from thermodynamic approach, but also due to "repulsive" interactions between polymer and aqueous domains during the rapid formation of the material.

We have shown here that the polymer induces phase transitions. Thus, the aggregation of the aqueous phase (part of the system) observed in the opaque films is caused by a phase (state of the system) separation phenomenon. The films represent a frozen-in- time-phase-separated systems. If not for the crosslinking of the material the polymer and the aqueous phase would be driven to physically separate. The presence of the crosslinking creates an insuperable kinetic barrier; which forces the polymer and AOT-water phases to coexist as a single film. In other words, the films are maintained far from equilibrium.

Table 5.1. Parameters of the polymers used in the study

Entry	MW	Polydispersity	Viscosity at 80°C (mPa s)	Density at 25°C (g/ml)
1	18 000	2	296	0.93
2	25 000	2	4356	
3	31 000	2.1	680	
4	44 000	2.4	1050	

Data from (18)

Table 5.2. The composition of microemulsions with water-to-surfactant ratio, W = 10

Microemulsion	HDDA (wt%)	DDA (wt%)	AOT (wt%)	H_2O (wt%)	H_2O (%)*	W**
5%	0.05	0.80	0.11	0.04	0.05	10.02
10%	0.04	0.68	0.20	0.08	0.10	10.00
15%	0.04	0.59	0.27	0.11	0.15	9.99
20%	0.03	0.50	0.33	0.13	0.20	10.10
25%	0.03	0.44	0.38	0.15	0.25	9.99
30%	0.02	0.38	0.43	0.17	0.30	10.00

*with respect to monomers

**calculated value

Table 5.3. The composition of microemulsions with the mass fraction of droplets maintained at 30

Microemulsion	HDDA (wt%)	DDA (wt%)	AOT (wt%)	H_2O (wt%)	H_2O (%)*	W**
w=3	3.93	65.80	26.94	3.33	4.55	3.05
w=5	3.92	65.26	25.70	5.12	6.89	4.92
w=7	3.97	66.01	23.50	6.51	8.51	6.84
w=10	4.08	66.03	21.31	8.57	10.89	9.93
w=12	3.89	65.98	20.31	9.82	12.32	11.94
w=15	4.14	65.80	18.73	11.34	13.95	14.95
w=16	3.98	65.73	18.18	11.85	14.52	16.09
w=17	3.96	65.76	17.75	12.19	14.89	16.96
w=18	3.91	65.71	17.34	12.58	15.30	17.91
w=19	3.98	65.75	16.93	13.02	15.74	19.00
w=20	4.04	65.74	16.54	13.27	15.98	19.81

*with respect to monomers

**calculated value

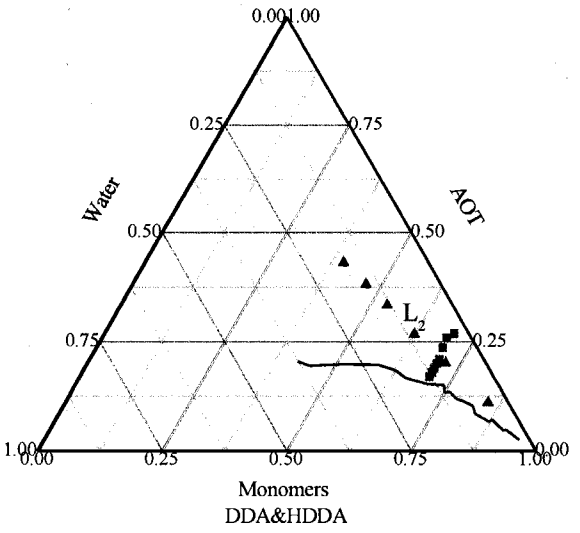

Figure 5.1. Ternary phase diagram of AOT-water-DDA&HDDA. (■) microemulsions with W = 10, (▲) microemulsions with 30 wt% of aqueous phase, area L_2 is the microemulsion region.

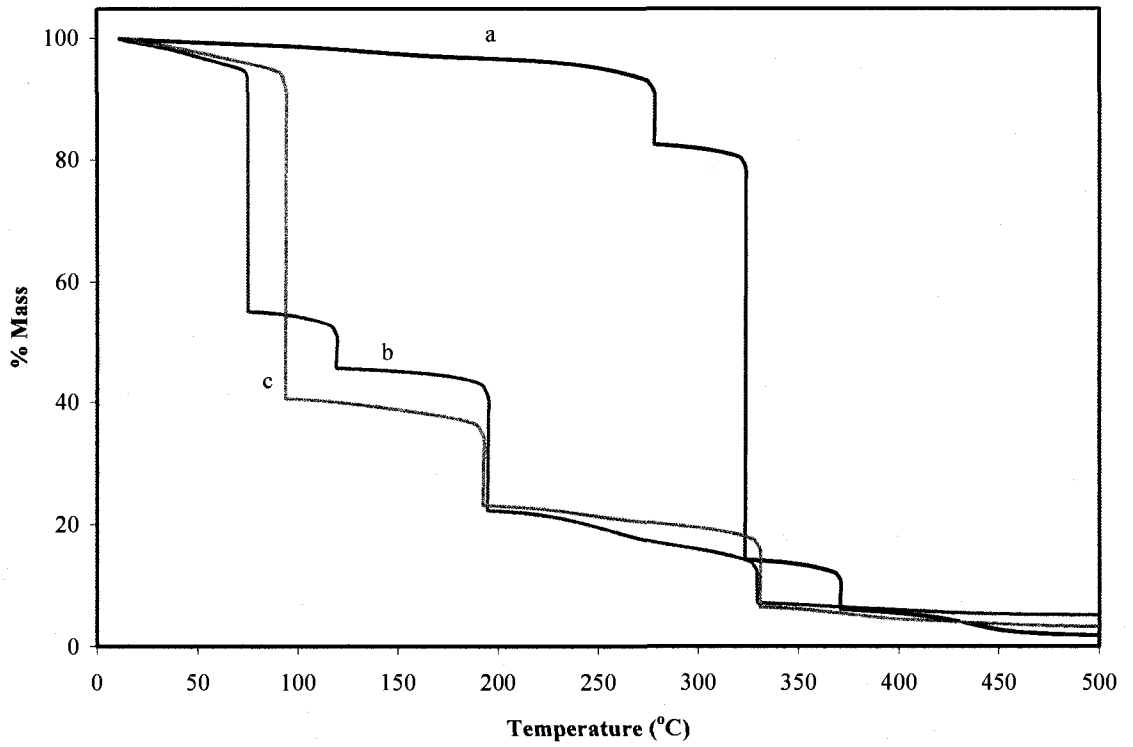

Figure 5.2. Thermal gravimetric analysis of the two phases that resulted from addition of the polymer(entry #2 from Table 5.1) to the 10% microemulsion; (b) bottom phase, (c) top phase. Additionally, trace (a) is the decomposition of pure polyDDA.

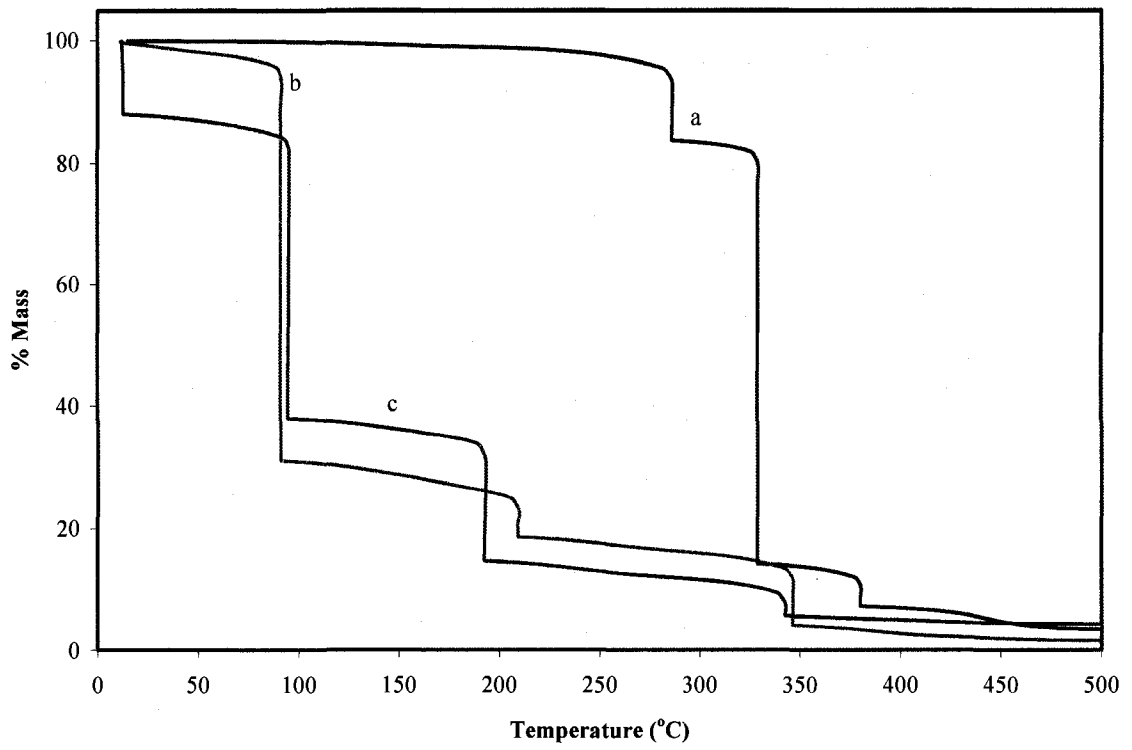

Figure 5.3. Thermal gravimetric analysis of the two phases that resulted from addition of the polymer(entry #3 from Table 5.1) to the W = 19 microemulsion; (b) bottom phase, (c) top phase. Additionally, trace (a) is the decomposition of pure polyDDA

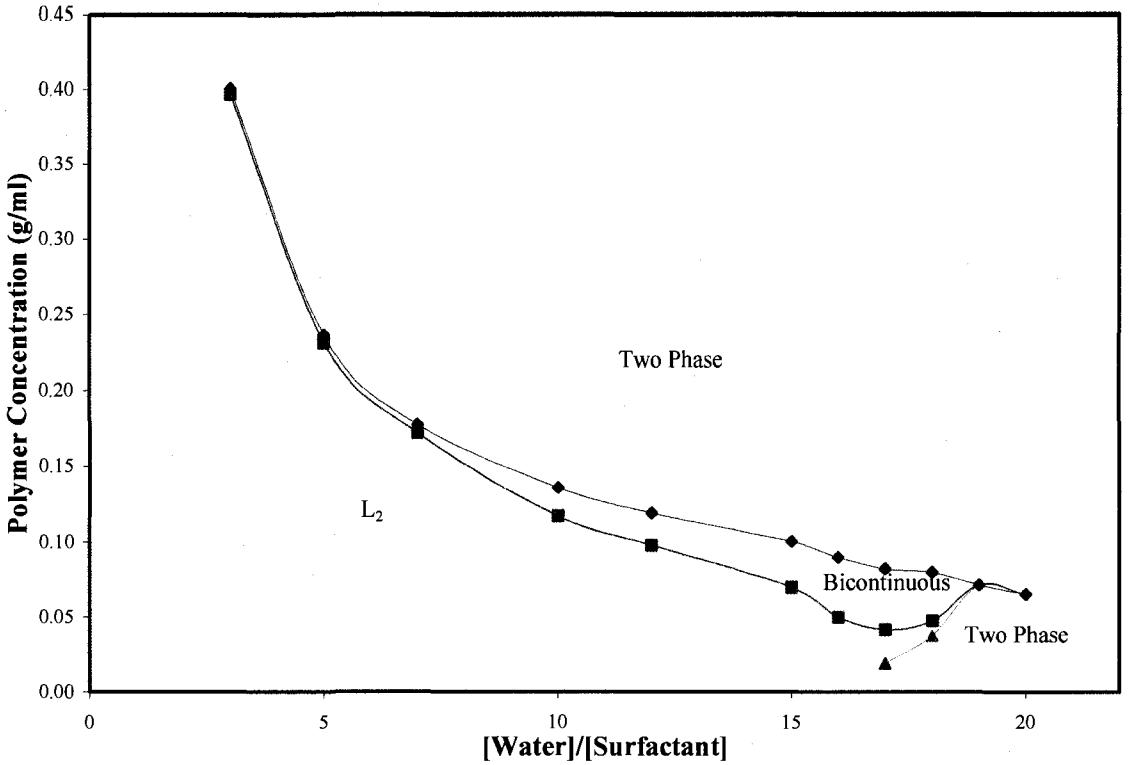

Figure 5.4. Critical polymer concentration as a function of W at 20°C.

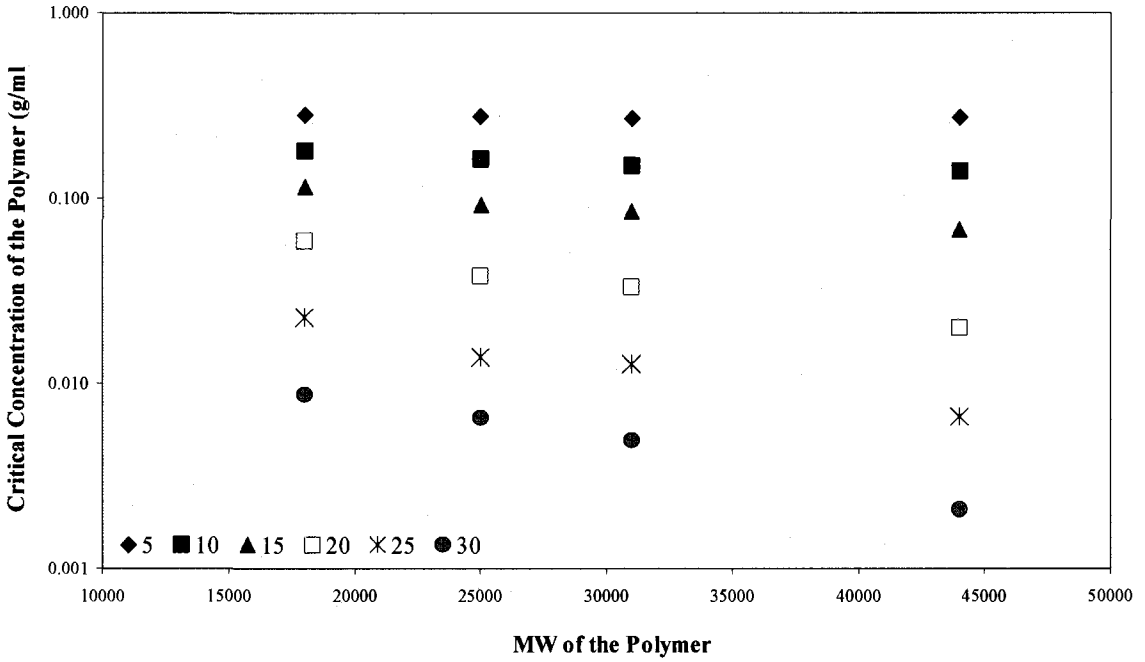

Figure 5.5. Critical polymer concentration as a function of the polymer molecular weight.

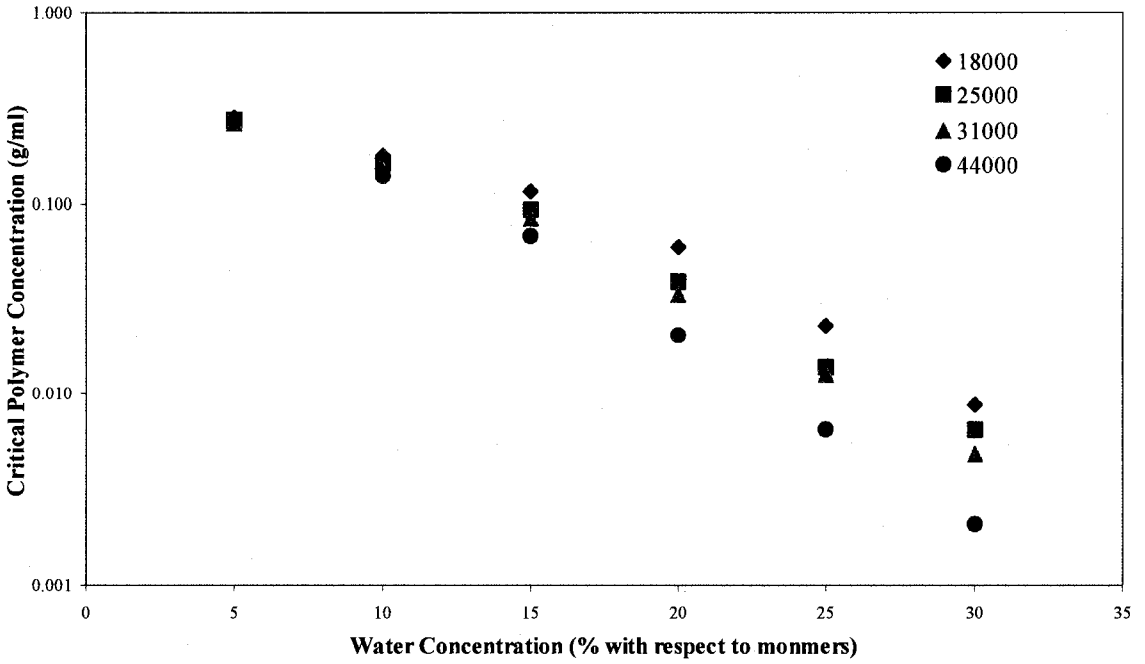

Figure 5.6. Critical polymer concentration as a function of the water content in the microemulsion.

References

(1) KJ Mutch, JS van Duijneveldt, J Eastoe: Colloid-polymer mixtures in the protein limit. Soft Matter 3 (2007) 155.

(2) L Piculell, K Thuresson, B Lindman: Mixed solutions of surfactant and hydrophobically modified polymer. Polymers for Advanced Technologies 12 (2001) 44.

(3) S Asakura, F Oosawa: Interaction between particles suspended in solutions of macromolecules. Journal of Polymer Science 33 (1958) 183.

(4) M Fuchs, KS Schweizer: Structure of collod-polymer suspensions. Journal of Physics: Condensed Matter 14 (2002) R239.

(5) X Ye, T Narayanan, P Tong, JS Huang, MY Lin, BL Carvalho, LJ Fetters: Depletition interaction in colloid-polymer mixtures. Physical Review E 45 (1996) 6500.

(6) M Kotlarchyk, S-H Chen, JS Huang, MW Kim: Structure of dense Sodium Di-2-ethylsulfosuccinate/D_2O/Decane Microemulsions. Physical Review Letters 53 (1984) 941.

(7) S Maccarrone, H Frielinghaus, J Allgaier, D Richter, P Lindner: SANS study of polymer-linked droplets. Langmuir 23 (2007) 9559.

(8) A Holmberg, L Piculell, P Schurtenberger, U Olsson: Oil-continous microemulsion mixed with an amphiphilic graft copolymer or with the parent homopolymer. Polymer-droplet interactions as revealed by phase behaavior and light scattering. Colloids and Surfaces A 250 (2004) 325.

(9) B Lemaire, P Bothorel, R D.: Micellar interaction in water-in-oil microemulsions. 1 Calculated ineraction potential. Journal of Physical Chemistry 87 (1983) 1023-28.

(10) A Vrij: Polymers at interfaces and the interactions in colloidal dispersions. Pure and Applied Chemistry 48 (1976) 471.

(11) JK Percus, GJ Yevick: Analysis of classical statistical mechanics by means of collective coordinates. Physical Review 110 (1958) 1.

(12) KJ Mutch, JS van Duijneveldt, J Eastoe, I Grillo, RK Heenen: Small-angle Neutron scattering study of microemulsion-polymer mixtures in the protein limit. Langmuir 24 (2008) 3053.

(13) D Vollmer, J Vollmer, B Stuhn, E Wehrli, H-F Eicke: Polymer-induced ordering in water-oil-surfactant mixtures. Physical Review E 52 (1995) 5146.

(14) A Holmberg, P Hansson, L Piculell, P Linse: Effect of an amphiphilic graft copolymer on an oil-continuous microemulsion. Journal of Physical Chemistry B 103 (1999) 10807.

(15) M Odenwald, H-F Eicke, W Meier: Transient networks by ABA triblock copolymers and microemulsions: a reological study. Macromolecules 28 (1995) 5069.

(16) R Nagarajan: Polymer-induced structural transitions in microemulsions. Langmuir 9 (1993) 369.

(17) DB Siano, J Bock: A microemulsion method for polymer molecular weight determination. Journal of Polymer Science: Polymer Letter Edition 20 (1982) 151.

(18) B Zoltowski, Y Chekanov, J Masere, JA Pojman, V Volpert: Evidence for the existance of an effective interfacial tension between miscible fluids. 2. Dodecyl acrylate-poly(dodecyl acrylate) in a spinning drop tensiometer. Langmuir 23 (2007) 5522.

(19) K-Q Xia, Y-B Zhang, P Tong, C Wu: Interactions in mixtures of a microemulsion and a polymer. Physical Review E 55 (1997) 5792.

(20) J Eastoe, BH Robinson, RK Heenen: Water-in-oil micreomulsions formed by ammonium and tetrapropylammonium salt of AOT. Langmuir 9 (1993) 2820.

(21) H Endo, J Allgaier, M Mihailescu, M Monkenbusch, G Gompper, D Richter, B Jakobs, T Sottmann, R Strey: Amphiphilic block copolymer as efficiency boosters in microemulsions: a SANS investigation of the role of polymers. Applied Physics A 74 (2002) S392.

(22) I Lynch, S Cornen, L Piculell: Investigation of the segregative phase separation induced by addition of polystyrene to AOT oil-continuous microemulsions. Journal of Physical Chemistry B 108 (2004) 5443.

(23) DJ Meier: Theory of polymeric dispersants. Statistics of constrained polymer chains. Journal of Physical Chemistry 71 (1967) 1861.

(24) FT Hesselink, A Vrij, JTG Overbeek: On the theory of the stabilization of dispersions by adsorbed macromolecules. II. Interaction between two flat particels. Journal of Physical Chemistry 75 (1971) 2094.

(25) PMR Paulo, CAT Laia, SMB Costa: Clusters in polymer-surfactant AOT microemulsions probed by excited state quenching kinetics. Journal of Physical Chemistry B 107 (2003) 1097.

(26) W Meier: Poly(oxyethylene) adsorption in water/oil microemulsions: a conductivity study. Langmuir 12 (1996) 1188.

CHAPTER VI

MATERIALS FORMED FROM PHOTOPOLYMERIZATION OF MICROEMULSIONS BASED ON THIOL-ENE CHEMISTRY

Introduction

The main objective of this chapter is to compare and contrast the influences of chain-growth and step-growth polymerizations on the aqueous phase aggregation. The different pathways of network formation in acrylates and thiol-enes were anticipated to result in a variety of films properties and morphologies. In order to perform the comparison, a novel system based on thiol-ene chemistry was sought.

As explained in Chapter 2, thiol-enes are photo-curable systems that polymerize through a free-radical step reaction. One of the main characteristics of the step-growth process is a late gelation of the system. The polymeric network is produced through the formation of dimers, trimers, and n-mers, before it finally reaches a gel point. The gel point is reached when an infinite polymer network is formed. In other words, one molecule coexists within the polymer phase and forms an insoluble polymer fraction.(1) In step-growth chemistry, the gel point occurs at much higher conversions of the monomers than in traditional multifunctional chain-growing free-radical polymerizations. In the polymerization of the acrylates, gelation can occur near zero conversion.(2)

Polymerization-induced phase separation of thiol-ene and acrylate systems has been used previously in the formation of polymer-dispersed liquid crystals (PDLC). It has been shown(3,4) that thiol-enes are better hosts for the phase separation process, especially for holographic polymer dispersed liquid crystals (HPDLC).(5) This is

because thiol-enes form a more uniform morphology in which the liquid crystals are confined in spherical droplets. In addition, thiol-ene polymers offer lower switching fields, higher diffraction efficiencies, better optical properties, and higher thermal stabilities than acrylate systems.(6)

Natarajan and coworkers(7) indicated reasons for the different morphologies in the photopolymerization-induced phase separation of the two systems. In acrylate mixtures, since multifunctional they polymerize via a chain-growth mechanism, the monomers are rapidly added to a growing chain. High-molecular weight polymer is formed nearly instantly, and the monomer concentration decreases steadily with time; the monomer is present until the polymerization is complete. Because the high-molecular weight polymer formed has limited solubility in the monomer/liquid crystal mixture, it phase separates early on and becomes a polymer-rich discontinuous phase. These small solid-polymer-rich nodes continue to grow via surface reactive groups and ultimately become attached to one another. In a multi-functional chain-growing system, diffusion-limited kinetics dominate the progress early in the reaction. The liquid crystal/monomer-rich phase resides in these areas of formation. The authors concluded that irregularly shaped domains are formed because of the local heterogeneity of the phase separation process.

In thiol-ene systems, the step-growth propagation mechanism causes a slow increase in the molecular weight of the polymer. Monomers convert into oligomers at the beginning of the reaction. As the number of oligomers increases above a critical concentration, phase separation occurs, which creates two liquid phases: oligomer-rich and liquid crystal-rich. Because both phases are liquid and the viscosity is low, as a result of surface tension the discontinuous phase droplets are typically spherical in shape.

As the reaction progresses, the growing oligomeric (polymeric) phase becomes immobile and traps the spherical domains in what is called a "swiss cheese" morphology.

Experimental

Materials

All reagents were used without further purification. Dioctyl sulfosuccinate sodium salt (AOT), 1,6-haxanedithiol (HDT), pentaerythitol allyl ether (APE), 1,9-decadiene (DDA), and tri(ethylene glycol) divinyl ether (PEG1) were purchased from Aldrich Chemical Co. Samples of Irgacure 369 photoinitiator were donated by Ciba Specialty Chemicals.

Preparation of Microemulsions

Microemulsions of AOT, HDT and APE, and deionized water were prepared with different water contents. The water to surfactant ratio was kept constant $[H_2O]/[AOT] = 10$. Solutions were prepared at water contents of 5, 7, 10, 15, 20, and 25 wt % (with respect to monomers). The solutions had a 1:1 molar ratio of SH groups to double bonds. First, AOT was added to the APE. After its dissolution the appropriate amount of water was added to APE-AOT solution. Irgacure 369, photoinitiator, at 5 mM concentration was added to the APE-AOT-water microemulsion to facilitate the initiation of the photopolymerization. As the last step, dithiol HDT was added. For example, to prepare a microemulsion with 10 wt% of water with respect to monomers, 0.8325 g ($1.87\ 10^{-3}$ mol) of AOT was dissolved in 1.5652 g ($6.10\ 10^{-3}$ mol) of APE overnight. Next, 0.017 g ($4.64\ 10^{-5}$ mol) of Irgacure 369 and 0.3377 g (0.018 mol) of DI-water was added and allowed to mix for 24 hours. Afterward, 1.4126 g ($9.39\ 10^{-3}$ mol) of HDT was added,

and the sample was shaken vigorously and shortly thereafter used to form films (within 2 hours). For the microemulsions containing tri(ethylene glycol) divinyl ether (PEG1) and 1,9-decadiene (DDA), the amount of divinyl to triene was varied, but the 1:1 ratio of SH to double bonds was conserved. For example, a sample with a 1:1 ratio of APE to PEG1, 10 wt% of water with respect to monomers, and W = 10 was prepared using the following procedure: 1.5034 g ($7.43\ 10^{-3}$ mol) of PEG1, 1.2674 g ($4.94\ 10^{-3}$ mol) of APE, and 1.3736 g ($3.09\ 10^{-3}$ mol) of AOT were mixed together overnight. Next, 0.0100 g ($2.73\ 10^{-5}$ mol) of Ingacure 369 and 0.5566 g ($0.031\ 10^{-3}$ mol) of DI water were added and allowed to mix. As the last step, 2.2297 g ($0.014\ 10^{-3}$ mol) of HDT was added and mixed.

Polymerization of Thin Films

The films were photo-polymerized with a 365 nm light with an intensity of 2.3 mW/cm^2 from low-intensity hand-held lamp. The exposure time was one minute for each side of the film. The thickness of the films was regulated using 0.2 mm (a cover glass) or 10 μm glass spacers. The microemulsion solution was pulled into the cell between two glass slides by capillary forces.

Phase Diagram Determination

Samples of known AOT concentrations were prepared in a 1:1 ratio of HDT:APE. DI water was added in a step-wise manner until a cloud point was reached, whereupon the mass of water was recorded. Next, small amounts of AOT were added to the cloudy microemulsion until it became clear again. An addition of DI water followed. At the water-induced cloud points, the composition of the samples was recalculated. This

process resulted in defining thee transition border shown in the ternary phase diagram in Figure 6.1.

Surfactant Dissolution

A small amount of the polymerized dry film was weighed and placed in a glass vial. The film was covered with DI-water, shaken, and left for at least 24 hours. After that time the film was removed from the vial and padded dry. Its weight was recorded, and it was placed in a new vial and covered again with fresh DI water. This cycle was repeated until the mass of the film did not change with two consecutive weighings. At that point the film was allowed to dry. When dry, the final mass was compared to the initial mass.

Instrumentation

Thermal gravimetric measurements were obtained using a TGA 2050 Thermogravimetric Analyzer from TA Instruments. Thermal stability was evaluated through a temperature ramp, and the composition evaluation was attempted using the quasi-isothermal (stepwise) method. Both methods used a temperature range from room temperature (about 15° C) to 600° C, and a heating rate of 5° C min^{-1}. However, in the step-wise method whenever the rate of weight change of the sample exceeded 0.5 % min^{-1}, an isothermal program was applied. The heat ramp was employed again whenever the rate of weight change fell below 0.05 % min^{-1}.

A kinetic analysis was conducted with real-time FTIR in order to plot conversion vs exposure time to light. Conversion vs. irradiation time was recorded on a modified Bruker 88 spectrometer with a 200 W high-pressure mercury-xenon lamp source. The two intensities used to initiate the polymerization were 12.5 mW/cm^2 and 1.56 mW/cm^2

at 365 nm. The thiol group conversion was monitored by measuring the area under the peak of the 2570 cm^{-1}. The peak at 3064 cm^{-1} was used to follow the conversion of the double bonds of the ene. The conversion was calculated according to the following:

$$\text{conversion} = \frac{H_0 - H_t}{H_0} \qquad \text{Equation 6.1}$$

where H_t is the peak at a given time and H_0 is the peak at the beginning of the reaction.

Results and Discussion

Phase Diagram

Various thiol and "ene" combinations were tried in an effort to prepare stable microemulsions. The limiting factor was the solubility of the surfactant (AOT) in the five tested thiols. It was found, that AOT dissolved in the simple carbon chain dithiol 1,6-hexanediol dithiol (HDT). The "ene" of choice was tri-functional pentaerythritol allyl ether (APE). A phase diagram was prepared for a 1,6-hexanediol dithiol/pentaerythritol allyl ether/AOT/Water system. By adding small amounts of water to the AOT solution in the 1:1 mixture of HDT and APE, the cloud points were determined. Placing the points of the critical composition on a ternary diagram revealed a region of a stable reverse microemulsion (labeled L_2). As shown in Figure 6.1, L_2 is a rather narrow compositional area when compared with the one for DDA/HDDA monomers. In addition, it was noticed that, after about an hour, the microemulsion would stay cloudy even when a large amount of AOT was added. It was concluded that the two monomers start to form a polymer network even without the addition of a photo-initiator; and further, that the presence of the polymer network also caused the "secondary"

clouding of the microemulsion. It was decided that the microemulsion would be prepared using a step procedure. First, the microemulsion in the ene part of the oil was prepared. Second, the thiol monomer was added. Microemulsions prepared in this manner were used to make films. Additionally, it should be noted that the microemulsions were always used within a half an hour of the mixing of the two monomers.

Appearances of the Films

Immediately upon polymerization, the films had a whitish color, similar to the color of the films formed from microemulsions based on acrylates. As described in the previous chapter, acrylate films change their appearance from opaque to transparent upon exposure to ambient humidity (< 100 % RH). That change always occurred within one hour. Unfortunately, the appearance of the films based on thiol-ene chemistry stayed the same even after 24 hours of exposure to the lab atmosphere. In Figure 6.2, a film based on HDT-APE monomers is depicted. Immediately after polymerization (Figure 6.2A) and still after exposure to an ambient atmosphere for 24 hours (Figure 6.2B), the film had a white color. Previously, growth of crystals was observed in the acrylate system, with increased cross-link density (addition of higher than 15% of difunctional monomer Figure 6.3). Thus, we hypothesize that the white color of the HDT-APE films is due to the presence of AOT crystals. The color persists even after water evaporates from the film, which prohibits the observation of the humidity response of these films, which was possible in the acrylate system.

Another interesting characteristic of the films prepared from microemulsions based on the HDT-APE system can be seen in the series of images taken of thin films with increasing water content. Figure 6.4 depicts four films that were prepared from the HDT-

APE microemulsions l(Table 6.1, entries 3, 4, 5, and 6). For a film prepared from microemulsion with 10 wt % of water, the size of the visible domains is approximately 50 microns (Figure 6.4a). The films with 15, 20 and 25 wt % of water show average domain sizes of 20, 13, and 8 microns, respectively (Figure 6.4b, c, d). It needs to be emphasized, that the increasing weight percent of water was always accompanied by an equivalent increase of surfactant to sustain a water-to-surfactant ratio of 10. We hypothesize that the composition of the visible domains changes as a consequence of the mutual increase in the so-called aqueous phase, which combines water and AOT. For microemulsions with smaller water contents, the domains visible in Figure 6.4a are composed mainly of water, with the surfactant on the interface of the domains. However, as the water and AOT increases, the domains' compositions shift, filling the domains with the aqueous phase rather than pure water. The thiol-ene network can compatibilize only a small amount of AOT, and the excess is moved to the aqueous domains.

The surface of the thin films was scanned to look for uniformity within the size of the domains. As depicted in Figures 6.5 and 6.6, the size of the domains varies within each film. Within one film the size of the domains varied from about 5 to 50 microns. In Figure 6.5 a representative set of pictures is shown. The pictures in this Figure were depict two films, under the same magnification, prepared from the same microemulsion, which had 20 wt% of water with respect to monomers and W = 10. The two films differed in thickness: 10 and 200 microns. The domains are generally spherical, as predicted from the phase separation mechanism,(7) but their size varied from approximately 5 to 25 microns. The spherical shape is also preserved in the thicker film (depicted in the lowest picture of Figure 6.5). An exception from the spherical shape is

visible for the film with low water content presented in Figure 6.6. This film was prepared from a microemulsion that contained 5 wt % of water with respect to monomers (entry# 1 in Table 6.1). In some parts of the film the phase separation resulted in spherical domains; however, in other parts a fingerprint texture was detected. The fingerprint texture resembled the chiral nematic morphology of liquid crystals.(8)

Water Content

The water amount of the films was determined with Thermal Gravimetric Analysis TGA. The analysis of the first film prepared from HDT-APE microemulsion showed that this film, immediately after polymerization, had the same water composition as the initial microemulsion of 5.6 wt% (Figure 6.7, entry #2 in Table 6.1). The same film after a 24-hour-long exposure to the open atmosphere lost most of this water, leaving approximately 2 wt%. Similarly, as in the case of the acrylate films, the remaining 2 wt% represented water strongly bonded to surfactant.

Figure 6.8 shows the thermal gravimetric analysis of the three films. The first was formed only from the monomers HDT-APE (plot c), the second from the monomers and surfactant HDT-APE-AOT (plot b), and the third from HDT-APE microemulsion with 7 wt% of water (plot a). Again, as in chapter 3, AOT decomposed at 200 °C and the network at 350 °C. Analysis with step-wise TGA, illustrated in Figure 6.9, showed that for the films with an increasing water amount, the water present in the microemulsions did not reappear in the films. The decomposition plots showed the water content of three films at only about 7 wt% (Figure 6.9, plot c, d, and e). The microemulsions that the films were prepared from were designed to have water contents of 10, 13, and 16 wt% (Table 6.1). Also, the film prepared from the microemulsion with 5 wt% of water (4.8 %

of total mass) showed only a 2% weight loss until high temperatures. There was no AOT decomposition temperature for the plot of this film, and only polymer network decomposition occurred at 350 °C.

A similar plot can be seen in Figure 6.10, which will be explained later. It has been mentioned above that the two monomers start to react instantaneously upon contact. After about an hour, all of the microemulsions listed in Table 6.1 became turbid, indicating phase separation occurring in the microemulsions. The formation of the polymer network was influencing the stability of the clear microemulsions. The samples were solid after 24 hours and were composed of two layers of material. The layers were analyzed with step TGA. The decomposition curve of the top layer (plot a in Figure 6.10) showed two discrete steps. At 200 °C there was a small decrease in mass. Then at 330 °C a 90 % mass drop occurred. The large mass decrease represented the decomposition of the polymer network, and the small decrease corresponded to AOT decomposition. That result indicated that the top layer contained mostly polymer network with a small amount of surfactant. On the other hand, the plot of the lower layer's decomposition (plot b in Figure 6.10) showed three distinct steps. Water evaporated at 34 °C, AOT decomposition occurred at 195 °C, and the polymer network decomposed at 330 °C.

There is an obvious compositional shift occurring during the self-polymerization of the HDT-APE microemulsions. From the microemulsion composition (Table 6.1, entry # 3), the network should account for 70 wt% of the sample. The polymer network represented only about 24 wt% of the bottom layer, whereas it was close to 90 wt% of the top layer. The mass loss at lower temperatures of the lower stratum represented

approximately 16 wt% of the sample, which was more than the initial 8 wt% water content of the microemulsion. The top part of the sample showed close to 2 wt% water content, again associated with approximately 5 wt% of surfactant in this material. The lower layer showed close to 57 wt% of AOT, which was close to three times the initial 20 wt% of surfactant content of the microemulsion (entry # 3 in Table 6.1).

In the case of self-initiated polymerization, the reaction proceeded at a much slower rate than when the films were photopolymerized with a lamp. This allowed a macroscopic separation of the two components to take place. As the polymer network was formed, its density was lower than the remaining aqueous phase; therefore, it floated to the top of the glass vial. In addition, the mobility of the two liquid phases facilitated a favorable, spherical, arrangement of the "included" phase.

Even though some of the surfactant stayed entangled within the forming network, a large majority of the AOT was associated with water and formed the lower layer of the material. A small amount of monomers resided within a "sea" of the aqueous phase. The polymer network was confined into small droplets depicted in Figure 6.11. This rearrangement resembled a direct emulsion, in which polymer particles are formed in an aqueous continuous phase. Because the system was not stirred, the size of the polymer droplets was not uniform, ranging from 30 to 130 microns.

To explain the unusual appearance of decomposition plot (Figure 6.9, plot a) of the film prepared from microemulsion with 5 wt% water (Table 6.1, entry # 1), we think that as the polymerization proceeded, the phase separation occurred, pushing the aqueous

phase out of the polymer. For that reason, the sample that was taken for TGA analysis showed neither water nor AOT.

Kinetic Analysis

Kinetic analysis was conducted to evaluate the influence of the aqueous phase on the rate of polymerization. The real-time FTIR was used to determine the conversion vs. exposure time plots for the samples containing only monomers, monomers with surfactant, and microemulsion. The conversion of the thiol group for HDT monomer was monitored by measuring the area under the peak of the 2570 cm^{-1}. The peak at 3064 cm^{-1} was used to follow the conversion of the double bonds of the APE monomer. The two peaks of interest are indicated in Figure 6.12.

The two intensities used to initiate the polymerization were 12.5 mW/cm^2 and 1.56 mW/cm^2 at 365 nm. The lower intensity light was chosen to imitate the light intensity of the lamp used for the films' preparation. Figure 6.13 shows the photopolymerization of the HDT-APE monomer solutions under the high intensity light of 12.5 mW/cm^2. Figure 6.13a shows the conversion of the ene functional groups (as a height of the peak) for three solutions exposed to light for 5 minutes: pure HDT-APE monomers, monomers with AOT in the amount needed for microemulsion with 5 wt% water and W = 10, and microemulsion with 5 wt% water and W = 10. It is evident that the reaction is very fast, as seen in the literature.(9) Focusing on the first seconds of the reaction (Figure 6.13b) it can be seen that the full conversion is reached within 15 seconds of exposure. Moreover, addition of the surfactant has no effect on the polymerization rate (Figure 6.13b, points

▲), and there is an insignificant change in the rate of conversion when water is present (Figure 6.13b, points ■).

Figure 6.14 illustrates the conversion-time plot of the photopolymerization under the light intensity of 1.56 mW/cm^2 of pure thiol-ene APE-HDT solution and two microemulsions. As expected, when the light intensity was lowered, the polymerization rate significantly decreased. In addition, the monomers did not attain 100 % conversion during the irradiation time. After 500 seconds of exposure to light the conversion of the 5% microemulsion, 10% microemulsion, and pure system was 92.0, 92.2, and 94.5 %, respectively. There was also a more defined lowering of the polymerization rate, as water is present in the system. Surprisingly however, there was no trend observed with water increase. This lack of trend with the water increase is most likely due to a computational error in obtaining the results.

The AOT Crystallization Problem

One problem we encountered had to do with the white color of the HDT-APE films, which limited observation of the humidity response of these materials. In this part of the research, we examined avenues to reduce the crystallization of the surfactant within the films. It was determined that two means were possible: a removal of AOT from already prepared samples, and a decrease in cross-link density by using a spacer monomer.

First we examined the removal of AOT. A dry film formed from the microemulsion with 7 wt% water was placed in a jar with DI-water. The film was swollen with water to dissolve the surfactant out. The immersion of the film was carried out for an extended time. The water was changed intermittently. After a two-week

period, the amount of the surfactant decreased from 19 wt% to 16 wt % (Figure 6.15). This result indicated that the polymer network was packed with cross-links (connection points) and therefore yielded a very tight net that "captured" the surfactant.

Next, we investigated the ways to decrease the crosslink density in the HDT-APE systems. The oil phase of the microemulsions was composed from stoichiometric amounts of difunctional and trifunctional monomers. Upon polymerization, the oil phase formed a network within which the aqueous phase was captured. As visualized in Figure 6.3, when this highly cross-linked network was formed the surfactant crystallized, thus turning the films white. A similar phenomenon was observed upon increasing the amount of cross-linker in the acrylate system. It was therefore assumed that decreasing the cross-linking density would prevent the crystallization of the surfactant.

To address this, tri(ethylene glycol) divinyl ether (PEG1) was used as a spacer between the cross-links. A stable microemulsion was achieved by using a 1:1 ratio of APE and PEG1. Upon photopolymerization, the film had a hazy look. Unfortunately, some crystallization occurred whenever the film was mechanically disturbed (cut). In addition, the thermal gravimetric analysis, Figure 6.17, revealed that, immediately after polymerization, only 4.6 wt% of the mass was represented by water in the film. The microemulsion used for the film preparation had 8 wt% of water in its total mass. Moreover, 20 wt% AOT content in the microemulsion was corresponded to 14 wt% in the film. We guess that the phase separation that occurred during the formation of this film affected the composition seen with TGA, as was the case for the undiluted system. Figure 6.16 shows a picture of the phase-separated film. The domains appeared to be of

uniform size throughout the film. They had a spherical shape with an average diameter estimated at around 25 μm.

The diffusion coefficient of water molecules was evaluated for the film with a 1:1 ratio of APE to PEG1. The mass change with time is presented in Figure 6.18. The value of the diffusion coefficient is calculated to be 1.4 10^{-7} cm^2 s^{-1}. In the acrylate system, the closest diffusion coefficient was shown for film with 15 wt% of water and W = 10. This shows that the HDT-APE-PEG1 film formed from 10% microemulsion had water molecules diffusion coefficient similar to that of DDA-HDDA film prepared from 15% microemulsion. It can be concluded, that the PEG1 monomer facilitates fast pathways for water transport.

In addition, the tri(ethylene glycol) divinyl ether part of the HDT-APE-PEG1 system most likely associated with the water domains equally in the microemulsion and in the film, we decided to use a more hydrophobic co-monomer. The monomer of choice was 1,9-decadiene (DDE). The microemulsion was formulated using 95 mol% DDE in the ene part of the oil. APE was used in smaller amounts as the crosslinking agent. Unfortunately, even when though the network crosslink density was strongly decreased, and similar to that of the acrylate system, the formed films had white color that remained even upon drying of the film. The morphology of the aqueous phase in the film was spherical droplets as shown in Figure 6.19.

Conclusions

The study of the fundamental properties and characteristics of thin films based on polymerizable microemulsion using thiol-ene chemistry was presented. The films

prepared from the HDT-APE microemulsions were white in appearance. In contrast to the films prepared from the acrylate-based microemulsion, they did not change their color upon water evaporation.

A narrow reverse microemulsion region in the phase diagram was determined through cloud point measurements. A short shelf-life for these microemulsions' stability was detected due to self-polymerization of the media even without an initiator.

Thermal gravimetric analysis confirmed that, as before, only a small amount of water was present in the dry white films. The color of the film was attributed to crystallization of the surfactant, which had been observed in the acrylate films with a higher crosslinker concentration. In addition, the films prepared from compositions designed to have low crosslink density also exhibited the white color. It is understood that the surfactant has low solubility in the thiol-ene network. The networks chemical structure cannot compatibilize the side chains of the AOT molecules. We recognize that the opposite is true for the acrylate network. The dodecyl acrylate introduces long side chains to the main chain that facilitates compatibility with the AOT's side chains.

Films showed distinct morphology due to the presence of two liquids during the phase separation. The majority of the domains had a spherical shape, as reported in the literature. Unfortunately, the sizes of the domains were not uniform within the films. The acrylate films had a mixture of spherical domains connected with bi-layers of surfactant. Again, we correlate these dissimilarities with the different compatibility of the networks and surfactant. The acrylate network allowed the surfactant to "dissolve" within the whole network. The thiol-ene network excluded the surfactant, forcing it into

large, spherical domains. It needs to be pointed out that a small amount of AOT can dissolve in the thiol-ene, as seen in the polymer layer of the self-polymerized samples; however, the acrylate system can absorb much larger amounts of AOT.

The HDT-APE systems showed self-induced polymerization. The phase separation in the self-polymerization resulted in a compositional shift; namely, the formation of the polymer network excluded the majority of the aqueous phase in a separate stratum.

The observation of the self-polymerization allowed us to test our hypothesis of what would happen with a reaction conducted infinitely slow. We expected to see full separation of the two immiscible systems, and in this case we did. This finding confirms that the rapid polymerization captures states far-from-equilibrium in the films.

Table 6.1. The Composition of microemulsions used in the study

#	APE (wt%)	HDT (wt%)	AOT (wt%)	H_2O (wt%)	Initiator (%)*	H_2O (%)*	W**
1	44.68	39.51	11.04	4.24	0.53	4.8	9.5
2	34.83	39.17	20.06	5.66	0.28	7.1	7.0
3	37.58	33.92	19.99	8.11	0.41	10.2	10.0
4	31.75	30.70	26.37	10.77	0.41	14.7	10.1
5	28.30	24.97	32.87	13.51	0.36	20.2	10.1
6	24.71	21.92	37.45	15.64	0.29	25.1	10.30

*with respect to monomers

**calculated value

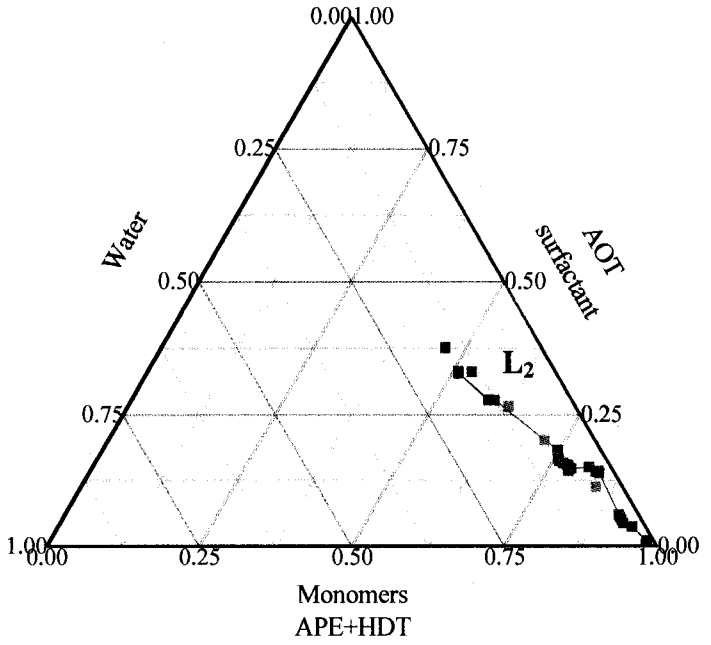

Figure 6.1. Ternary phase diagram for APE-HDT system with marked L_2 phase and set of microemuslsions (■) used in the study.

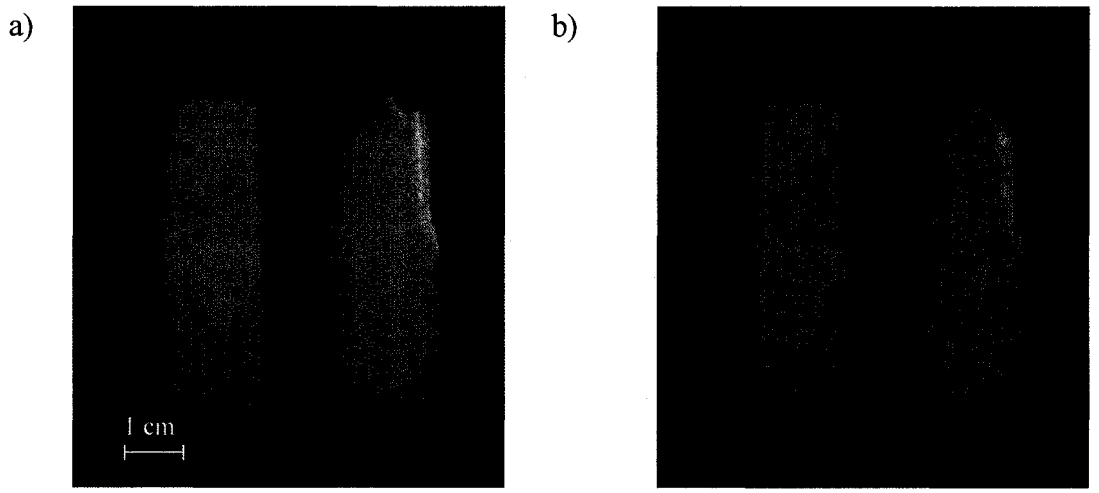

Figure 6.2. Pictures of the two stages of the films prepared from thiol-ene based microemulsion: (a) right after polymerization, (b) after 24-hour-long exposure to open atmosphere.

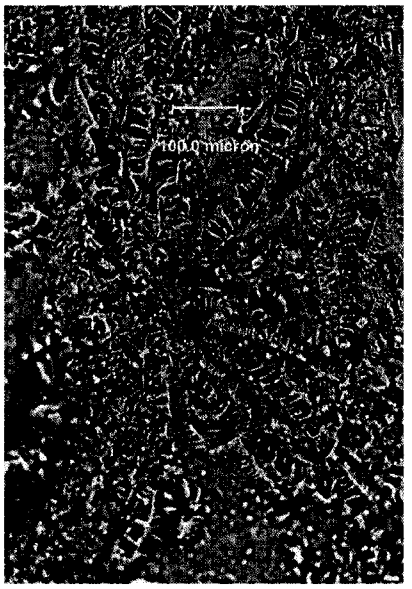

Figure 6.3. Image of a growing AOT crystal in a film prepared from HDT-APE microemulsion.

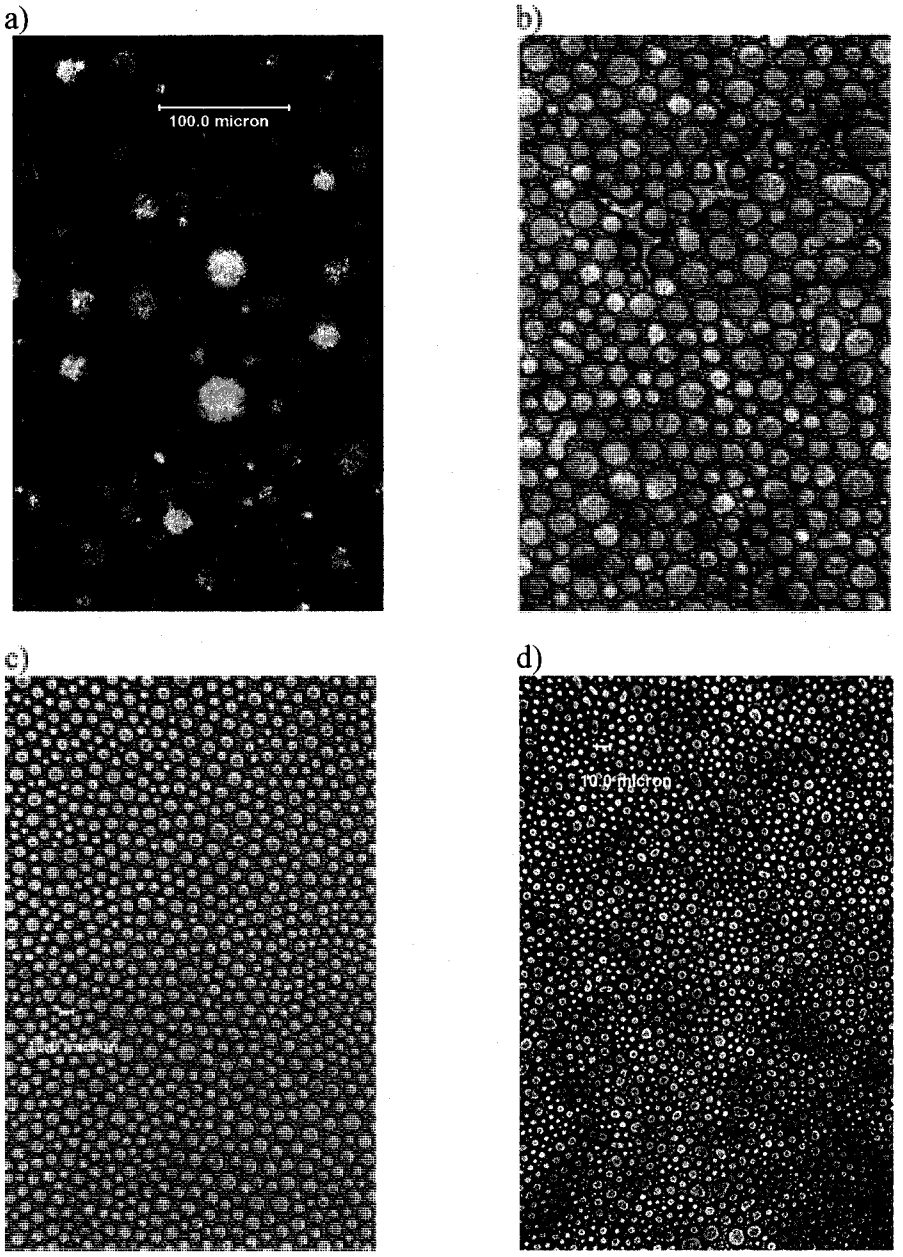

Figure 6.4. Images of thin films photopolymerized from microemulsions based on HDT-APE with increasing water amount: (a) 10, (b) 15, (c) 20, (d) 25 wt % with respect to monomers. All taken at the same magnification. Image (a) represents top most layer of a thick film 0.2 mm, images (b), (c), and (d) are of the thin films.

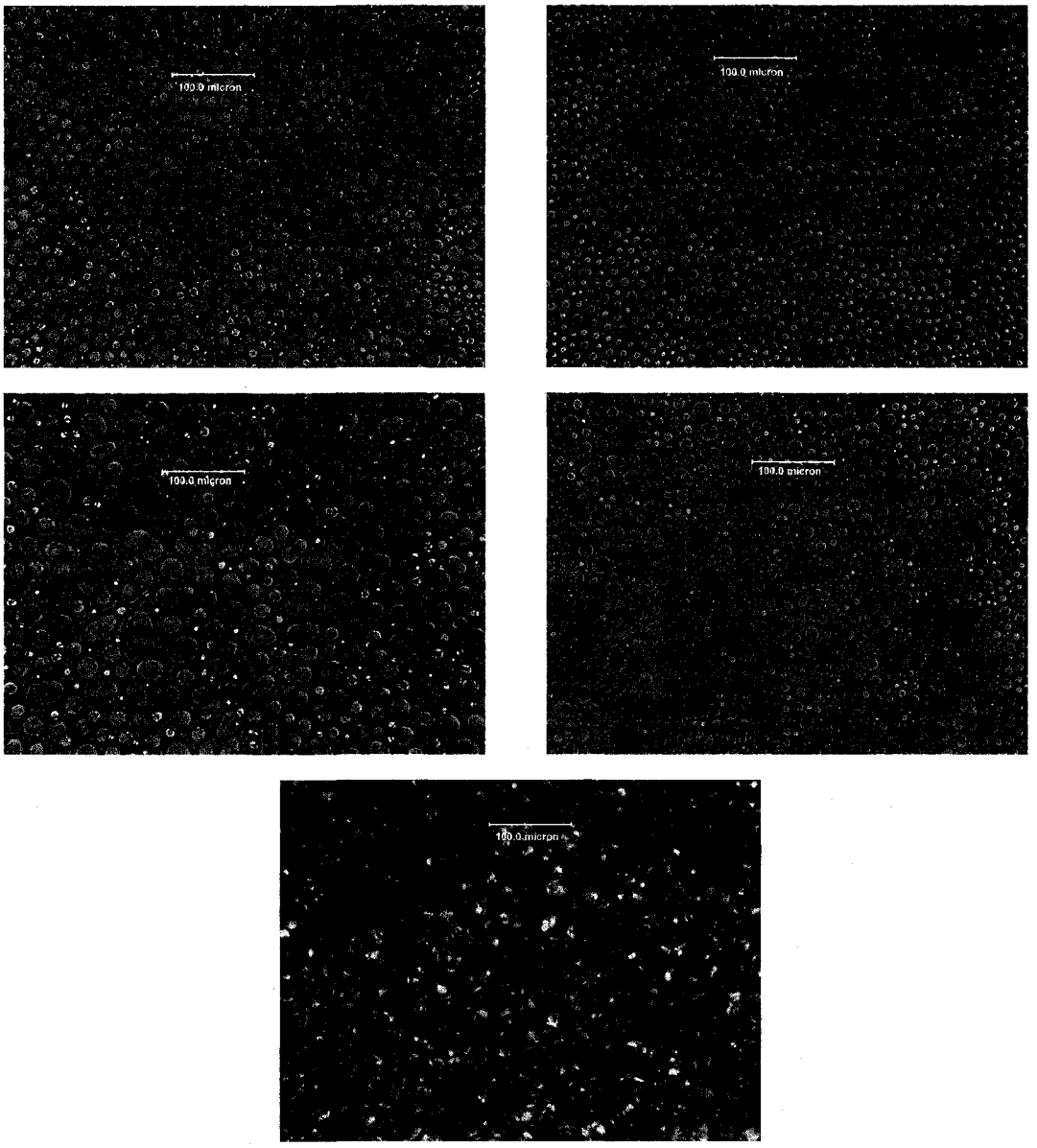

Figure 6.5. Images of two films photopolymerized from the 20 wt% microemulsion based on HDT-APE. Top images taken of a 10-micron film, the lower image represents the top most layer of a thick film 0.2 mm. All images taken at the same magnification, the scale bar represents 100 microns.

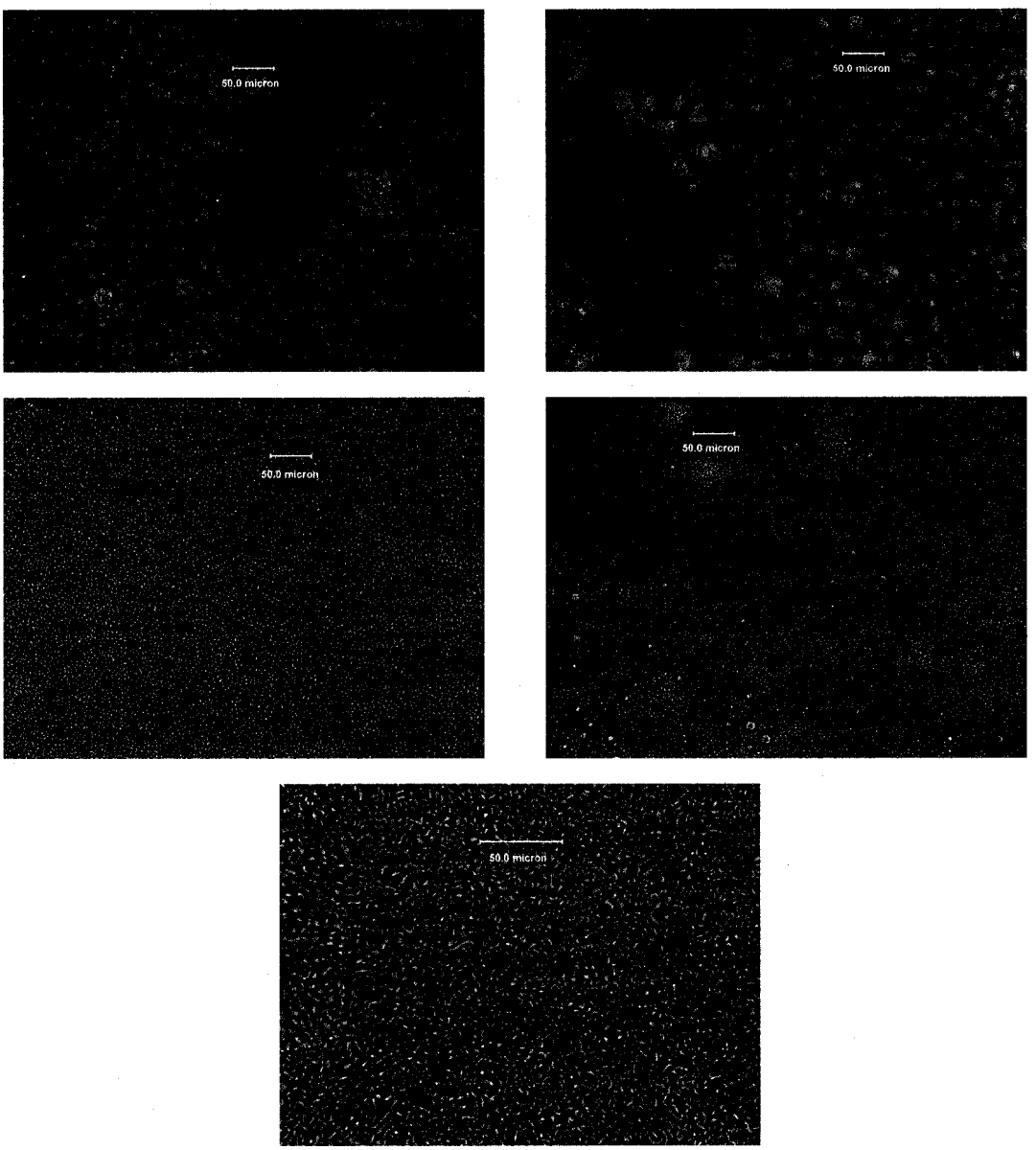

Figure 6.6. Images of a thin film prepared from the 5 wt% microemulsion based on HDT-APE. All images taken at the same magnification, the scale bar represents 50 microns.

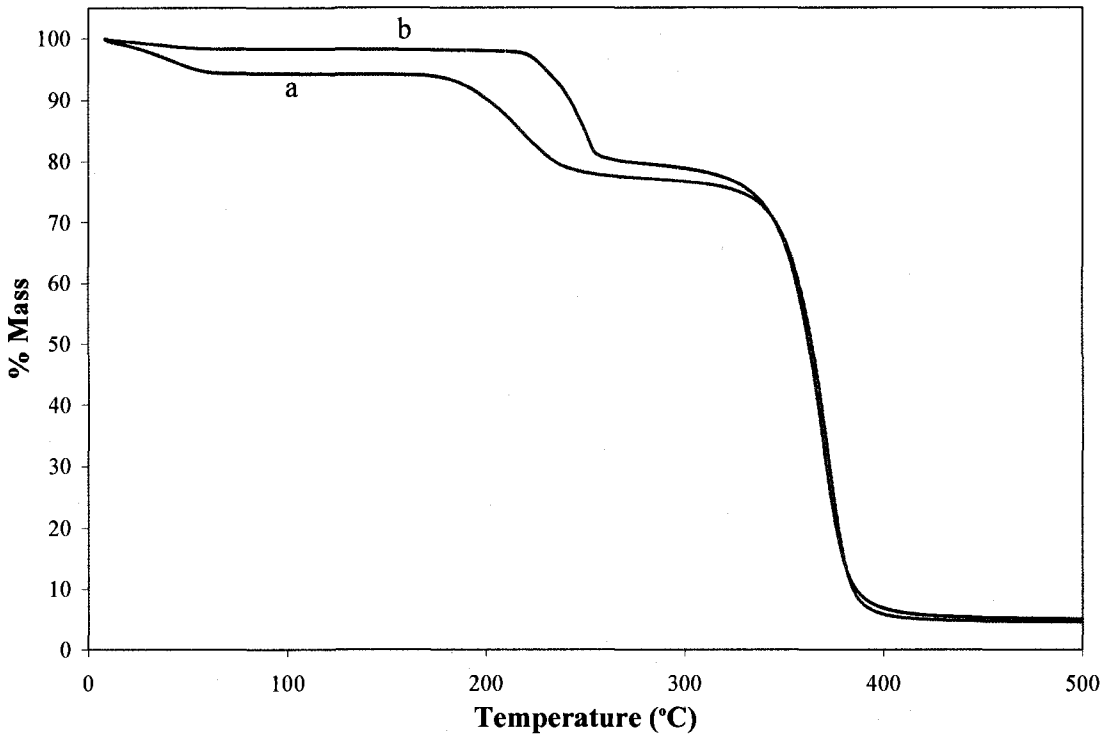

Figure 6.7. Thermal gravimetric analysis of films prepared from APE-HDT microemulsion that had 7 wt % of water with respect to monomers: (a) the film immediately after polymerization, (b) the same film after 24 hour exposure to open atmosphere.

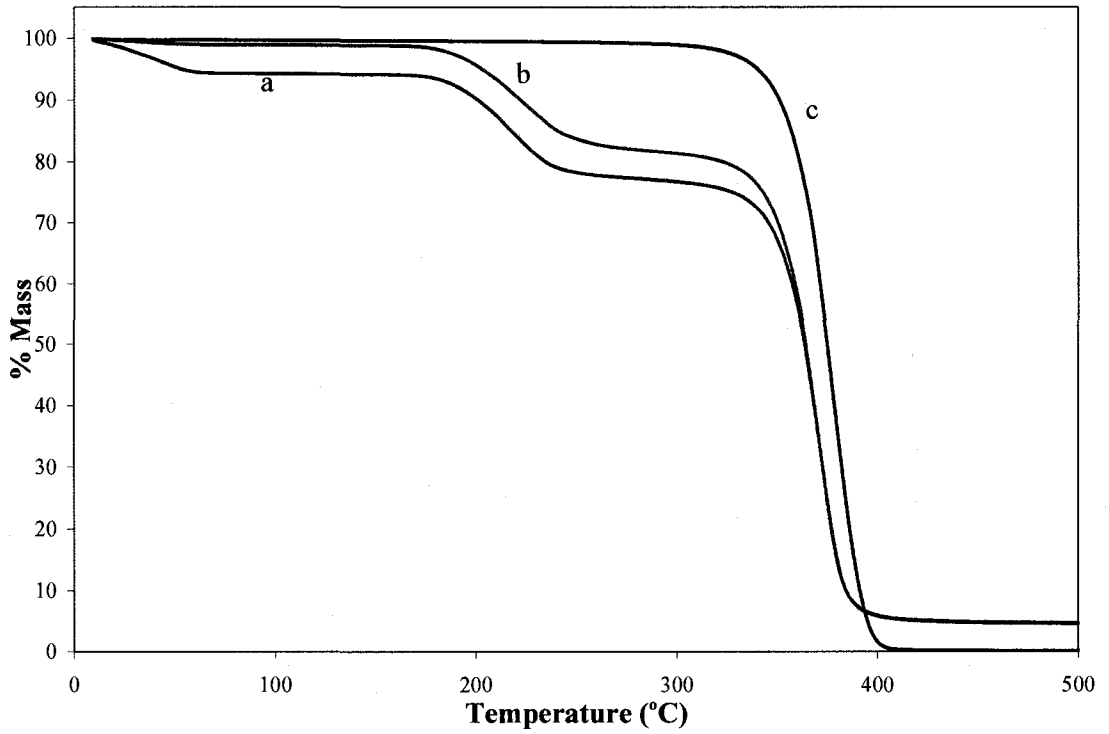

Figure 6.8. Thermal gravimetric analysis of films prepared from: (a) microemulsion that had 7 wt % of water with respect to monomers immediately after polymerization, (b) APE-HDT monomers and AOT, (c) APE-HDT monomers only.

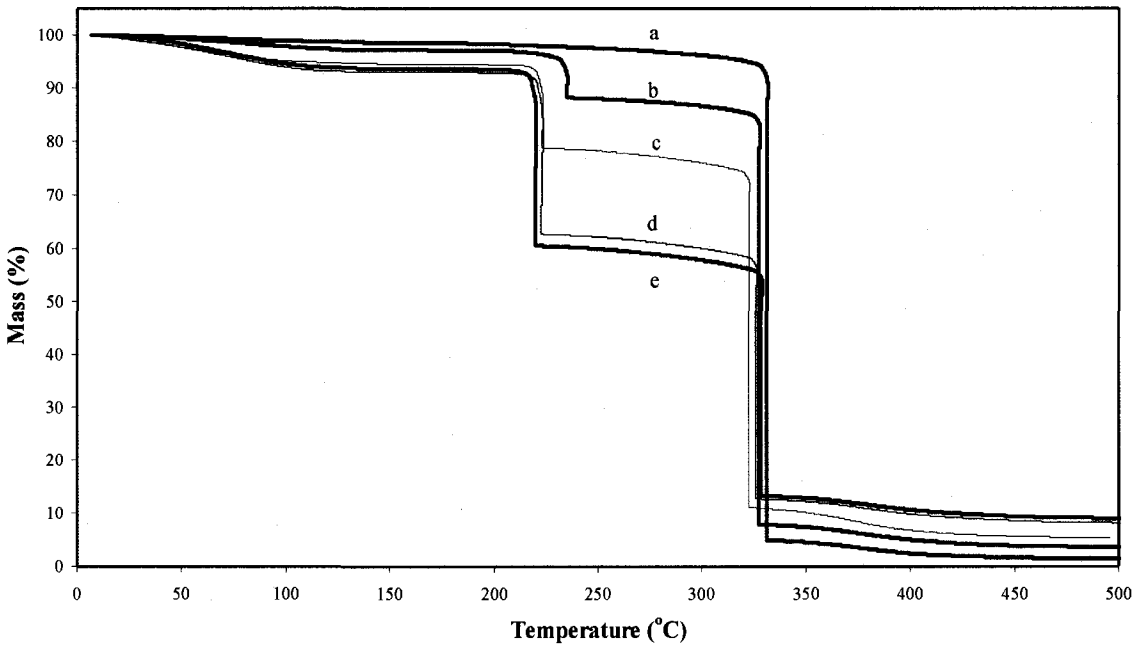

Figure 6.9. Thermal gravimetric analysis of films prepared from HDT-APE microemulsions with W = 10 and increasing water content with respect to monomers: (a) 5 wt %, (b) 10 wt %, (c) 15 wt %, (d) 20 wt %, (e) 25 wt %.

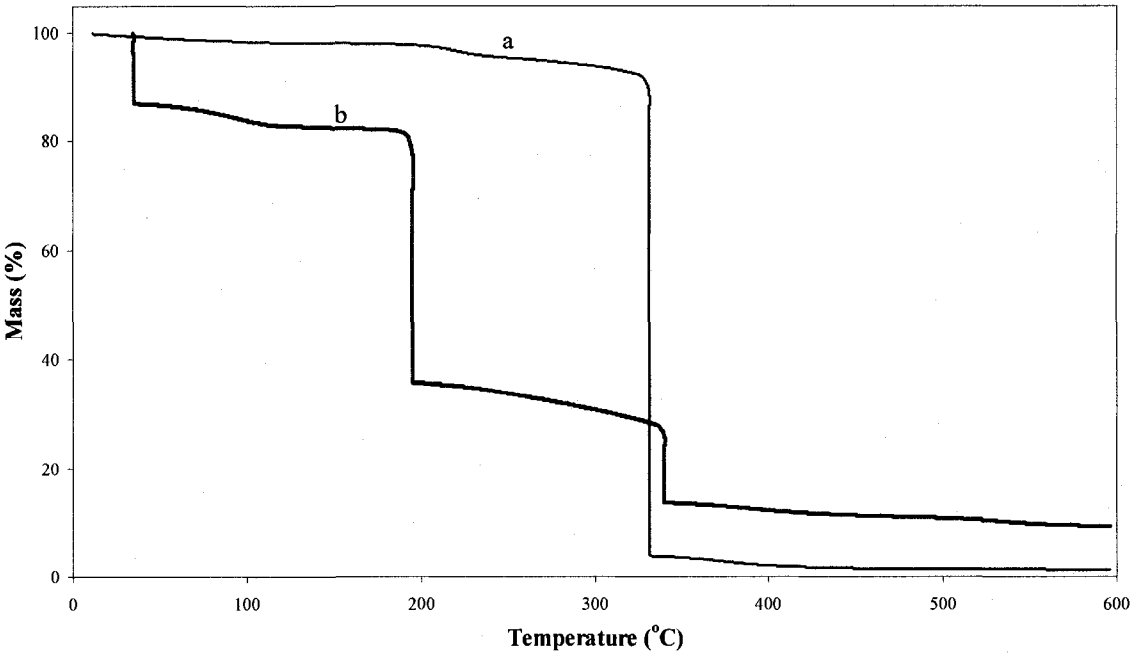

Figure 6.10. Thermal gravimetric analysis of two layers of sample that self-polymerized from HDT-APE microemulsions with W = 10 and 10% of water; (a) top layer, (b) lower layer.

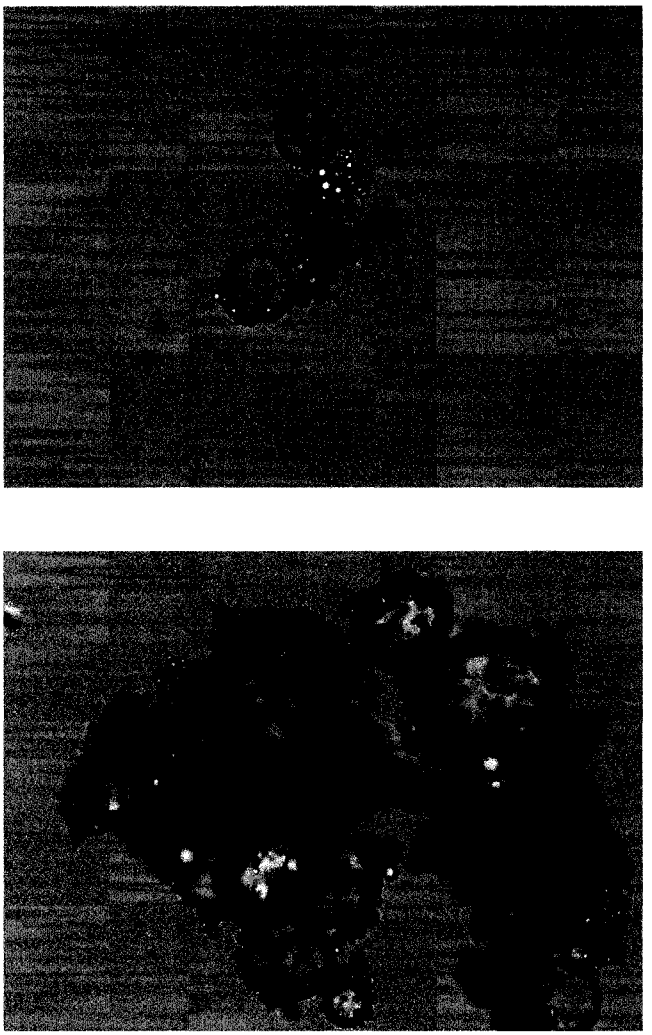

Figure 6.11. Polymer droplets washed out of the lower layer of self-polymerized microemulsion with 15 wt% of water and W = 10. The scale bar represents 100 microns.

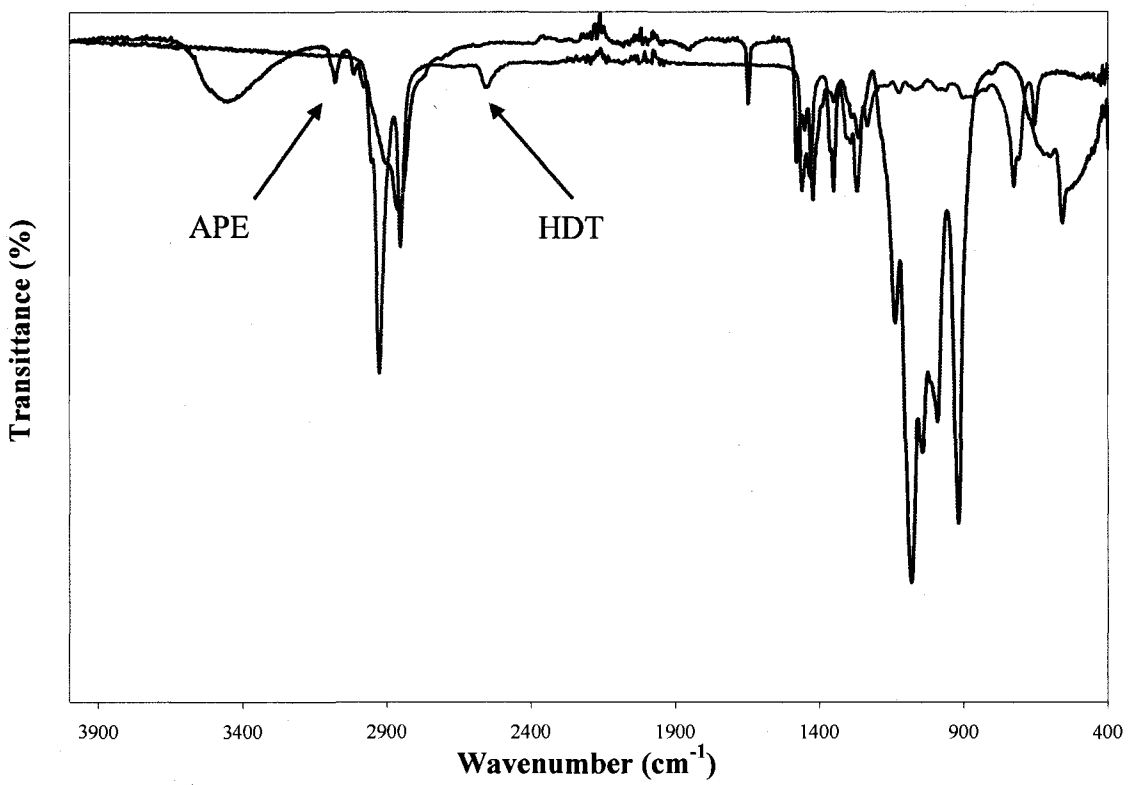

Figure 6.12. IR spectra of the two reacting monomers with indicated groups of interest.

a)

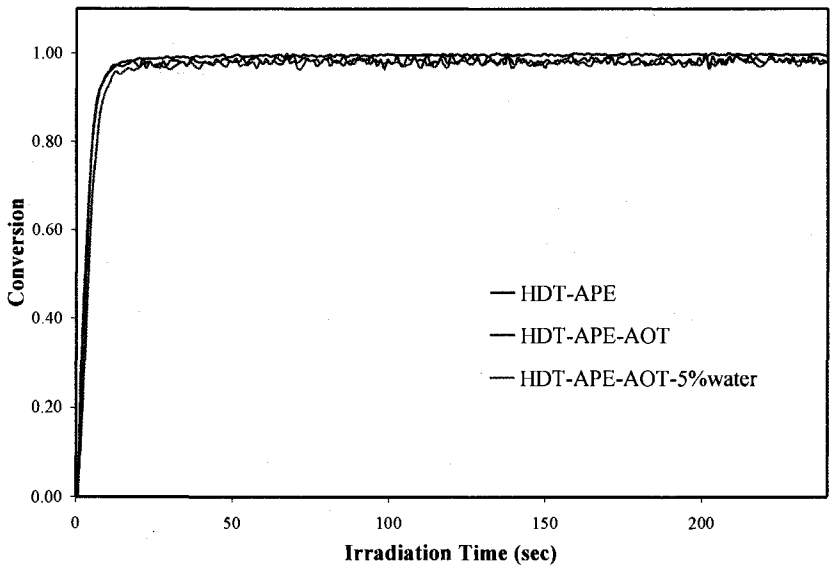

b)

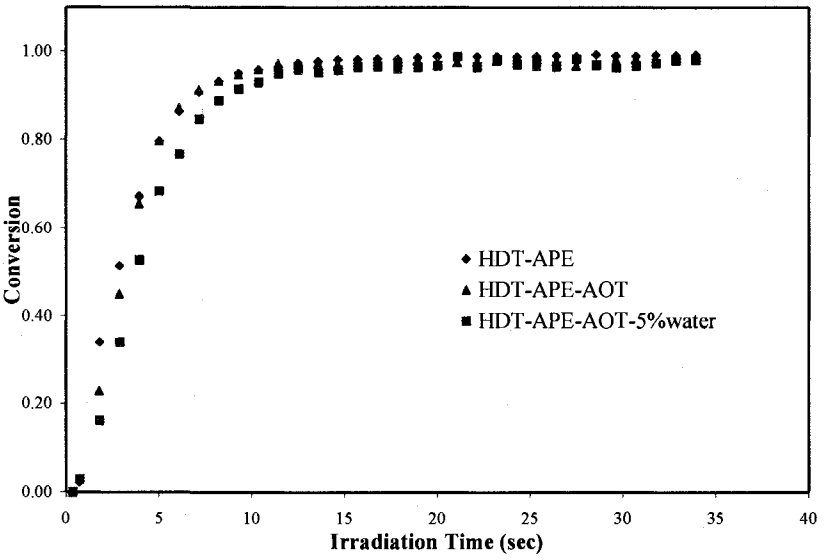

Figure 6.13. RTIR conversions of the double bond in the ene monomer: (◆) APE-HDT, (▲) APE-HDT-AOT (■) microemulsion APE-HDT-AOT-H_2O (5 wt% water with respect to monomers. Part (a) - full view on the process, Part (b) enlargement of the first seconds of the reaction. Light intensity 12.5 mW/cm^2, high-pressure mercury-xenon lamp source.

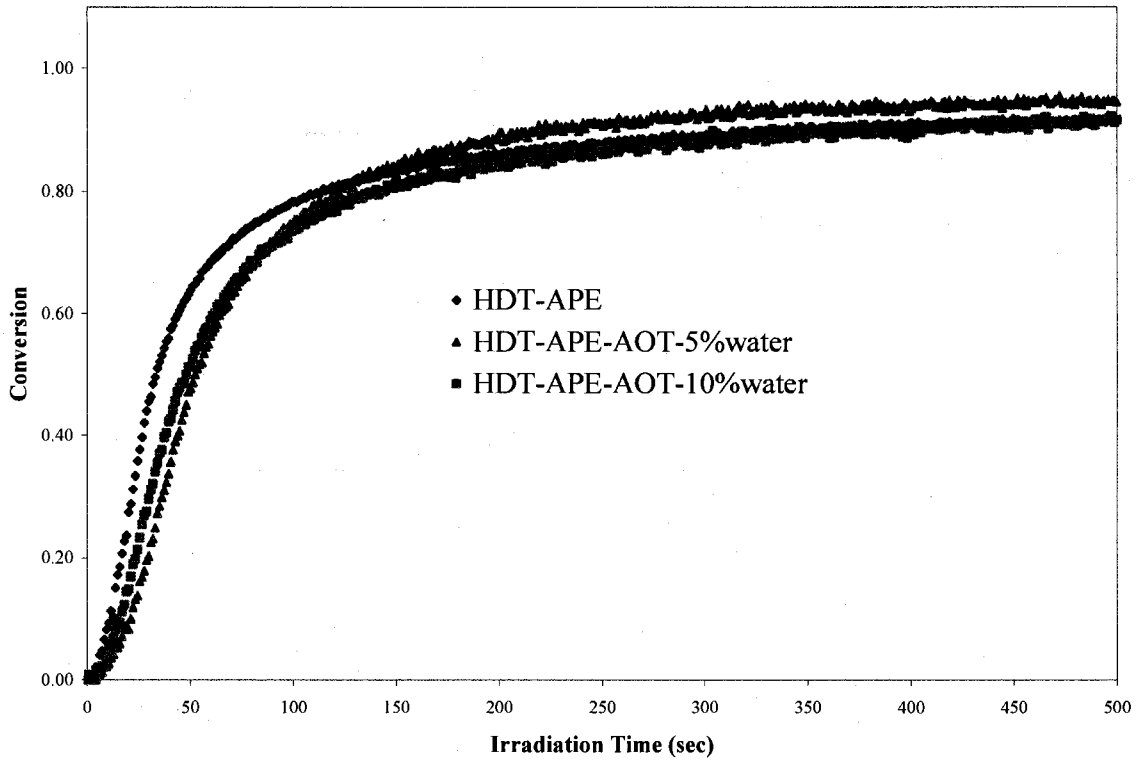

Figure 6.14. RTIR conversions of the double bond in the ene monomer: (◆) APE-HDT, (▲) APE-HDT-AOT-H_2O microemulsion 5 wt% of water, (■) APE-HDT-AOT-H_2O microemulsion 10 wt% of water. Light intensity 1.56 mW/cm^2 at 365 nm, high-pressure mercury-xenon lamp source.

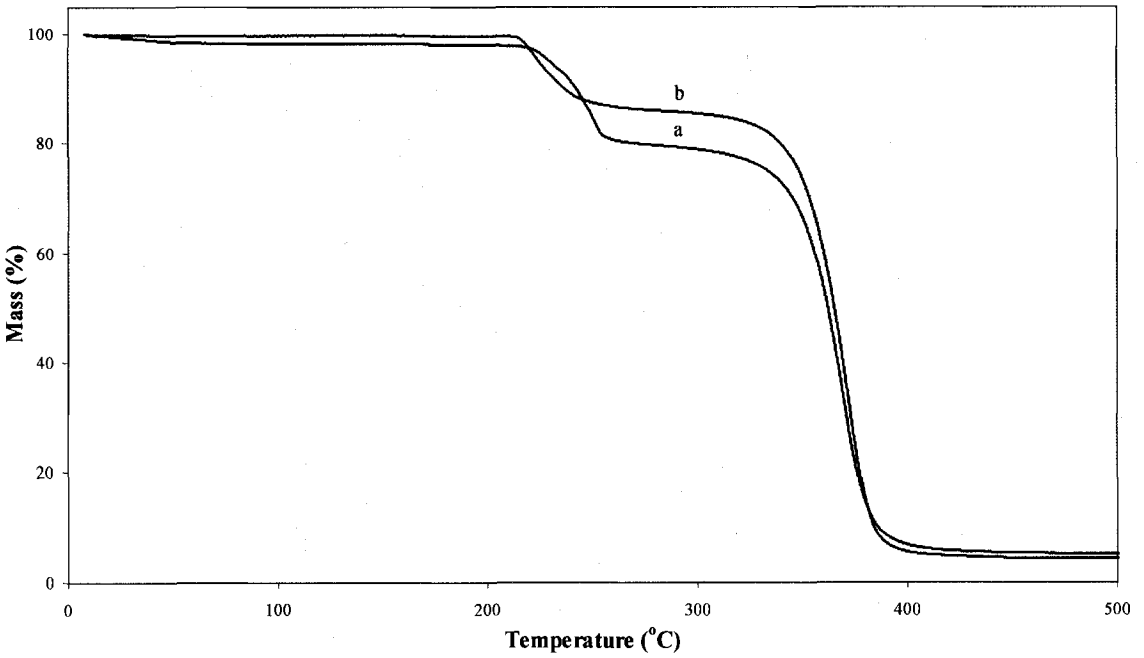

Figure 6.15. Thermal gravimetric analysis of a film polymerized from HDT-APE microemulsions with W = 10 and 10 wt% of water; (a) dry film before immersion in water, (b) the same film with "removed" surfactant.

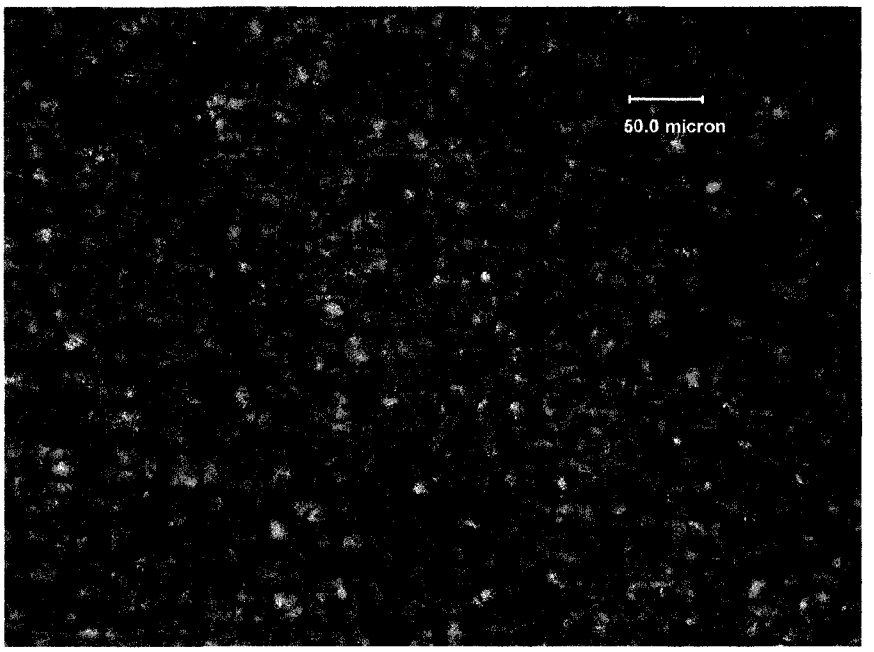

Figure 6.16. Image of a film photopolymerized from a microemulsion based on HDT-APE-PEG1 with 10 wt% water and W = 10. The scale bar represents 50 microns.

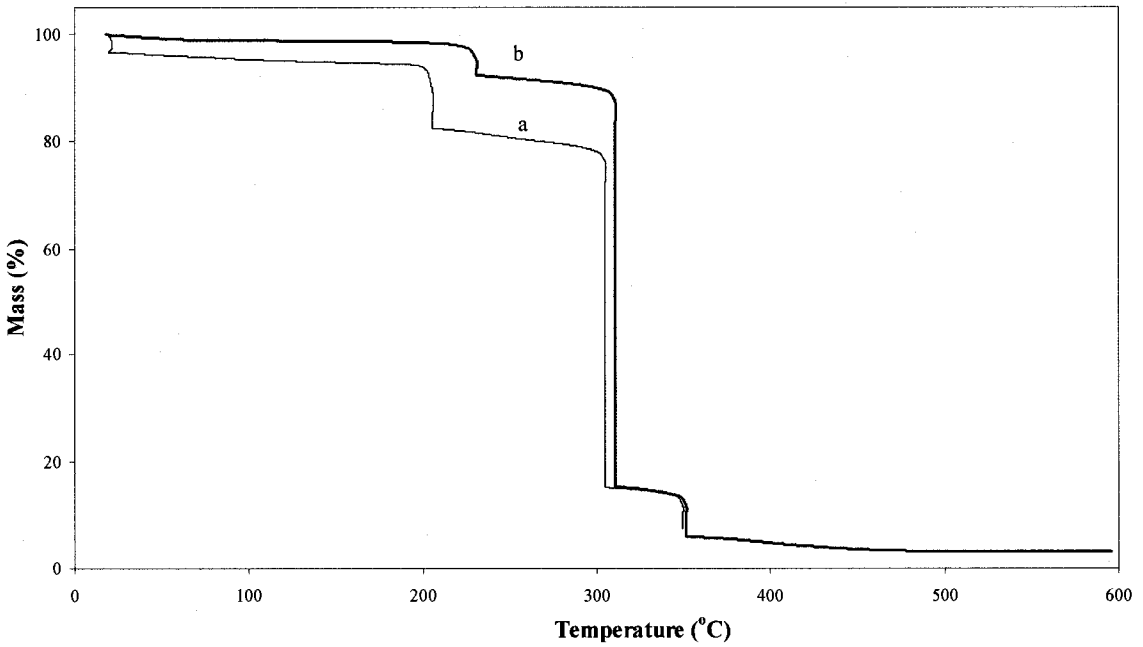

Figure 6.17. Thermal gravimetric analysis of films prepared from the HDT-APE-PEG1 microemulsion that had 10 wt% of water and W = 10, (a) right after polymerization, (b) the same film after 24 hour exposure to open atmosphere.

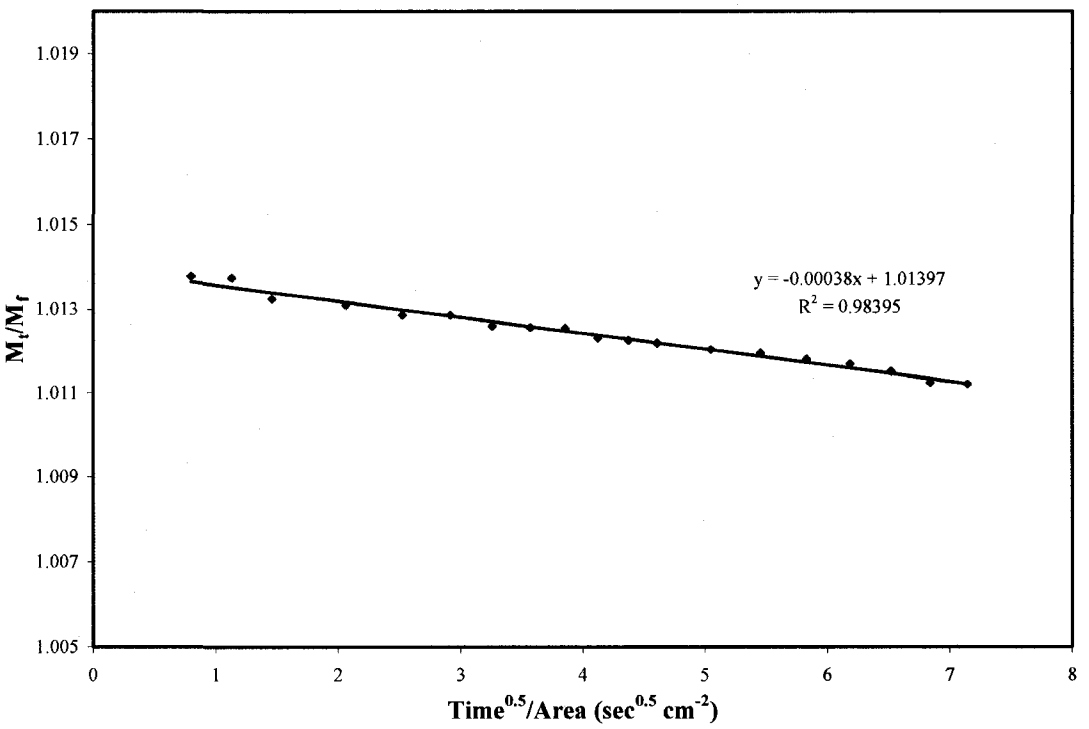

Figure 6.18. Diffusion coefficient determination for a film prepared from microemulsion based on HDT-APE-PEG1 system.

a)

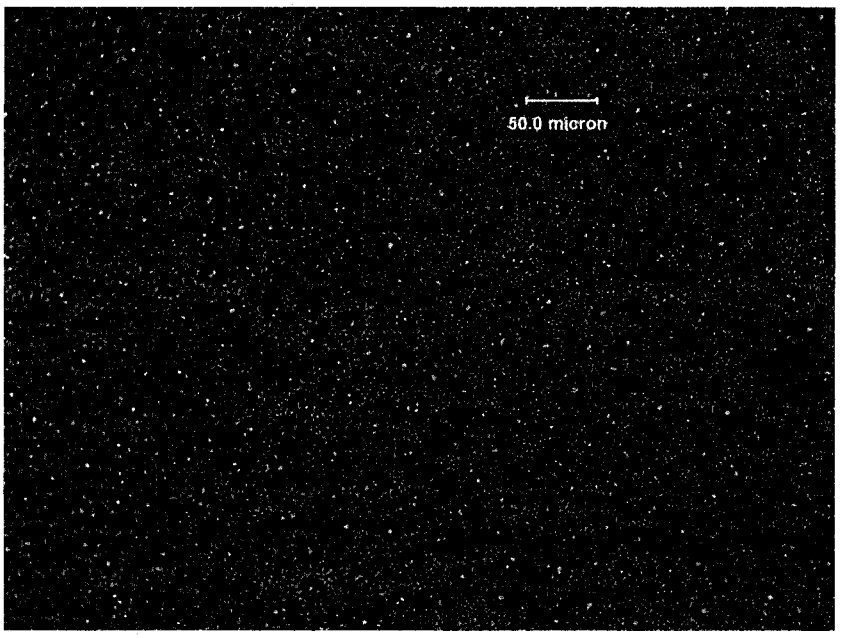

b)

Figure 6.19. Images of a film photopolymerized from a microemulsion based on HDT-APE-DDE with 10 wt% water and W = 10. (a) Part of a thin film (10 μm), (b) Top layer of a thick film (~0.2 mm). The scale bar represents 50 microns.

Reference

(1) G Odian: Principles of Polymerization, 4th Ed., Wiley, New York, 2004.

(2) TJ Tuling, M Tirrell: Toward a molecular theory of the Trommsdorff effect. Macromolecules 14 (1981) 1501.

(3) ER Beckel, NB Caramer, AW Harant, BC N.: Electro-optic properties of thiol-ene polymer stabilized ferroelectric liquid cryatal. Liquid Crystals 30 (2003) 1343-50.

(4) D Nwabunma, T Kyu: Phase behaviour of mixtures of low molar mass nematic liquid crystal and in situ photo-cross-linked polymer network. Macromolecules 32 (1999) 664.

(5) AF Senyurt, G Warren, JB Whitehead, CE Hoyle: Matrix physical structure effect on the electro-optic characteristics of thiol-ene based H-PDLS films. Polymer 47 (2006) 2741.

(6) M Date, Y Takeuchi, K Kato: A memory-type holographic polymer dispersed liquid crystal (HPDLC) refrective display device. Journal of Physics D: Applied Physics 31 (1998) 2225.

(7) LV Natarajan, CK Shepherd, DM Brandelik, RL Sutherland, S Chandra, VP Tondiglia, D Tomlin, TJ Bunning: Switchable Holographic polymer-dispersed liquid crystal reflection gratings based on thiol-ene photopolymerization. Chemistry of Matrials 15 (2003) 2477.

(8) PJ Collings, M Hird: Introduction to Liquid Crystals Chemistry and Physics, Taylor & Francis, 1998.

(9) CE Hoyle, TY Lee, TM Roper: Thiol-enes: chemistry of the past with promise for the future. Journal of Polymer Science: Part A: Polymer Chemistry 42 (2004) 5301.

CHAPTER VII

CONCLUSIONS AND FINAL REMARKS

It has been shown that the morphology of polymers formed through photopolymerization of reverse microemulsions is strongly influenced by dynamical and chemical factors. When a clear microemulsion with nanoscale structures was polymerized, it transformed into opaque, white films. The appearance of the films resulted from large aggregates that scattered light.

The chemical structures of the monomers, long-chained acrylates or thiol-enes, affected the morphology of the formed materials. When the microemulsion was composed of acrylate monomers, the formed polymer had two different structures. The droplets, which were mainly filled with water, were large enough to scatter visible light and gave the films their opacity. However, the droplets were too small to be observable under the optical microscope. Secondly, some portion of the surfactant self-assembled into a bilayer structure connecting the larger pools of water. The bilayers were formed due to favorable interactions between the surfactant and polymer chains.

In the case of microemulsions based on thiol-ene chemistry, the films morphology was noticeably different. In the films, large droplets with sizes varying from 2 to 100 μm were visible under the magnification of the optical microscope. Also, the surfactant was less compatible with the thiol-ene network than with acrylate and was promptly excluded from that network. As a consequence, the composition of the aggregates changed depending on the microemulsion's composition. When more of the aqueous phase was

present in the microemulsion, the domains were filled not only with water but also with an aqueous phase composed of water and surfactant.

The morphologies of both systems are sensitive to the rate of the polymerization. When the thiol-ene microemulsion was allowed to self-polymerize, the phase separation occurred. A top layer was mainly composed of a polymer. A lower water-rich stratum had a small amount of polymer confined in droplets. This result proved that films formed through the light-induced reaction are frozen in a far-from-equilibrium state.

A humidity response was seen in the acrylate system. The films underwent a transition from opaqueness to clearness upon exposure to low humidity of the surroundings. This process was reversible. It was supposed that the opaqueness is a result of large domains in the films. We were able to confirm this assumption with SANS and USANS analysis of films right after polymerization and in the opaque state. It would be desirable to analyze the structure of these films as a function of humidity. We would expect a decrease in the size of domains as water leaves from the films.

Another interesting aspect of this research is the influence of the polymer presence on the stability of the microemulsion phase. We conducted preliminary analysis of these perturbed systems through dynamic light scattering, DLS. Quickly it was discovered, that some of the compositions would have a very weak scattering signal, when others showed multiple decay modes. This complicated response requires further analysis, which could result in a complementary doctoral work.